Title

The Expression and Function of Down Syndrome Cell Adhesion Molecule B in the Larval Zebrafish Nervous System

Author

Julien, Donald Patrick

Publication Date

2017

Peer reviewed|Thesis/dissertation

UNIVERSITY OF CALIFORNIA

Los Angeles

The Expression and Function of Down Syndrome Cell Adhesion Molecule B in the Larval Zebrafish Nervous System

A dissertation submitted in partial satisfaction of the requirements for the degree

Doctor of Philosophy in Neuroscience

by

Donald Patrick Julien

2017

ASTRACT OF THE DISSERTATION

The Expression and Function of Down Syndrome Cell Adhesion Molecule B in the Larval Zebrafish Nervous System

by

Donald Patrick Julien

Doctor of Philosophy in Neuroscience

University of California, Los Angeles, 2017

Professor Alvaro Sagasti, Chair

The brain is composed of complex neuronal circuits that provide the physiological basis for our cognition, perception, and behavior. Unraveling how neurons establish these circuits and the myriad of molecular signals that guide their development is one of the most daunting tasks in neurobiology. Down Syndrome Cell Adhesion Molecules (DSCAMs) play an evolutionarily conserved role in regulating key aspects of neuronal wiring, including programmed cell death, neuronal migration, axon guidance, neurite branching, branch spacing, and synaptic targeting. However, despite being expressed broadly throughout the vertebrate nervous system, there remains a paucity of in vivo investigations of the functions of DSCAM family members across different regions of the brain. Additional studies could shed light on how well DSCAM functions are conserved across the diversity of neuronal cells types in different neuronal systems.

In the present study, I leveraged the genetic tractability and optical accessibility of the larval zebrafish model to investigate the expression and function of a DSCAM family member, *dscamb*, throughout the developing brain. Using targeted mutagenesis, I created the first

dscamb loss-of-function mutant lines, and through a combination of transgenic approaches, I provided the first characterization of *dscamb* expression. Using these genetic tools, I uncovered that, similar to DSCAM family members in other species, Dscamb is expressed broadly throughout the brain, spinal cord, and peripheral nervous system. However, I also identified several regions of expression, particularly in the peripheral nervous system and muscle cells, that have not been described for other DSCAM family members. Unlike other vertebrate DSCAMs, I found no evidence that Dscam is required for retinal development. Moreover, *dscamb* loss-of-function did not affect the overall structural organization of the brain and spinal cord. Despite an absence of apparent anatomical defects a series of behavioral analyses revealed that *dscamb* mutants are severely deficient in their ability to find or capture food, suggesting that this protein has a critical, and perhaps subtle, function in the wiring of neuronal systems that underlie feeding behavior.

The dissertation of Donald Patrick Julien is approved.

S. Lawrence Zipursky

Kelsey C. Martin

Bennett G. Novitch

Alvaro Sagasti, Chair

University of California, Los Angeles

2017

DEDICATION

For Jill and Jeff

For Family and Friends

TABLE OF CONTENTS

LIST OF FIGURES AND TABLES

ACKNOWLEDGEMENTS

I am incredibly grateful for the guidance of my adviser, Dr. Alvaro Sagasti. The breadth and depth of his scientific understanding is exceeded only by his curiosity and interests. No matter what direction my research went—and it went in many directions, typically moving further away from the purview of our lab—Alvaro was always engaged, supportive, and able to provide profound insight. His guidance was always balanced with trust and respect, and with that, the freedom to also work and think independently. This has allowed me to grow immeasurably as both a scientist and an individual.

I thank the rest of my inspiring dissertation committee: Larry Zipursky, Kelsey Martin, and Bennett Novitch. Although, I could never help but feel nervous walking into our meetings—a reflection of my profound admiration for your scientific and professional achievements—your enthusiasm, encouragement, and perspicacity always left me feeling inspired and eager to do more.

Thank you to all the members of the Sagasti lab, past and present, for your scientific, technical, and creative input during many hours of group meetings and through many discussions across the bays in lab. Thank you also for your comradery over wine and smorgasbords of TJ's snacks. I have been truly fortunate to have had such a wonderful group of colleagues.

Thank you to my parents, my siblings, and my lifelong friends for your love, companionship, and support long before and throughout my doctoral education. To the new friends that I have made and my wonderful cohort in the NSIDP, thank you for supporting me and one another through the tribulations and triumphs of graduate school. I would not be who I am today without all of you.

Most of all, thank you Esther, for being my companion and my best friend. Your warmth and strength has been my greatest source of comfort and inspiration.

The research presented in this thesis was supported by National Institute of Arthritis and Musculoskeletal and Skin Diseases (R01 AR064582). Graduate student support was provided by a scholarship from the Achievement Rewards for College Scientists (ARCS) Foundation and the UCLA Philip Whitcome Predoctoral Training Program in Molecular Biology.

All of the research presented in this thesis is currently being collated and abridged into a publication. Authorship will include Donald P Julien, Joshua P Barrios, Alex W Chan, Adam Douglass, and Alvaro Sagasti.

Except for the examples stated below, I personally designed, performed, and analyzed all of the experiments contained in this thesis.

In Chapter 2, Alex W Chan conducted the confocal imaging and cell counting in Et1(dscamb^{t2b}:Gal4)/BAC(trpa1b:GFP) coexpression analysis.

In Chapter 3, Marianne Cilluffo and the UCLA Electron Microscopy Core, carried out all of the histological processing for photoreceptor TEM. I performed the TEM image acquisition.

In Chapter 3, Alex W Chan collected the data for somatosensory function assays and mutant mortality experiments, and I performed the data visualization and statistical analyses. Joshua Barrios (PhD graduate student in the laboratory of Dr. Adam Douglass) performed the auditory

function assays, including the behavioral data collection, data visualization, and statistical analyses. I genotyped the larvae after auditory testing.

VITA

EDUCATION

2007-2011	University of Missouri, Columbia, MO BS in Biological Sciences Minor in Chemistry

HONORS & AWARDS

2011-2016	Achievement Rewards for College Scientists (ARCS) Scholarship
2013-2015	UCLA Philip Whitcome Training Program in Molecular Biology
2013	UCLA Dept of MCDB Annual Retreat Poster Prize
2011	UCLA Chancellor's Prize Scholarship
2011	MU Professor Stanley Zimmering Prize in Biology

RESEARCH

2012-present	Alvaro Sagasti, PhD University of California, Los Angeles, CA PhD Thesis lab: The expression and function of Dscamb in the larval zebrafish nervous system
2012	Istvan Mody, PhD University of California, Los Angeles, CA PhD rotation: Structural changes in perineurial nets surrounding cortical interneurons in mouse models of schizophrenia
2012	Patricia Phelps, PhD University of California, Los Angeles, CA PhD rotation: Identification of Disabled-1 mutant cortical neurons in primary culture
2010-2011	Andrew McClellan, PhD University of Missouri, Columbia, MO Undergraduate research: Temperature modulation of spinal cord regeneration in the larval lamprey
2010	Scott Hultgren, PhD Washington University, St. Louis, MO Summer undergraduate research: Generating and characterizing strains of uropathogenic E. coli with mutations in pili-encoding genes

PUBLICATIONS & ABSTRACTS

Articles:

Benes JA, House KN, Burks FN, Conaway KP, **Julien DP**, Donley JP, Iyamu MA, McClellan AD (2017) Regulation of axonal regeneration following spinal cord injury in the lamprey. J Neurophysiol 118:1439–1456.

Julien DP, Sagasti A (2014) Synaptic specificity: when the neighbors are away, sensory axons turn promiscuous. Curr Biol 24:R1168–R1170.

Wang F*, **Julien DP***, Sagasti A (2013) Journey to the skin: Somatosensory peripheral axon guidance and morphogenesis. Cell Adh Migr 7:388–394.

*co-first authorship

Recent Abstracts and Poster Presentations:

Julien DP, Chan AW, Sagasti A. Identifying zebrafish somatosensory subtypes using CRISPR/Cas9-directed transgene integration. Poster presentation at LPM International Congress on Genome Editing and Gene Modulation. University of Oxford, April 2016.

Julien DP, Chan AW, Sagasti A. Identifying zebrafish somatosensory subtypes using CRISPR/Cas9-directed transgene integration. Poster presentation at the CSHL Meeting on Genome Engineering: The CRISPR/Cas9 Revolution. Cold Spring Harbor, NY, Sept 2015.

Julien DP, Tellez G, Wang F, Sagasti A. The molecular mechanisms of somatosensory axon branch spacing. Poster presentation at the CSHL Meeting on Axon Guidance, Synapse Formation and Regeneration. Cold Spring Harbor, NY, Sept 2014.

Julien DP, Tellez G, Wang F, Sagasti A. The molecular mechanisms of somatosensory axon branch spacing. Poster presentation at the GSA 11th International Conference on Zebrafish Development and Genetics. Madison, WI, June 2014.

CHAPTER 1

Introduction

1.1 THE IMMUNOGLOBULIN SUPERFAMILY AND NEURONAL DEVELOPMENT

The brain is composed of numerous, morphologically complex neurons, which elaborate incredibly intricate axonal and dendritic arbors and traverse large distances to connect disparate regions of the brain. Organizing these complex, intermingling neuronal arbors into the circuits that underlie behavior and cognition requires the precise coordination of several developmental events: neuronal migration and differentiation, neurite outgrowth and elongation, axonal guidance, axonal and dendritic branching, and synaptic formation and refinement. Coordinating these already complex processes across numerous and diverse neuronal populations requires a diversity of molecular cues and receptors (Langley, 1895; Sperry, 1963; Lawrence Zipursky and Sanes, 2010). Uncovering the vast repertoire of molecular signals that govern the assembly of neuronal circuits is arguably one of the most important and daunting tasks in neurobiology.

The immunoglobulin superfamily (IgSF) of cell adhesion molecules (CAMs) is one of the largest protein families in vertebrates, and represents some of the most abundant CAMs expressed in the brain. The diversity of these proteins and the broad range of their binding interactions (Vaughn and Bjorkman, 1996) make IgSF CAMs an ideal substrate for organizing complex neuronal circuits. One family of IgSF proteins, the Down Syndrome cell adhesion molecules (DSCAMs), has attracted considerable attention due to its location on the Down syndrome critical region (DSCR) of chromosome 21 (Yamakawa et al., 1998), trisomy of which is sufficient to manifest the developmental and intellectual disability defects associated with Down syndrome (Korenberg et al., 1992, 1994; Delabar et al., 1993). DSCAMs are single-pass transmembrane proteins, with a conserved extracellular domain organization consisting of 10 Ig domains and 6 fibronectin repeats (Agarwala et al., 2001a; Barlow et al., 2001). In mice, DSCAM is expressed broadly throughout brain, spinal cord, and peripheral nervous system (Yamakawa et al., 1998; Agarwala et al., 2001a; Barlow et al., 2001, 2002a, 2002b). Expression is particularly enriched in the cerebral cortex, cerebellum, and hippocampus, all of which have reduced size in Down

Syndrome individuals, making DSCAM an enticing candidate for mediating Down Syndrome neuropathology.

Further interest in DSCAMs was raised by studies of the fruit fly (*Drosophila melanogaster*) ortholog *dscam1*, and its role in neurite self-recognition and avoidance. The *dscam1* allele has a unique mechanism of alternative splicing, which is capable of generating up to 19,008 different extracellular domains that engage in precise homophilic binding. Stochastic expression of different isoforms in each neuron encodes individual identity and allow branches of the same neuron to recognize and avoid one another (Schmucker, 2007; Hattori et al., 2008; Millard and Zipursky, 2008). At least two DSCAM family members have been identified in vertebrates: DSCAM and the closely-related DSCAM-like 1 (DSCAML1) (Yamakawa et al., 1998; Agarwala et al., 2001c). Neither gene is capable of extensive alternative splicing. Indeed extensive alternative splicing of DSCAMs appears to be specific to arthropods. However, the highly conserved extracellular structure of these proteins suggests that DSCAM plays an important role in neuronal development that does not require extensive molecular diversity.

1.2 DSCAMS REGULATE NEURONAL BRANCH SPACING

Studies in leech touch-sensing neurons provide the first evidence of neuronal self-avoidance

The highly branched axonal and dendritic arbors of many neurons must space themselves appropriately to comprehensively innervate a target area. Self-avoidance is a tendency of neurite branches originating from the same neuron to avoid contacting one another. This process was proposed nearly 50 years ago by Nicholls and Baylor (Nicholls and Baylor, 1968) while mapping the receptive territories of touch-sensing neurons in the skin of the leech (*Hirudo medicinalis*). They characterized three subtypes of touch-sensing neurons that were responsive to different magnitudes of skin deformation (i.e. different levels of pressure). Neighboring sensory neurons of the same subtype have receptive territories that largely exclude one

another, but exhibit some overlap on the edges of their receptive fields. They also noted that some sensory neurons project two axon branches towards the periphery. Cutting one of these axon branches ablated half of the receptive field, suggesting that individual sensory neurons can project multiple axon branches that innervate neighboring subfields. Unlike the receptive territories of different sensory neurons (which partially overlapped) these subfields arising from the same neuron were almost completely segregated. This observation led them to hypothesize that axons originating from the same neuron repel one another during development.

These findings were later validated by Kramer and Stent (Kramer and Stent, 1985). Working with another leech model (Haementeria ghilianii), Kramer and Stent identified a large touch-sensing neuron that projected three axon branches to the periphery, where they arborized into adjacent, but mutually-exclusive patches of the skin. They crushed one of these peripheral branches and visualized the response of the neighboring sister arbor by injecting the cell with a fluorescent dye. The spared arbor expanded its territory into the now vacant field of its ablated sister arbor, suggesting that axon branches of the same cell repel one another in the skin. They speculated that self-repulsion could be a general principle for axonal and dendritic arbors across other regions of the nervous system. This process would ensure that arbors spread evenly across their innervation territory, and the ability to recognize self from nonself would allow different arbors to coexist within the same territory. At the time, Kramer and Stent, speculated that one possible molecular mechanism could be “that the peripheral axons carry cell-specific, or idiosyncratic, labels,” but that “the number of such labels would have to be quite large” (Kramer and Stent, 1985). This insight would prove to be prescient years later with the discovery of the role of Dscam1 in self-avoidance in the fly nervous system.

Drosophila Dscam1 mediates self-avoidance through molecular diversity and homophilic binding

The Drosophila gene, *dscam1*, is the most well-characterized DSCAM family member, particularly for its role in self-avoidance. The *dscam1* locus is unique in its ability to undergo extensive alternative splicing. Specifically, the exons encoding the second, third, and seventh extracellular Ig domains each contain multiple potential alternatively-spliced exons; there are 12, 48, and 33 alternatively spliced exons encoding the second, third, and seventh extracellular Ig domains (exon 4, 6, and 9, respectively) (Schmucker et al., 2000). Two alternative exons encode the transmembrane domain and regulate the selective trafficking of Dscam1 proteins to either dendrites or axons (Wang et al., 2004; Shi et al., 2007; Yang et al., 2012). Consequently, the *dscam1* locus is capable of generating over 19,008 alternatively spliced ectodomains, providing an ideal molecular substrate for achieving the "quite large" number of labels that Kramer and Stent initially proposed for satisfying self-avoidance.

Despite such extensive molecular diversity Dscam1 isoforms participate in precise homophilic binding. Dscam1 homophilic binding was initially characterized by coating fluorescent beads with single Dscam1 isoforms and measuring their ability to adhere to other beads or cultured cells presenting the same or different Dscam1 isoforms. These studies demonstrated that Dscam1 isoforms bind exclusively with proteins of the same isoform. Homophilic binding requires the presence of all three variable Ig domains, and even a mismatch of one variable domain disrupts binding (Wojtowicz et al., 2004). A high-throughput ELISA-based binding assay, capable of testing thousands of different combinations of Dscam1 ectodomains, validated that, with few exceptions, Dscam1 isoforms engage in precise homophilic binding (Wojtowicz et al., 2007).

The role of Dscam1 in neuronal self-avoidance is perhaps most clearly demonstrated in the touch-sensing neurons of fly larvae. (Hughes et al., 2007; Matthews et al., 2007; Soba et al., 2007). This sensory system is composed of four subtypes of dendritic arborization (da) of

sensory neurons (Class I, II, III, and IV) that elaborate sensory dendritic arbors in the epidermis to detect different types of touch stimuli. Neurons within each subtype exhibit highly stereotyped dendritic arbor morphologies and innervation territories, with little overlap between dendritic branches of the same arbor or neighbors of the same subtype, but extensive overlap between neighbors of different subtypes (Grueber et al., 2002). In *dscam1* mutant larvae, the sensory branches of individual da neurons crossed over and fasciculated extensively with one another, indicating a failure of self-avoidance. This phenotype was observed across all da neuron subtypes. *dscam1* mutant neurons also showed no significant deficits in total dendritic length, numbers of branches, or repulsion between neighboring neurons, suggesting that Dscam1 functions specifically in self-avoidance in da sensory neurons. Expression of a single isoform of Dscam1 was sufficient to rescue self-avoidance defects. Moreover, when a single isoform was ectopically expressed in neighboring neurons of different subtypes—whose dendrites overlap — it drove neighboring branches to avoid one another.

Dscam1 also regulates self-repulsion in the fly CNS. During development, mushroom body axons bifurcate into two sister axons, each projecting to a different target region. In *dscam1* mutants, these axons fail to segregate and grow towards the same target regions, suggesting a defect in axon self-repulsion. Expression of a single Dscam1 isoform in individual cells was sufficient to rescue the proper segregation of mushroom body axons (Hattori et al., 2007). Therefore, Dscam1 appears to regulate self-repulsion in both axons and dendrites and across different regions of the fly nervous system.

Individual cells express multiple isoforms of Dscam1 in a probabilistic manner

The aforementioned studies demonstrated a role for Dscam1 in regulating neuronal self-avoidance, but how does the fly brain leverage this extensive molecular diversity to enable hundreds of thousands of neuronal arbors to intermingle, while also recognizing and avoiding

themselves? Neves et al analyzed the expression of individual fly photoreceptors using a custom built microarray chip designed to probe all 93 alternative exons(Neves et al., 2004). Although this approach does not detect the combination of alternative exons in each mRNA transcript, they were able to estimate that individual cells express 14-50 isoforms of Dscam1, and that the array of isoforms differs between cells (Neves et al., 2004). Similar studies in mushroom body neurons also identified that individual neurons express multiple isoforms that vary between neurons (Zhan et al., 2004). Interestingly, an analysis of transgenic reporters for each of the 12 exon 4 variants identified that different cell populations are more likely to express certain alternative exons over others, and that this preference varies across cell types (Miura et al., 2013). These studies also found that the expression of exon 4 variants can change over time.

To determine how much Dscam1 diversity is required for individual neurons to reliably distinguish self from other, Hattori et al (2009), used homologous recombination to generate multiple lines where they reduced the number of possible Dscam1 isoforms from 19008 to 14256, 4752, 576, and 12. In da sensory neurons, self-repulsion was rescued with as few as 12 Dscam1 isoforms. However, these cells also aberrantly repelled from neighboring neurons with which they usually overlap. This defect was restored to wild type levels when 4752 potential isoforms were available, suggesting that the fly nervous systems requires thousands of Dscam1 isoforms for accurate self-recognition (Hattori et al., 2009).

Collectively, these studies point to a model in which each neuron expresses a unique array of 14-50 Dscam1 isoforms that act as a molecular barcode for self-recognition and avoidance. When branches of the same neuron contact one another, they engage in precise homophilic binding that signals them to repel each other. When branches of different neurons interact, the reduced homophilic binding is unable to trigger the repulsive response. This model provides a

satisfying and logical molecular explanation for how numerous, intermingling neurites can reliably distinguish self from nonself; however, several outstanding questions remain. The fact that certain cells types are biased in their expression of certain exon 4 variants, raises the possibility that neighboring neurons could occasionally express at least one identical isoform at the same time. Theoretically this would cause neighboring cells to mis-identify and repel one another. It is possible that low frequencies of misidentification are tolerable in circuit development. Another possibility is that Dscam1 molecules interact combinatorially in cis to provide an added measure of specificity in binding. Perhaps the most interesting and fundamental question, however, is how neurons manage to exert any kind of preference in the face of so many possible spliceforms, and what are the molecular mechanisms that underlie the selection of some variants over others.

Dscams regulate tiling in the Drosophila visual system

A robust mechanism of self-recognition allows neuronal arbors to spread branches evenly across their innervation territory even as they intermingle extensively with neighboring arbors. Just as critical to the formation of neuronal circuits, however, is how those neighboring arbors recognize one another and space themselves appropriately. When neurons performing a similar function innervate the same target, they often segregate their arbors into mutually exclusive territories. This interaction is referred to as “tiling,” because the resulting arrangement resembles tiles across a kitchen floor. Tiling minimizes redundancy between neighbors, while ensuring that the entire target area is comprehensively innervated. Although numerous molecular signals have been implicated in tiling, DSCAMs are one of the only protein families identified where this function that are highly conserved across different species (Grueber and Sagasti, 2010).

The Drosophila visual system has a repeating and highly modular structure with many neuronal subtypes that tile with like neighbors. The fly compound eye is composed of ~800 independent units, called ommatidia. Each ommatidium contains eight photoreceptors (R1-8) that project axons terminating in two different glomeruli in the optic lobe: the lamina (R1-R6 axons), and the medulla (R7 and R8 axons). In the lamina, R1-R6 axons that originate from separate ommatidia, but encode the same point in visual space, converge into repeating neuropil structures, called cartridges, where they form synapses with the dendrites of multiple types of interneurons (L1-L5). L1-L5 interneurons, in turn, project axons into the medulla, where they synapse in specific laminae of repeating column units. L1-L5 axons are tiled across medullar columns, such that each column receives only one axons from each interneuron subtype (Clandinin and Zipursky, 2002).

The DSCAM family member, Dscam2, regulates tiling between multiple subtypes of L-type interneurons in the optic lobe. Dscam2 binds homophilically and is expressed in L1 neurons, which tile their axons into discrete columns in the medulla. In *dscam2* mutants, L1 axons terminate in the appropriate sublaminae, but their axons extend laterally to invade neighboring columns. Dscam2 is required both autonomously and in neighboring columns to prevent tiling defects (Millard et al., 2007). An analysis of the expression of two alternative splice forms of Dscam2 (Dscam2A and Dscam2B) revealed that L1 neurons exclusively express Dscam2B. Knockout of Dscam2B, but not Dscam2A resulted in tiling defects (Lah et al., 2014). Thus, L1 axons repel one another into separate columns through Dscam2B-mediated homophilic binding.

L-type interneurons also project dendrites that tile within neuropil cartridges of the lamina. L4 neurons, for instance, project two posterior dendrites to innervate neighboring cartridges and a single anterior dendrite to innervate its home cartridge. This invariant pattern of dendritic branches, creates a tiled arrangement, where each L4 neuron innervates three cartridges, and

each cartridge is innervated by three L4 dendrite branches. In *dscam2* mutants, the anterior dendrite develops normally, but the two posterior branches expand to innervate an additional one or two cartridges (Tadros et al., 2016). A similar phenotype was also observed in *dscam4* mutants, suggesting that these two proteins function in the same pathway. In contrast to L1 axons, where Dscam2 signaling acts to mutually repel axons into a tiled arrangement, neighboring L4 dendrites ordinarily contact and synapse with one another in each cartridge, suggest that a non-repulsive mechanism is at play. Indeed, the authors found that *dscam2*/*dscam4* L4 dendrites fail to adhere to their appropriate targets early in development, causing them to overshoot and invade neighboring cartridges. These studies provide a compelling example of how Dscams can regulate the appropriate spacing of both axonal and dendritic arbors, and that tiled arrangements can be generated through disparate cellular interactions, such as repulsion and adhesion.

Dscams regulate homotypic branch spacing and mosaic patterning in the mouse retina

Two DSCAM family members have been identified in the vertebrate genome: DSCAM (Yamakawa et al., 1998) and the closely-related Dscam-like 1 (DSCAML1) (Agarwala et al., 2001c). Although vertebrate DSCAMs do not undergo extensive alternative splicing (Yamakawa et al., 1998; Barlow et al., 2002b), they do engage in homophilic binding (Agarwala et al., 2000, 2001c) and share some striking functional parallels to their fly counterparts in the development of the visual system. Similar to the fly visual system, the vertebrate retina is stratified into well-characterized cellular and synaptic domains. The outer nuclear layer (ONL) contains the photoreceptors (PRs) that transduce light into electrochemical signals. At the outer plexiform layer (OPL), these signals are relayed from the PRs to bipolar cells (BCs) in the inner nuclear layer (INL). The INL also contains two other neuronal cell types critical for processing these sensory signals: horizontal cells (HCs) and amacrine cells (ACs). At the inner plexiform layer (IPL), sensory information is transferred from BCs to retinal ganglion layer (RGL), where retinal

ganglion cells (RGCs) serve as the output cells of the retina, conveying sensory information to downstream regions of the brain. Each of the five major cell types in the retina (PR, HC, BC, AC, and RGC), are divided into several—sometimes many—subtypes. Neurons of the same subtype are distributed across the retina in regularly spaced “mosaics”, with neighbors evenly spaced from one another and varying degrees of overlap between neighboring arbors. This arrangement ensures that the entire visual field is equally competent for processing visual information (Masland, 2012).

DSCAM and DSCAML1 are expressed in non-overlapping retinal cell types in the mouse retina. DSCAM is expressed in most RGCs and several AC subtypes (TH+, bNOS+), while DSCAML1 is expressed in the PRs, rod bipolar cells (PKC-beta1+), and a subset of ACs (Dab+) (Fuerst et al., 2008, 2009). In *Dscam* and *Dscaml1* mutants, the INL and IPL are significantly expanded and disorganized, largely due to decrease in developmental cell death. Amongst the cell types that ordinarily express these proteins, mosaic spacing was severely disrupted in mutant retinas, with cells aggregating into large clumps with fasciculated processes. Increased density from reduced cell death was not sufficient to recapitulate this phenotype, nor was artificially decreasing cell number through knockout of *Brn3b* able to rescue the fasciculation and aggregation defects in *Dscam* mutants (Fuerst et al., 2012; Keeley et al., 2012). Closer inspection revealed that cell types aggregated and fasciculated independently of one another. Fascicles were composed of branches of the same neuron and neighbors of the same cell type, indicating that DSCAMs are required for self-avoidance and to maintain proper spacing between homotypic cells and their processes. Wildtype cells transplanted into *Dscam* mutant retinas also fasciculated and clumped with their mutant neighbors, suggesting that homophilic DSCAM signaling between cells is required for homotypic spacing (Fuerst et al., 2012). For many of these retinal cell types, branches ordinarily exhibit some degree of overlap during development, arguing that DSCAMs does not act as a direct repulsive cue, but rather as a “nonstick coating”

that masks adhesive cues and prevents homotypic branch fasciculation (Fuerst et al., 2009). Thus, despite diverse mechanisms of alternative splicing in flies and mice, DSCMs have a conserved role in regulating self-avoidance and branch spacing.

1.3 DSCAMS REGULATE SYNAPTIC REFINEMENT

DSCAMs regulate synaptic coupling and lamination in the vertebrate retina

The retinal IPL is composed of axonal and dendritic processes from BCs, ACs, and RGCs, which can be further subdivided into many subtypes that synapse in distinct sublaminae. Targeting each subtype to its appropriate laminae and synaptic targets is critical for visual function, because different retinal circuits compute distinct aspects of visual stimuli. In the chick retina, Dscams and the closely-related Sidekick1 and Sidekick2 (Sdk1 and Sdk2) IgSF proteins are expressed in non-overlapping cell types and are enriched in distinct sublaminae of the IPL (Yamagata et al., 2002; Yamagata and Sanes, 2008). Neuronal subtypes expressing each of these IgSF molecules are present in both the INL and RGL and project to complementary sublaminae in the IPL, suggesting that they could play a role in synaptic coupling. RNAi-mediated knockdown of these proteins disrupted lamination in RGCs that ordinarily expressed these proteins, causing them to overshoot their target laminae (Yamagata and Sanes, 2008). Conversely, ectopic expression of each IgSF molecule redirected processes to the specific sublamina where the over-expressed protein is enriched (Yamagata et al., 2002; Yamagata and Sanes, 2008). Although these studies did not investigate the role of Dscams and Sdks in self-avoidance and fasciculation in the chick retina, they demonstrate that DSCAMs and similar cell adhesion molecules also regulate neuronal lamination.

In contrast to their roles in chicks, mouse DSCAM and DSCAML1 proteins show a more diffuse localization throughout the retina, instead of being concentrated in distinct sublaminae (Fuerst et al., 2009; de Andrade et al., 2014a, 2014b). Initial studies in mice did not identify lamination

defects in the Dscam mutant retinas (Fuerst et al., 2008, 2009). This may be due to genetic variability, as the first Dscam mutant alleles characterized were perinatal lethal on the commonly used C57BL/6 inbred strain and had to be maintained on outbred genetic backgrounds. A more recently discovered *Dscam* null allele (*Dscam*^{2J}) is viable on an inbred background, allowing for a more reliable characterization of gene function in neuronal patterning with less phenotypic variation (Fuerst et al., 2010). Analysis of retinal development in this mouse line corroborated the homotypic aggregation and fasciculation defects observed in previous mutants lines; however, *Dscam*^{2J} mutants also showed lamination defects in specific subtypes of retinal neurons, such as bNOS+ ACs and cholinergic (ChAT+) ACs. These finding demonstrate that DSCAM regulates retinal lamination in the mouse retina through a mechanisms that are influenced by genetic background. Future studies to identify genetic modifiers that account for this phenotypic variation could identify molecular partners that modulate DSCAM signalling.

Further interrogation of DSCAM function in retinal lamination, using a Cre-inducible *Dscam* null allele, found that lamination defects occur only when *Dscam* is ablated in both ACs and RGCs, but not just one or the other (Fuerst et al., 2012). Interestingly, ChAT+ ACs do not express DSCAM, and do not exhibit fasciculation or mosaic defects in *Dscam* mutants, suggesting that DSCAM regulates ChAT+ laminar targeting indirectly through its effects in other cell types. bNOS+ ACs, on the other hand, do express, DSCAM. The fact that proper lamination can still be achieved in bNOS+ ACs with DSCAM loss-of-function in either ACs or RGCs, but not both cell types, further indicates that lamination requires a coordinated interaction between multiple cell types and multiple molecular cues, and not solely homophilic DSCAM signaling between synaptic partners (Fuerst et al., 2012). Similar studies with targeted ablation of DSCAM in the INL and RGL would be required to determine if DSCAMs are also required pre- and post-synaptically for proper lamination in the chick retina.

DSCAM also has dosage-dependent effects on retinal lamination. Wildtype TH+ ACs project dendritic arbors to the S1 sublamina, but completely refine their projections to the S3 layer at later stages (Li et al., 2015). Heterozygous mutants TH+ ACs failed to refine their dendrites and were bistratified between the S1 and S3 layers. When *Dscam* was overexpressed across the retina, TH+ ACs segregated more precociously than wild-type ACs the S3 layer. Thus, increased DSCAM dosage drives more dendritic refinement to the S3 layer, suggesting that DSCAM is required in TH+ ACs to destabilize misprojected dendrites and promote synaptic refinement (Li et al., 2015).

Drosophila Dscam1 dosage orchestrates sensory axon synaptic refinement

In contrast, increased Dscam1 dosage in Drosophila DA sensory neurons elicits more profuse arborization of axon terminals in the ventral nerve cord. DA neuron axon terminals in this area have a stereotyped branching pattern. In *dscam1* null mutants, axon terminals are markedly stunted in their presynaptic arbor growth and branching. Although expression of a single *Dscam1* isoform on a null mutant background rescued the presynaptic arbor size, terminal branches misprojected to inappropriate targets, suggesting that Dscam1 diversity is dispensable for growth but not synaptic targeting. Dscam1 overexpression through either introduction of an extra allele, overexpression of positive regulators (Wnd or FMRP), or knockout of negative regulators (Hiw) caused profuse overgrowth of da axon terminals (Kim et al., 2013; Sterne et al., 2015). Similar experiments in an adult mechanosensory neurons (scutellar [Sc] neurons), in which Dscam1 expression was increased through either introduction of a third allele or knockout of FMRP, resulted in an increased frequency of mistargeted axon collaterals in the ventral nerve cord (Cvetkovska et al., 2013). Sc axon mistargeting also occurs with reduced Dscam1 isoform diversity, and complete loss-of-function prevents axon arborization (Chen et al., 2006; Hattori et

al., 2009; He et al., 2014), indicating that Dscam1 diversity and proper dosage are both required for Sc axon arborization and synaptic targeting.

DSCAM is required for proper sensory axon synapse formation in the mouse spinal cord

Defective sensory axon synapse formation in the CNS is also seen *Dscam* mutant mice. *Dscam* mutant mice have defective locomotor coordination (Xu et al., 2011; Lemieux et al., 2016; Thiry et al., 2016). Sensory feedback is a critical aspect of motor coordination, and DSCAM is expressed in both motor neurons and sensory neurons in dorsal root ganglia (DRG) (Thiry et al., 2016). Electrophysiological recordings from spinal motor circuits identified reduced mono- and polysynaptic sensory reflexes in *Dscam* mutant mice. Immunohistochemical analysis demonstrated that, despite normal numbers of DRG sensory neurons in *Dscam* mutant mice, there was a significant decrease in the number of sensory synapses on spinal motor neurons, suggesting that reduced sensory feedback was due to defective sensory synapse formation that was not secondary to sensory neuron loss (Thiry et al., 2016). Although additional studies are required to determine the specific molecular and cellular basis of this synaptic defect in *Dscam* mutant mice, these studies raise the intriguing possibility that DSCAMs could play a conserved role in sensory synaptic targeting between invertebrates and vertebrates.

Dscam is required for sensorimotor synapse formation and refinement in Aplysia

Studies of Aplysia neurons suggest a potential molecular mechanism for DSCAM regulation of sensorimotor synapse formation (Li et al., 2009). When cultured together, Aplysia sensory neurons and motor neurons, their postsynaptic partners, spontaneously synapse with one another. Both types of neurons express Dscam. In sensory neurons, Dscam accumulated in stable presynaptic varicosities, which were opposed by postsynaptic aggregations of AMPA-like receptors, where Dscam was also concentrated. Inhibition of Dscam signaling or expression either pre- or postsynaptically prevented the clustering of postsynaptic AMPA-like receptors.

Dscam was also required in both cell types for learning-associated synapse remodeling and postsynaptic glutamate receptor clustering (Li et al., 2009). It is interesting that DSCAMs regulate sensory axon synaptic targeting across both invertebrates and vertebrates. In Aplysia, like vertebrates, Dscam is not extensively spliced, raising the intriguing possibility that this function predates the evolution of Dscam1 alternative splicing in arthropods.

DSCAM regulates dendritic spine maturation in the mouse cortex

DSCAM also regulates the formation of dendritic spines in the mouse cortex, the primary postsynaptic compartment of excitatory pyramidal neurons (Maynard and Stein, 2012). In *Dscam* knockout mice, pyramidal neurons show a transient decrease in total number of spines during postnatal development. Although the total number of spines eventually recovered, there was a persistent increase in the proportion of immature spines with short, narrow morphologies suggesting at least a partial role for DSCAM in cortical neuron synapse maturation (Maynard and Stein, 2012). Taken together, the aforementioned studies demonstrate that DSCAMs play a conserved role in guiding synaptic targeting across different species and neuronal circuits.

1.4 DSCAMS REGULATE NEURONAL BRANCHING

In addition to self-avoidance, Dscam1 also regulates axonal and dendritic branch formation in the fly nervous system. As previously mentioned, Dscam1 knockout in mechanosensory Sc neurons completely blocked axon arborization in the ventral nerve cord. This phenotype could not be rescued with expression of a single Dscam1 isoform, and reduced Dscam diversity also caused milder defects in arborization (Chen et al., 2006; Hattori et al., 2009; He et al., 2014), indicating that Dscam1 expression and diversity are required for Sc axon branching. RNAi-mediated knockdown of Dscam1 in an identified motor neuron (MN5) increased dendritic arborization without causing any apparent defects in self-avoidance (Hutchinson et al., 2014). However, the opposite effect on dendritic arborization was observed with enhanced Dscam1

knockdown (via Dicer2 overexpression) suggesting that, like da and Sc axons, proper MN dendrite branching requires a balance of Dscam1 protein levels.

In vitro studies suggest that DSCAMs also regulate axonal and dendritic arborization in the mouse brain. RNAi-mediated knockdown of DSCAM in cultured embryonic mouse cortical neurons blocks Netrin-induced axonal branching, indicating that DSCAM functions in collaboration with Netrin to positively regulate axonal branching (Huang et al., 2015). Dendritic arborization, on the other hand, increased in cultured cortical neurons upon knockdown of either DSCAM or DSCAML1, suggesting that DSCAMs act as negative regulators of dendritic arborization (Cui et al., 2013; Zhang et al., 2015). This theory is supported by studies of cultured hippocampal neurons, in which DSCAM over-expression decreased dendritic arbor complexity (Alves-Sampaio et al., 2010). In vivo analysis of cortical pyramidal neurons in postnatal *Dscam* mutant mice also identified an increase in apical branch number, although there was a corresponding decrease in mean apical branch length and a decrease in total basal dendrite length (Maynard and Stein, 2012). These phenotypes were also transient, and dendritic branching recovered to normal numbers and length during postnatal development. Isolated cortical neurons in culture also showed significant decreases in secondary (although not primary and tertiary) dendrite branch number and length. More detailed quantification of the DSCAM knockdown phenotype in culture could resolve these differences. It is also possible that DSCAM knockdown has off-target or transient effects that are not recapitulated in null mutant lines. While it is clear that additional studies are required, these observations argue that vertebrate DSCAMs also regulate axonal and dendritic branching.

1.5 DSCAMS REGULATE AXON GROWTH AND GUIDANCE

To form precise neuronal circuits, axons must traverse large distances through the complex environment of the developing brain. While making this journey, growing axons use a variety of

receptors to detect diffusible and substrate-bound molecular cues in the local environment. These receptor-ligand interactions can mediate either attractive or repulsive responses, both of which are critical for instructing axons to change directions, continue growing, or halt once they reach their appropriate targets. Decades of research have uncovered many IgSF family members that regulate axon growth and pathfinding. Initial studies characterizing the subcellular localization in cultured mouse neurons revealed that the DSCAM protein is distributed throughout the axon, raising the possibility that DSCAMs could also regulate axon guidance (Agarwala et al., 2001b).

Mouse Dscams stimulate axon growth

Stimulation of continued axon growth is a prerequisite step in guiding axons to their appropriate targets. Cultured DRG neurons (Amano et al., 2009) and RGC explants (Bruce et al., 2017), both of which normally express DSCAM, showed longer and more abundant axon outgrowth when cultured on DSCAM-containing substrates. This effect was abolished when *Dscam* mutant neurons were cultured in the same conditions, indicating that DSCAM stimulates axon growth through homophilic binding. In *Dscam* mutant mice, RGC axons maintain a normal trajectory as they grow through the optic chiasm to the dorsal thalamus (Bruce et al., 2017); however, after crossing the optic chiasm, many axons stalled and fewer reached the dorsal thalamus. Moreover, knocking down DSCAM or DSCAML1 in the mouse cortex using RNAi also impaired cortical axon growth into the corpus callosum (Zhang et al., 2015). Thus, in vitro and in vivo evidence suggests that DSCAM acts to promote axon growth, likely through homophilic binding with DSCAM in the surrounding environment, and that this function is conserved in its ortholog DSCAML1.

Drosophila Dscam1 regulates axon guidance through self-avoidance dependent and independent mechanisms

Once positive growth is established, axons still face a daunting task of navigating a complex extracellular environment to reach their appropriate synaptic targets. As previously described, early investigations of Dscam1 function in the Drosophila mushroom body axons identified a mutant phenotype in axon guidance: instead of bifurcating to innervate distinct separate glomeruli, mutant axons fasciculated and projected in the same direction (Wang et al., 2002). Additional studies identified a defect in self-avoidance as the underlying cause for this defective axon targeting (Zhan et al., 2004; Hattori et al., 2007), demonstrating that self-avoidance can play a critical role in axon guidance. However, studies in other regions of the Drosophila brain demonstrate that Dscam1 regulates axon guidance through mechanisms that are presumably independent of self-avoidance. For example, Dscam1 regulates olfactory receptor neuron (ORN) targeting to appropriate glomeruli in the drosophila antennal lobe (Hummel et al., 2003). Subtypes of ORNs terminate their axons in distinct glomeruli within the antennal lobe. Knocking out Dscam1 caused a subset of ORN axons to misproject their axons to inappropriate glomeruli, as well as ectopic regions outside of the antennal lobe (Hummel et al., 2003). Many mutant ORNs also failed to send projections across the midline to innervate the contralateral antennal lobe, demonstrating that Dscam1 regulates ORN axon guidance to target glomeruli and, potentially, midline crossing.

Subsequent studies in Drosophila support and expand upon the role for Dscam1 in commissural axon guidance. Netrin is an evolutionarily-conserved attractive signal in axon guidance. In both vertebrates and invertebrates, Netrin signaling through its receptor, deleted in colorectal cancer (DCC), plays a critical role in commissural axon guidance (Tessier-Lavigne and Goodman, 1996). In Drosophila, knockout of either *dcc/frazzled* or *netrins* impairs (but does not completely abolish) the formation of midline commissures in the ventral nerve cord (Andrews et al., 2008). In vitro experiments showed that Drosophila Dscam1 also binds to Netrin. Although knockout of *dscam1* alone resulted in only subtle defects in axon commissures, *dscam1/dcc* double mutants

had dramatic defects that were more severe than *dcc* single mutants, suggesting that Dscam1 and DCC interact to regulate commissural axon guidance. Over-expression of Dscam1 in neurons that do not ordinarily cross the midline was also sufficient to drive ectopic midline crossings. Interestingly, this phenotype was not rescued in *netrin* mutants (Andrews et al., 2008). These results suggest that Dscam1 and DCC act in parallel pathways to regulate commissural axon guidance, and that Dscam1 likely regulates this process through its interaction with Netrins, in addition to other as yet unidentified signaling molecules.

Slit is another ligand that signals through Dscam1 to regulate axon guidance at the midline (Dascenco et al., 2015; Alavi et al., 2016). In Sc mechanosensory neurons, *slit* mutations cause a selective loss of axon collaterals that project across the midline in the ventral nerve cord. Similar commissural branch defects were observed in Drosophila mutant lines with either 1) reduced expression of the receptor tyrosine phosphatase, RPTP69D, or 2) *dscam1* reduced isoform diversity (Dascenco et al., 2015). Phenotypic analysis using various combinations of mutant alleles for *dscam1*, *slit*, and *rptp69d*, demonstrated that these genes interact genetically, likely in the same pathway, to stimulate the formation of commissural axon collaterals. Biochemical experiments uncovered the molecular basis of these interactions: Slit, produced at the ventral midline, binds to the extracellular domain of Dscam1, enhancing its direct binding to RPTP69D; RPTP69D then dephosphorylates the *Dscam1* intracellular domain, which stimulates the formation and growth of axon collaterals to the midline. Interestingly, no defects in Sc axon guidance were observed in mutants for the canonical Slit receptor, Robo. Coupled with biochemical studies, which showed that Slit binds directly to Dscam1, these studies provide strong evidence that Dscam1 is a novel receptor for Slit-mediated axon guidance, which is independent of Robo signaling (Dascenco et al., 2015). Conversely, studies of longitudinal axon growth along the ventral nerve cord demonstrate that Dscam1 binding to Slit can also stimulate its association with Robo1 to promote growth across segment boundaries (Alavi et al., 2016).

Taken together, these studies demonstrate that Dscam1 functions as a Slit receptor through both Robo-dependent and -independent mechanisms, depending on the cellular context.

Vertebrate DSCAMs regulate commissural axon guidance in the spinal cord

There is conflicting evidence on the function of DSCAM in vertebrate commissural axon guidance. Mouse DSCAM localizes to spinal cord commissural axons, and biochemical studies demonstrate that DSCAM can bind both Netrin and DCC, suggesting that these signaling molecules may also collaborate in axon guidance across the midline (Ly et al., 2008; Liu et al., 2009). This hypothesis was corroborated through in vivo and spinal cord explant experiments, which demonstrated that DSCAM knockdown through RNAi impaired commissural axon outgrowth and ventral midline crossing (Ly et al., 2008; Liu et al., 2009). These initial studies, however, conflict with in vivo analyses of a *Dscam* null mutant mouse line, which had no defects in commissural axon pathfinding (Palmesino et al., 2012). A later study, using a separate *Dscam* mutation on a different genetic background, also found that commissural axons crossed the midline normally, but did so in greater numbers, possibly due to decreased programmed cell death—similar to the mouse retina—although additional studies are required to verify this possibility (Thiry et al., 2016). A possible explanation for these conflicting results is that genomic knockout of *Dscam* activates compensatory mechanisms (e.g. upregulation of an alternative guidance receptor), which does not occur on the shorter timescale of RNAi-mediated knockdown. Indeed, knockdown of DSCAM or DCC in rat spinal cord explants revealed that Dscam and DCC can mediate Netrin-induced axon guidance independently of each other (Ly et al., 2008), suggesting that DSCAM may function redundantly and secondarily to DCC. Nonetheless, these studies demonstrate that mouse DSCAM can bind heterophilically with Netrin to attract growing axons towards a target.

Vertebrate DSCAMs function as chemorepulsive receptors

In vitro studies suggest that DSCAM can also regulate axonal chemorepulsive pathways. Biochemical studies demonstrated that DSCAM interacts physically with UNC5, another Netrin receptor that mediates growth cone collapse and axon repulsion. Knockdown of UNC5 or DSCAM individually in cultured cerebellar granule neurons abolished Netrin-mediated growth cone collapse, suggesting that both proteins are required for Netrin-induced repulsion. Partial knockdown of both proteins simultaneously also abolished the repulsive response, indicating that DSCAM and UNC5 may interact in the same pathway to transduce Netrin-mediated repulsion (Purohit et al., 2012). DSCAM also binds the secreted ligand, Draxin (Ahmed et al., 2011), a chemorepulsive signal that has been implicated in spinal cord and forebrain commissural axon guidance (Islam et al., 2009). Although the biological relevance of DSCAM's associations with both UNC5 and Draxin has yet to be demonstrated in vivo, these studies raise the interesting possibility that DSCAM may also regulate axonal pathfinding through chemorepulsion.

In summary, investigations into the function of DSCAMs in axon guidance demonstrate that these proteins are capable of engaging in a variety heterophilic interactions. The expanded repertoire of DSCAM binding partners includes other IgSF proteins, such as DCC, Robo, and UNC5, in addition to non-IgSF ligands, including Netrin, Slit, and Draxin. Thus, DSCAM is a highly versatile signaling molecule, capable of guiding growing axons through both attractive and repulsive signaling pathways. Intriguingly, Dscam1 homophilic binding in Drosophila appears to modulate its heterophilic interactions and signaling. For instance, reduced Dscam1 isoform diversity, which presumably increases the probability of homophilic binding, impairs the projection of axon collaterals towards the midline, suggesting that homophilic binding inhibits the interaction between Dscam1 and Slit, RPTP69D, or both proteins (Dascenco et al., 2015). Future experiments could uncover how Dscam1 homophilic and heterophilic binding interact to

regulate different aspects of neuronal development, and whether this cross-talk also modulates DSCAM function in vertebrates.

1.6 GOALS OF THE PRESENT STUDY

In conclusion, DSCAMs are implicated in many of the key steps in neuronal circuit formation, including axon growth and guidance, axonal and dendritic branching, neurite self- and neighbor-avoidance, synaptic targeting, and synapse formation. Several of these functions, such as programmed cell death, dendritic branching, and spine formation, correlate with neuroanatomical defects in Down Syndrome, suggesting that DSCAM could play a key role in disease pathogenesis. Initial studies in mice determined that DSCAM is expressed broadly throughout the nervous system during development and into adulthood. However, to date, most in vivo studies of vertebrate DSCAM function have focused on the retina, with a few other studies in the spinal cord and cerebral cortex. Analysis of DSCAM function across other regions of the brain could identify new roles for these proteins or shed light on the conservation of their functions across different neuronal circuits. A more detailed understanding of DSCAM function could facilitate our understanding of Down Syndrome pathophysiology and identify potential therapeutic targets.

Zebrafish are a promising model for investigating the function of DSCAMs. The external fertilization and optical transparency of the zebrafish embryo makes it easy to observe the development of the entire brain in living animals. Moreover, recent advances in genome editing, such as TALENS and CRISPR/Cas9 gene editing systems, make it easy and efficient to knockout and assess the function of almost any gene of interest in zebrafish. In the present study, I leveraged the genetic tractability of the zebrafish system to investigate the expression and function of the DSCAM family member, *dscamb,* across the developing nervous system. I used TALEN and CRISPR/Cas9 gene targeting systems to generate the first *dscamb* null

mutant lines as well as targeted enhancer trap insertions. Using these enhancer trap reporters, and a novel *dscamb* BAC reporter line, I found that Dcamb is expressed widely throughout the nervous system, similar to other DSCAM family members. I used *dscamb* null mutant lines to assess gene function in the retina, as well as other regions where DSCAM function has not been investigated in vertebrates. By coupling cellular investigations with sensory and behavioral analyses, I identified a novel role for *dscamb* in feeding that has not been previously reported in other studies of DSCAM family members.

1.7 REFERENCES

Agarwala KL, Ganesh S, Amano K, Suzuki T, Yamakawa K (2001a) DSCAM, a Highly Conserved Gene in Mammals, Expressed in Differentiating Mouse Brain. Biochem Biophys Res Commun 281:697–705.

Agarwala KL, Ganesh S, Suzuki T, Akagi T, Kaneko K, Amano K, Tsutsumi Y, Yamaguchi K, Hashikawa T, Yamakawa K (2001b) Dscam is associated with axonal and dendritic features of neuronal cells. J Neurosci Res 66:337–346.

Agarwala KL, Ganesh S, Tsutsumi Y, Suzuki T, Amano K, Yamakawa K (2001c) Cloning and functional characterization of DSCAML1, a novel DSCAM-like cell adhesion molecule that mediates homophilic intercellular adhesion. Biochem Biophys Res Commun 285:760–772.

Agarwala KL, Nakamura S, Tsutsumi Y, Yamakawa K (2000) Down syndrome cell adhesion molecule DSCAM mediates homophilic intercellular adhesion. Brain Res Mol Brain Res 79:118–126.

Ahmed G, Shinmyo Y, Ohta K, Islam SM, Hossain M, Naser IB, Riyadh MA, Su Y, Zhang S, Tessier-Lavigne M, Tanaka H (2011) Draxin inhibits axonal outgrowth through the netrin receptor DCC. J Neurosci 31:14018–14023.

Alavi M, Song M, King GLA, Gillis T, Propst R, Lamanuzzi M, Bousum A, Miller A, Allen R, Kidd T (2016) Dscam1 Forms a Complex with Robo1 and the N-Terminal Fragment of Slit to Promote the Growth of Longitudinal Axons. PLoS Biol 14:e1002560.

Alves-Sampaio A, Troca-Marín JA, Montesinos ML (2010) NMDA-mediated regulation of DSCAM dendritic local translation is lost in a mouse model of Down's syndrome. J Neurosci 30:13537–13548.

Amano K, Fujii M, Arata S, Tojima T, Ogawa M, Morita N, Shimohata A, Furuichi T, Itohara S, Kamiguchi H, Korenberg JR, Arata A, Yamakawa K (2009) DSCAM deficiency causes loss of pre-inspiratory neuron synchroneity and perinatal death. J Neurosci 29:2984–2996.

Andrews GL, Tanglao S, Farmer WT, Morin S, Brotman S, Berberoglu MA, Price H, Fernandez GC, Mastick GS, Charron F, Kidd T (2008) Dscam guides embryonic axons by Netrin-dependent and -independent functions. Development 135:3839–3848.

Barlow GM, Lyons GE, Richardson JA, Sarnat HB, Korenberg JR (2002a) DSCAM: an endogenous promoter drives expression in the developing CNS and neural crest. Biochem Biophys Res Commun 299:1–6.

Barlow GM, Micales B, Chen X-N, Lyons GE, Korenberg JR (2002b) Mammalian DSCAMs: roles in the development of the spinal cord, cortex, and cerebellum? Biochem Biophys Res Commun 293:881–891.

Barlow GM, Micales B, Lyons GE, Korenberg JR (2001) Down syndrome cell adhesion molecule is conserved in mouse and highly expressed in the adult mouse brain. Cytogenet Cell Genet 94:155–162.

Bruce FM, Brown S, Smith JN, Fuerst PG, Erskine L (2017) DSCAM promotes axon fasciculation and growth in the developing optic pathway. Proc Natl Acad Sci U S A 114:1702–1707.

Chen BE, Kondo M, Garnier A, Watson FL, Püettmann-Holgado R, Lamar DR, Schmucker D (2006) The molecular diversity of Dscam is functionally required for neuronal wiring specificity in Drosophila. Cell 125:607–620.

Clandinin TR, Zipursky SL (2002) Making Connections in the Fly Visual System. Neuron 35:827–841.

Cui S, Lao L, Duan J, Jin G, Hou X (2013) Tyrosine phosphorylation is essential for DSCAML1 to promote dendrite arborization of mouse cortical neurons. Neurosci Lett 555:193–197.

Cvetkovska V, Hibbert AD, Emran F, Chen BE (2013) Overexpression of Down syndrome cell adhesion molecule impairs precise synaptic targeting. Nat Neurosci 16:677–682.

Dascenco D, Erfurth M-L, Izadifar A, Song M, Sachse S, Bortnick R, Urwyler O, Petrovic M, Ayaz D, He H, Kise Y, Thomas F, Kidd T, Schmucker D (2015) Slit and Receptor Tyrosine Phosphatase 69D Confer Spatial Specificity to Axon Branching via Dscam1. Cell 162:1140–1154.

de Andrade GB, Kunzelman L, Merrill MM, Fuerst PG (2014a) Developmentally dynamic colocalization patterns of DSCAM with adhesion and synaptic proteins in the mouse retina. Mol Vis 20:1422–1433.

de Andrade GB, Long SS, Fleming H, Li W, Fuerst PG (2014b) DSCAM localization and function at the mouse cone synapse. J Comp Neurol 522:2609–2633.

Delabar JM, Theophile D, Rahmani Z, Chettouh Z, Blouin JL, Prieur M, Noel B, Sinet PM (1993) Molecular mapping of twenty-four features of Down syndrome on chromosome 21. Eur J Hum Genet 1:114–124.

Fuerst PG, Bruce F, Rounds RP, Erskine L, Burgess RW (2012) Cell autonomy of DSCAM function in retinal development. Dev Biol 361:326–337.

Fuerst PG, Bruce F, Tian M, Wei W, Elstrott J, Feller MB, Erskine L, Singer JH, Burgess RW (2009) DSCAM and DSCAML1 function in self-avoidance in multiple cell types in the developing mouse retina. Neuron 64:484–497.

Fuerst PG, Harris BS, Johnson KR, Burgess RW (2010) A novel null allele of mouse DSCAM survives to adulthood on an inbred C3H background with reduced phenotypic variability. Genesis 48:578–584.

Fuerst PG, Koizumi A, Masland RH, Burgess RW (2008) Neurite arborization and mosaic spacing in the mouse retina require DSCAM. Nature 451:470–474.

Grueber WB, Jan LY, Jan YN (2002) Tiling of the Drosophila epidermis by multidendritic sensory neurons. Development 129:2867–2878.

Grueber WB, Sagasti A (2010) Self-avoidance and tiling: Mechanisms of dendrite and axon spacing. Cold Spring Harb Perspect Biol 2:a001750.

Hattori D, Chen Y, Matthews BJ, Salwinski L, Sabatti C, Grueber WB, Zipursky SL (2009) Robust discrimination between self and non-self neurites requires thousands of Dscam1 isoforms. Nature 461:644–648.

Hattori D, Demir E, Kim HW, Viragh E, Zipursky SL, Dickson BJ (2007) Dscam diversity is essential for neuronal wiring and self-recognition. Nature 449:223–227.

Hattori D, Millard SS, Wojtowicz WM, Zipursky SL (2008) Dscam-mediated cell recognition regulates neural circuit formation. Annu Rev Cell Dev Biol 24:597–620.

He H, Kise Y, Izadifar A, Urwyler O, Ayaz D, Parthasarthy A, Yan B, Erfurth M-L, Dascenco D, Schmucker D (2014) Cell-intrinsic requirement of Dscam1 isoform diversity for axon collateral formation. Science 344:1182–1186.

Huang H, Shao Q, Qu C, Yang T, Dwyer T, Liu G (2015) Coordinated interaction of Down syndrome cell adhesion molecule and deleted in colorectal cancer with dynamic TUBB3 mediates Netrin-1-induced axon branching. Neuroscience 293:109–122.

Hughes ME, Bortnick R, Tsubouchi A, Bäumer P, Kondo M, Uemura T, Schmucker D (2007) Homophilic Dscam interactions control complex dendrite morphogenesis. Neuron 54:417–427.

Hummel T, Vasconcelos ML, Clemens JC, Fishilevich Y, Vosshall LB, Zipursky SL (2003) Axonal targeting of olfactory receptor neurons in Drosophila is controlled by Dscam. Neuron 37:221–231.

Hutchinson KM, Vonhoff F, Duch C (2014) Dscam1 is required for normal dendrite growth and branching but not for dendritic spacing in Drosophila motoneurons. J Neurosci 34:1924–1931.

Islam SM, Shinmyo Y, Okafuji T, Su Y, Naser IB, Ahmed G, Zhang S, Chen S, Ohta K, Kiyonari H, Abe T, Tanaka S, Nishinakamura R, Terashima T, Kitamura T, Tanaka H (2009) Draxin, a repulsive guidance protein for spinal cord and forebrain commissures. Science 323:388–393.

Keeley PW, Sliff BJ, Lee SCS, Fuerst PG, Burgess RW, Eglen SJ, Reese BE (2012) Neuronal clustering and fasciculation phenotype in Dscam- and Bax-deficient mouse retinas. J Comp Neurol 520:1349–1364.

Kim JH, Wang X, Coolon R, Ye B (2013) Dscam expression levels determine presynaptic arbor sizes in Drosophila sensory neurons. Neuron 78:827–838.

Korenberg JR, Bradley C, Disteche CM (1992) Down syndrome: molecular mapping of the congenital heart disease and duodenal stenosis. Am J Hum Genet 50:294–302.

Korenberg JR, Chen XN, Schipper R, Sun Z, Gonsky R, Gerwehr S, Carpenter N, Daumer C, Dignan P, Disteche C (1994) Down syndrome phenotypes: the consequences of chromosomal imbalance. Proc Natl Acad Sci U S A 91:4997–5001.

Kramer AP, Stent GS (1985) Developmental arborization of sensory neurons in the leech Haementeria ghilianii. II. Experimentally induced variations in the branching pattern. J Neurosci 5:768–775.

Lah GJ-E, Li JSS, Millard SS (2014) Cell-specific alternative splicing of Drosophila Dscam2 is crucial for proper neuronal wiring. Neuron 83:1376–1388.

Langley JN (1895) Note on Regeneration of Prae-Ganglionic Fibres of the Sympathetic. J Physiol 18:280–284.

Lawrence Zipursky S, Sanes JR (2010) Chemoaffinity Revisited: Dscams, Protocadherins, and Neural Circuit Assembly. Cell 143:343–353.

Lemieux M, Laflamme OD, Thiry L, Boulanger-Piette A, Frenette J, Bretzner F (2016) Motor hypertonia and lack of locomotor coordination in mutant mice lacking DSCAM. J Neurophysiol 115:1355–1371.

Li H-L, Huang BS, Vishwasrao H, Sutedja N, Chen W, Jin I, Hawkins RD, Bailey CH, Kandel ER (2009) Dscam mediates remodeling of glutamate receptors in Aplysia during de novo and learning-related synapse formation. Neuron 61:527–540.

Li S, Sukeena JM, Simmons AB, Hansen EJ, Nuhn RE, Samuels IS, Fuerst PG (2015) DSCAM promotes refinement in the mouse retina through cell death and restriction of exploring dendrites. J Neurosci 35:5640–5654.

Liu G, Li W, Wang L, Kar A, Guan K-L, Rao Y, Wu JY (2009) DSCAM functions as a netrin receptor in commissural axon pathfinding. Proc Natl Acad Sci U S A 106:2951–2956.

Ly A, Nikolaev A, Suresh G, Zheng Y, Tessier-Lavigne M, Stein E (2008) DSCAM is a netrin receptor that collaborates with DCC in mediating turning responses to netrin-1. Cell 133:1241–1254.

Masland RH (2012) The neuronal organization of the retina. Neuron 76:266–280.

Matthews BJ, Kim ME, Flanagan JJ, Hattori D, Clemens JC, Zipursky SL, Grueber WB (2007) Dendrite self-avoidance is controlled by Dscam. Cell 129:593–604.

Maynard KR, Stein E (2012) DSCAM contributes to dendrite arborization and spine formation in the developing cerebral cortex. J Neurosci 32:16637–16650.

Millard SS, Flanagan JJ, Pappu KS, Wu W, Zipursky SL (2007) Dscam2 mediates axonal tiling in the Drosophila visual system. Nature 447:720–724.

Millard SS, Zipursky SL (2008) Dscam-mediated repulsion controls tiling and self-avoidance. Curr Opin Neurobiol 18:84–89.

Miura SK, Martins A, Zhang KX, Graveley BR, Zipursky SL (2013) Probabilistic splicing of Dscam1 establishes identity at the level of single neurons. Cell 155:1166–1177.

Neves G, Zucker J, Daly M, Chess A (2004) Stochastic yet biased expression of multiple Dscam splice variants by individual cells. Nat Genet 36:240–246.

Nicholls JG, Baylor DA (1968) Specific modalities and receptive fields of sensory neurons in CNS of the leech. J Neurophysiol 31:740–756.

Palmesino E, Haddick PCG, Tessier-Lavigne M, Kania A (2012) Genetic analysis of DSCAM's role as a Netrin-1 receptor in vertebrates. J Neurosci 32:411–416.

Purohit AA, Li W, Qu C, Dwyer T, Shao Q, Guan K-L, Liu G (2012) Down syndrome cell adhesion molecule (DSCAM) associates with uncoordinated-5C (UNC5C) in netrin-1-mediated growth cone collapse. J Biol Chem 287:27126–27138.

Schmucker D (2007) Molecular diversity of Dscam: recognition of molecular identity in neuronal wiring. Nat Rev Neurosci 8:915–920.

Schmucker D, Clemens JC, Shu H, Worby CA, Xiao J, Muda M, Dixon JE, Zipursky SL (2000) Drosophila Dscam is an axon guidance receptor exhibiting extraordinary molecular diversity. Cell 101:671–684.

Shi L, Yu H-H, Yang JS, Lee T (2007) Specific Drosophila Dscam juxtamembrane variants control dendritic elaboration and axonal arborization. J Neurosci 27:6723–6728.

Soba P, Zhu S, Emoto K, Younger S, Yang S-J, Yu H-H, Lee T, Jan LY, Jan Y-N (2007) Drosophila sensory neurons require Dscam for dendritic self-avoidance and proper dendritic field organization. Neuron 54:403–416.

Sperry RW (1963) CHEMOAFFINITY IN THE ORDERLY GROWTH OF NERVE FIBER PATTERNS AND CONNECTIONS. Proc Natl Acad Sci U S A 50:703–710.

Sterne GR, Kim JH, Ye B (2015) Dysregulated Dscam levels act through Abelson tyrosine kinase to enlarge presynaptic arbors. Elife 4 Available at: http://dx.doi.org/10.7554/eLife.05196.

Tadros W, Xu S, Akin O, Yi CH, Shin GJ-E, Millard SS, Zipursky SL (2016) Dscam Proteins Direct Dendritic Targeting through Adhesion. Neuron 89:480–493.

Tessier-Lavigne M, Goodman CS (1996) The molecular biology of axon guidance. Science 274:1123–1133.

Thiry L, Lemieux M, D Laflamme O, Bretzner F (2016) Role of DSCAM in the development of the spinal locomotor and sensorimotor circuits. J Neurophysiol 115:1338–1354.

Vaughn DE, Bjorkman PJ (1996) The (Greek) key to structures of neural adhesion molecules. Neuron 16:261–273.

Wang J, Ma X, Yang JS, Zheng X, Zugates CT, Lee C-HJ, Lee T (2004) Transmembrane/juxtamembrane domain-dependent Dscam distribution and function during mushroom body neuronal morphogenesis. Neuron 43:663–672.

Wang J, Zugates CT, Liang IH, Lee C-HJ, Lee T (2002) Drosophila Dscam is required for divergent segregation of sister branches and suppresses ectopic bifurcation of axons. Neuron 33:559–571.

Wojtowicz WM, Flanagan JJ, Millard SS, Zipursky SL, Clemens JC (2004) Alternative splicing of Drosophila Dscam generates axon guidance receptors that exhibit isoform-specific homophilic binding. Cell 118:619–633.

Wojtowicz WM, Wu W, Andre I, Qian B, Baker D, Zipursky SL (2007) A vast repertoire of Dscam binding specificities arises from modular interactions of variable Ig domains. Cell 130:1134–1145.

Xu Y, Ye H, Shen Y, Xu Q, Zhu L, Liu J, Wu JY (2011) Dscam mutation leads to hydrocephalus and decreased motor function. Protein Cell 2:647–655.

Yamagata M, Sanes JR (2008) Dscam and Sidekick proteins direct lamina-specific synaptic connections in vertebrate retina. Nature 451:465–469.

Yamagata M, Weiner JA, Sanes JR (2002) Sidekicks: synaptic adhesion molecules that promote lamina-specific connectivity in the retina. Cell 110:649–660.

Yamakawa K, Huot YK, Haendelt MA, Hubert R, Chen XN, Lyons GE, Korenberg JR (1998) DSCAM: a novel member of the immunoglobulin superfamily maps in a Down syndrome region and is involved in the development of the nervous system. Hum Mol Genet 7:227–237.

Yang Z, Huh SU, Drennan JM, Kathuria H, Martinez JS, Tsuda H, Hall MC, Clemens JC (2012) Drosophila Vap-33 is required for axonal localization of Dscam isoforms. J Neurosci 32:17241–17250.

Zhang L, Huang Y, Chen J-Y, Ding Y-Q, Song N-N (2015) DSCAM and DSCAML1 regulate the radial migration and callosal projection in developing cerebral cortex. Brain Res 1594:61–70.

Zhan X-L, Clemens JC, Neves G, Hattori D, Flanagan JJ, Hummel T, Vasconcelos ML, Chess A, Zipursky SL (2004) Analysis of Dscam diversity in regulating axon guidance in Drosophila mushroom bodies. Neuron 43:673–686.

CHAPTER 2

Generation and characterization of Dscamb mutants and transgenic reporters

2.1 INTRODUCTION

The genetic tractability and optical clarity of the zebrafish make it an ideal model for investigating the function of DSCAM family members in the developing nervous system. The zebrafish genome contains three DSCAM genes: *dscama*, *dscamb*, and *dscaml1*. Like in other vertebrates, zebrafish DSCAMs are not extensively alternatively splicing. Despite the absence of molecular diversity, vertebrate DSCAMs are implicated in almost every aspect of neuronal development and circuit formation, including programmed cell death, neuronal migration, self- and neighbor-avoidance, axonal and dendritic branching, axon guidance, and synaptic targeting. Many of these functions are conserved between flies and vertebrates, demonstrating that DSCAMs are important regulators of vertebrate neuronal development, even in the absence of molecular diversity. To date, there has been only one published study investigating the expression and function of a dscam family member in zebrafish development (Yimlamai et al., 2005). Tissue in situ hybridization against *dscama* mRNA found that it is expressed broadly throughout the brain and spinal cord at larval stages of development. Morpholino-mediated knockdown of Dscama expression was embryonic lethal due to early defects in cell migration during gastrulation (Yimlamai et al., 2005), precluding an analysis of its function in neuronal development, which occurs at later developmental stages. For this reason, we decided to focus on the closely-related paralog, *dscamb*. We generated multiple novel genetic tools, including genetic null mutant and transgenic reporter lines, to characterize the expression and function of *dscamb* in the larval zebrafish central and peripheral nervous systems.

2.2 RESULTS

dscamb null mutations impair survival to adulthood, but produce no obvious anatomical defects

To investigate the function of Dscamb in zebrafish neuronal development, we used TALENs to generate null mutant lines. We selected two target sites within the coding region of *dscamb*: 1)

the translational start codon, and 2) a region in the middle of exon 2 (Figure 2.1A). We engineered a pair of TALENs flanking each target site with Fok1 obligate homodimerization endonuclease domains (Cermak et al., 2011) and injected mRNA encoding each pair of TALENs into embryos at the single cell stage. For each target site, we used Restriction Fragment Length Polymorphism (RFLP) and sequencing to identify multiple founders with germline frameshift mutations that generate premature stop codons (Figure 2.1B). We established four mutant *dscamb* lines with unique mutant alleles—two mutations for each target site: *dscamb*^{t1a}, *dscamb*^{t1b}, *dscamb*^{t2a}, and *dscamb*^{t2b}.

Across both target sites and mutant alleles, we detected no obvious developmental or anatomical defects between wild-type, heterozygous, and homozygous mutant siblings, when observed up to 7 days post-fertilization (dpf). However, homozygous mutants had almost complete mortality by the time fish reached sexual maturity (~3 months old). Moreover, heterozygous siblings were significantly underrepresented relative to their wild-type siblings at the same ages, suggesting that the *dscamb* gene confers a developmental deficit that impairs survival to older stages.

A BAC transgenic reporter identifies Dscamb expression across numerous neuronal and sensory systems

Closer inspection of the specific tissues expressing Dscamb could pinpoint developmental defects underlying mutant mortality. To date, however, no studies have investigated the expression pattern of *dscamb*. To identify cell types expressing Dscamb, we used BAC transgenics to generate a Gal4-based reporter line (Bussmann and Schulte-Merker, 2011; Suster et al., 2011). We identified a 41 kb BAC containing the first exon of *dscamb,* in addition to 22.3 kb upstream and 18.5kb downstream non-coding sequence (Figure 2.2A). Using in-vitro

homologous recombination, we inserted a Gal4-containing transgene at the translational start codon of the first exon of *dscamb,* located within the BAC. The BAC construct was integrated randomly into the genome [BAC(dscamb:gal4)] and crossed to a UAS:GFP line to observe expression.

Brain expression

We investigated the expression of BAC(dscamb:gal4) at late embryonic and larval stages (2, 3, and 7 dpf). With the exception of a few facial muscle fibers, GFP was expressed primarily in neurons scattered throughout the central and peripheral nervous systems (Figure 2.2). At all three time-points, a dense cluster of GFP-expressing neurons neurons in the olfactory bulb of the forebrain expressed GFP (Figure 2.1E). In the midbrain, a cluster of cells—likely, neurons of the optic tectum—was consistently labeled at 2 and 3 dpf, but largely absent by 7 dpf (Figure 2.2E). In the hindbrain, GFP expression was most prominent in a group of cells resembling the nucleus of the vagus nerve (cranial nerve X) (Figure 2.2F).

Spinal cord expression

GFP+ cells were scattered sparsely throughout the spinal cord (Figure 2.2G). Many of these cells appeared to be interneurons. GFP-labeled motor axons could also be seen innervating muscle fibers in the body wall, demonstrating that our BAC reporter also labels motor neurons. Occasional Rohon-Beard (RB) somatosensory neurons were distinguished by their large, dorsally-located cells bodies and peripheral axons that arborize within the skin.

Dscamb is not required for Rohon-Beard peripheral axon self-avoidance

Drosophila Dscam1 is required for self-avoidance in peripheral touch-sensing neurons (Hughes et al., 2007; Matthews et al., 2007; Soba et al., 2007). We hypothesized that Dscamb may play

a similar role in zebrafish somatosensory neurons. To test this hypothesis, we injected *dscamb* mutant embryos with our BAC(dscamb:Gal4) and a UAS:GFP plasmid to obtain sparse labeling. This allowed us to distinguish individual RB neurons and analyze their peripheral arbors in the skin for self-avoidance defects (Figure 2.3). After quantifying the number of self-crossover events between RB peripheral axon branches, we did not observe a significant difference in homozygous mutant embryos (Figure 2.3C). Total peripheral axon length and number of branches were also normal in mutant RB neurons (Figure 2.3D,E), demonstrating that Dscamb is not required for self-avoidance or the normal morphological development of RB somatosensory neurons.

Cranial ganglia expression

At 3dpf, BAC(dscamb:gal4) was expressed abundantly in the vagal sensory ganglia (gX) (Figure 2.2D), and also in the glossopharyngeal ganglia (gIX). A few GFP+ neurons were also seen in the posterior lateral line ganglion (pLLg). GFP-filled axons from these neurons coursed down the trunk where they innervated mechanosensory neuromasts along the lateral side of the body (Figure 2.2G). We observed a few labeled cells just posterior to the eye, likely representing neurons of either the anterior lateral line or trigeminal ganglia (data not shown).

Retinal expression

At 2 and 3 dpf, extensive, bright reporter expression was observed in the photoreceptor (PR) layer of the retina (Figure 2.2C). PR expression persisted as late as 7 dpf. A few BAC(dscamb:gal4)-expressing cells were also seen scattered throughout other retinal layers at 2-3 dpf (data not shown). The zebrafish retina develops in an inside-out fashion, with the first RGCs differentiating around 1 dpf, followed closely by cells of the inner nuclear layer (bipolar, amacrine, and horizontal cells), and lastly, PRs, in the outermost cell layer (Avanesov and

Malicki, 2010). The BAC(dscamb:gal4) expression patterns suggests that Dscamb is expressed early and abundantly in PR development, but more sparsely in other retinal cell types.

Olfactory expression

BAC(dscamb:gal4) was expressed in the olfactory system. At 1 dpf, sparse GFP expression was detected in the developing olfactory placode. By 2 dpf, a subset of differentiated olfactory sensory neurons (ORNs) were labeled in the olfactory sensory epithelium. Sensory axons from labeled ORNs were observed projecting to the olfactory glomeruli where they interlaced with dendrites from numerous GFP-expressing neurons in the olfactory bulb (data not shown). ORN expression was not detectable at 3 dpf, but was still present in the olfactory bulb (Figure 2.2E). Expression in the olfactory bulb was also detected at 7 dpf. These observations are consistent with the expression pattern of DSCAM expression in mice (Agarwala et al., 2001b), and suggest that Dscamb could be involved in the development of the olfactory system.

Statoacoustic expression

In zebrafish, the otic placode-derived otic vesicle gives rise to the inner ear sensory organs that detect auditory (hearing) and vestibular (balance) stimuli. Sensory transduction is mediated by five patches of mechanosensory hair cells (ovHCs): two macula (utricular and saccular) and three cristae (anterior, posterior, and lateral) (Whitfield et al., 2002). Numerous GFP-expressing ovHCs were visible in all five of these ovHC clusters at both 2 and 3 dpf (Figure 2.2D), suggesting that Dscamb could play a role in ovHC development.

CRISPR/Cas9-directed enhancer trap integration upstream of *dscamb* show similar patterns of expression regardless of orientation or loss-of-function mutations.

Since the BAC reporter could be missing key regulatory sequences, and integration into the genome can cause positional effects that alter reporter expression, we made and enhancer trap at the endogenous *dscamb* locus. To create a *dscamb* enhancer trap reporter, we used CRISPR/Cas9-guided mutagenesis to target the insertion of a reporter transgene upstream of *dscamb* (Figure 2.4A). This approach has been used successfully for targeted enhancer trap insertion (Kimura et al., 2014). Moreover, by integrating the enhancer trap upstream of the mutant allele, we could more readily identify heterozygous and mutant embryos, making it easier to identify loss-of-function phenotypes in Dscamb-expressing cells. We selected two gRNA target sites upstream of the *dscamb* locus: 1) gRNA-Et1, located 69bp upstream of the transcriptional initiation site, and 2) gRNA-Et2, located 4bp upstream of the transcriptional initiation site. Individual *dscamb*-targeting gRNAs were injected into single-cell embryos along with a donor transgene plasmid—containing a minimal heatshock promoter, driving expression of Gal4FF (Asakawa and Kawakami, 2009)—were injected along with Cas9-encoding mRNA, and a second gRNA to cut and linearize the donor plasmid in vivo (Mbait gRNA) (Figure 2.4A). Using this approach, we generated three lines with stable enhancer trap integrations upstream of the wiltype allele, and one line with an integration upstream of the *dscamb*^{t2b} mutant allele (Figure 2.4B-E). Of the wild-type enhancer trap lines, two were integrated at the gRNA-Et1 target site: Et1(dscamb^{wt}:gal4)^{i}, Et1(dscamb^{wt}:gal4)^{o}. The remaining wild-type enhancer trap line was integrated at the sgRNA-Et2 target site: Et2(dscamb^{wt}:gal4). Integration upstream of the mutant allele occurred at the gRNA-Et1 target site: Et1(dscamb^{t2b}:gal4).

Using this CRISPR/Cas9-targeted enhancer trap method, the enhancer trap plasmid could integrate in either forward or reverse orientations, and multiple copies of the plasmid can integrated tandemly at the target site. Previous studies using this approach, saw only minor changes in enhancer trap expression between forward and reverse integration upstream of the genes investigated (Kimura et al., 2014). To identify the orientation of each enhancer trap

insertion, we used a PCR assay with three primers: 1) a forward genomic primer that bound upstream of the gRNA target sites, 2) a reverse genomic primer that bound downstream of the target sites, and 3) an outward-facing donor-plasmid primer that bound to either the 5' or 3' end of the linearized donor plasmid. The donor-plasmid, in combination with one of the genomic primers, will amplify a product of different sizes, depending on the orientation of the integration. Using this approach, we found that all three of our gRNA-Et1 enhancer trap lines were in the reverse orientation (Figure 2.4B-D). Interestingly, our gRNA-Et2 line showed evidence of both a reverse and forward integration (Figure 2.4E), suggesting that this line contains at least two tandemly integrated donor plasmids: a reverse integration at the most upstream end of the insertion site, and a forward integration at the most proximal end, relative to the *dscamb* transcriptional start site. Notably, the gRNA-Et1 enhancer trap lines may also contain multiple copies of the donor plasmid integrated into the genome that could have been missed using this PCR detection assay.

We crossed each of our enhancer trap lines to a Tg(5xUAS:GFP) line to compare their expression patterns at 5 dpf (Figure 2.4B-E). GFP expression was similar regardless of integration at either the gRNA-Et1 or gRNA-Et2 target sites, suggesting that integration at either target site does not disrupt critical regulatory elements for *dscamb* expression. The overall pattern of *dscamb* expression was similar between the three reverse integration lines [Et1(dscamb^{wt}:gal4)^{i}, Et1(dscamb^{wt}:gal4)^{o}, and Et1(dscamb^{t2b}:gal4)] and the gRNA-Et2 enhancer line, which also contained a forward orientated donor [Et2(dscamb^{wt}:gal4)]. Therefore, the orientation of the donor plasmid integration appears to have minimal effects on the enhancer trap integration. Integrations upstream of the wild-type and mutant alleles also showed similar patterns of GFP expression, indicating that *dscamb* loss-of-function mutations do not dramatically alter enhancer trap expression. UAS transgene positional effects were also minimal, as there was little change in the overall expression pattern visualized with other

transgenic UAS lines (UAS:KikGR, UAS:nfsb-mCherry). Since there were no obvious differences in expression between lines, we focused on the mutant enhancer trap line [Et1(dscamb^{t2b}:gal4)] for remaining experiments in this study. This allowed us to simultaneously characterize the expression pattern of Dscamb while comparing and contrasting development in heterozygous and homozygous mutants.

Enhancer trap lines identify a broad pattern of *dscamb* expression throughout the central and peripheral nervous system

Embryonic brain expression

Compared to BAC(dscamb:gal4), which was concentrated in a few neuronal populations in the brain, our Et1(dscamb^{t2b}:gal4) line exhibited a much broader pattern of expression in the brain and spinal cord (Figure 2.5). To better characterize this expression pattern, we crossed our enhancer trap line [Et1(dscamb^{t2b}:gal4), Tg(5xUAS:GFP)] to a pan-neuronal line: [Tg(nbt:RFP)], and imaged its expression at embryonic (1 dpf) and larval (4-5 dpf) stages.

At 1 dpf, enhancer trap was expressed broadly throughout the nascent embryonic brain (Figure 2.5A). In the peripheral nervous systems, GFP+ cells were seen in all the the early sensory ganglia, including the trigeminal, anterior lateral line, posterior lateral line, and octaval/statoacoustic ganglia (Figure 2.5A). At this time-point, the enhancer trap was also abundantly expressed in the olfactory placode, which gives rise to the olfactory epithelium (data not shown, but ORN expression at 3dpf is presented in Figure 2.7). Although many of the GFP+ cells observed in the CNS and PNS were also RFP+, we also observed many cells that were exclusively RFP+, suggesting that dscamb is not expressed in all neurons. Conversely, many cells were only GFP+, suggesting that the nbt:RFP transgene incompletely labels neurons and/or that Dscamb is also expressed in nbt:RFP-negative glial cells. Comparing the overall

structure and organization of these tissues in heterozygous [Et1(dscamb^{t2b}:gal4)/wt; henceforth referred to simply as “heterozygous”] and homozygous [Et1(dscamb^{t2b}:gal4)/dscamb^{t2b}; henceforth referred to simply as “homozygous”] mutant embryos did not reveal obvious structural defects (Figure 2.5A).

Dscamb is expressed in a subpopulation of somatosensory neurons that partially overlaps with TrpA1b

Like the BAC reporter, our enhancer trap also labeled RB somatosensory neurons in the spinal cord, although it was clearly expressed in a subpopulation. Previous research in our lab and others have characterized subtypes of RB somatosensory neurons based on the expression of different genes (Faucherre et al., 2013; Gau et al., 2013; Palanca et al., 2013). To better characterize the Dscamb-expressing subpopulation of somatosensory neurons we crossed Et1(dscamb^{t2b}:Gal4) to BAC(trpa1b), which has been shown to label an RB subtype that comprises about 40% of the total population (Palanca et al., 2013). We imaged the spinal cord in these embryos at 2dpf and found that Dscamb is expressed in 30% of TrpA1b-expressing RB subtype. Conversely, we detected many Dscamb-expressing RB that were TrpA1b-negative enhancer; however, due the dense labeling in other cell-types in the spinal cord, we could accurately quantify the number of Dscamb+/TrpA1b- RB neurons. Nonetheless, these findings demonstrate that the Dscamb-expresing subpopulation of RB somatosensory neurons partially overlaps with the TrpA1b-expressing subtype.

Olfactory system

Consistent with the BAC reporter, Et1(dscamb^{t2b}:Gal4) was expressed in ORNs and the olfactory bulb (Figure 2.7), raising the possibility that Dscamb could regulate axon guidance or synaptic coupling between these two tissues. In *D. melanogaster*, *dscam1* is required to maintain the

normal arrangement of ORN axons and projection neuron dendrites in the olfactory glomeruli (Hummel et al., 2003; Zhu et al., 2006). Because Et1(dscamb^{t2b}:Gal4) was expressed in both ORNs and the olfactory bulb, it was difficult to differentiate ORN axon endings in the olfactory bulb. To circumvent this issue, and evaluate the morphology of mutant ORN axon terminals, we crossed Et1(dscambt2b:Gal4) to a UAS line expressing a photoconvertible fluorescent protein (KikGR), which switches from green to red fluorescence upon exposure to UV light. Using a UV laser, we selectively photoconverted KikGR in the ORNs, allowing us to distinguish the red-filled ORN axons in the olfactory bulb. We imaged red ORN axon endings in both heterozygous and homozygous mutant larvae. Mutant axons innervated the olfactory bulb and coalesced into glomeruli in a pattern that closely resembled their heterozygous siblings (Figure 2.7).

Larval brain expression

At 4-5 dpf, the enhancer trap was broadly expressed in the forebrain, midbrain, and hindbrain (Figure 2.5B), including many regions that were not observed with the BAC reporter. In addition to the olfactory bulb, Et1(dscamb^{t2b}:gal4) was also observed across other regions of the forebrain. GFP+ cells were also seen in the midbrain optic tectum, but there were also many RFP+/GFP- single positive cells, suggesting that Dscamb is expressed in a subtype of tectal neurons. The tectal neuropil, where retinal RGC axons synapse with tectal neurons, was also filled with GFP+ processes. GFP expression in the hindbrain was much more abundant than the BAC reporter. In particular, the cerebellum, which was not labeled in the BAC reporter, was clearly marked with many enhancer trap-expressing cells. The more caudal regions of the hindbrain were also more extensively labeled than in the BAC reporter. *dscamb* mutation did not cause any obvious defects in the development or organization of these tissues (Figure 2.5B).

Cranial ganglia expression

Consistent with the BAC reporter, we observed enhancer trap expression in larval cranial sensory ganglia at 4-5 dpf (Figure 2.5B). GFP was similarly expressed in the vagal and glossopharyngeal ganglia, but the enhancer trap labeled more cells than the BAC reporter in the posterior lateral line, anterior lateral line, and trigeminal ganglia. However, GFP was clearly expressed only in a subset of these neurons in each of these regions. Homozygous *dscamb* mutants showed no obvious defects in the organization of these ganglia (Figure 2.5B).

Statoacoustic expression

In contrast to the BAC reporter, the enhancer trap was expressed in cells of the statoacoustic ganglion (Figure 2.5A-B). The enhancer trap reporter also corroborated Dscamb expression in all five patches of hair cells in the otic vesicle (Figure 2.5B). GFP+ axons, likely efferents originating from the statoacoustic ganglion, coursed into the ovHC patches of the anterior, lateral, and posterior cristae. No pronounced changes in the sensory ovHC patches or innervating GFP+ axons were detected in *dscamb* homozygous mutants.

Facial muscle fiber expression

Similar to the BAC reporter, the enhancer trap reporter labeled a specific population of facial muscle fibers, located just anterior-ventral to the otic vesicle (Figure 2.5B). In the enhancer trap, this expression pattern also included muscle fibers on the ventral side of the head (Figure 2.8). These muscle fibers are responsible for the movement of the operculum (bony gill cover) and jaw, and serve critical functions in feeding and gill ventilation. Defects in these behaviors could explain the mortality of homozygous mutants. To address this possibility, we investigated the structure and innervation of these the lateral and ventral muscle fibers in *dscamb* mutants at 5 dpf and 4 dpf, respectively. At these stages, there were no obvious differences in the structure or organization of these muscle fibers between heterozygous and homozygous mutant siblings.

Using the nbt:RFP line to distinguish motor axons, we found that both the lateral (data not shown) and ventral muscle fibers (Figure 2.8) are innervated. Although subtle morphological or synaptic defects in motor axon innervation would not have been detected in our analysis.

Spinal cord expression

The enhancer trap reporter, was broadly expressed in the spinal cord (Figure 2.5C). GFP expression appeared to be slightly more abundant in the dorsal half of the spinal cord. Elongated GFP+/RFP- cells were also observed around the outer edge of the spinal cord, particularly on the ventral side. These cells may be oligodendrocyte precursor cells, but additional expression analysis would be required to confirm this identification. Similar to the BAC reporter, GFP+ motor axons were observed exiting the spinal cord to innervate the body wall (Figure 2.5C). Closer inspection of these axons and their terminal endings in the periphery, suggested that Dscamb is expressed in all three of the zebrafish primary motor axons (RoP, MiP, CaP) (data not shown). Comparing heterozygous and homozygous mutant siblings, we did not detect any obvious structural changes in the organization of the spinal cord or peripheral motor axons (Figure 2.5C).

Enteric nervous system expression

Et1(dscambt2b:Gal4) was expressed in neurons of the enteric nervous system (ENS), scattered along the entire length of the gut tube (Figure 2.5C). Analyzing coexpression with nbt:RFP revealed that the enhancer was expressed in some, but not all, ENS neurons (Figure 2.9A). Subset-specific enhancer trap expression was also observed with a Sox10 reporter [Tg(Sox10:Cre), Tg(loxP-BFP-loxP-RFP)], which labels cells of neural crest origin, including ENS neurons (data not shown). In both cases, we observed many GFP+/RFP- ENS cells, suggesting that our Sox10 and nbt reporters both incompletely label the ENS.

We hypothesized that Dscamb could be required for the migration of zebrafish neurons along the length of the gut. To test this hypothesis, we imaged Et1(dscambt2b:Gal4)-expressing neurons in the distal region of the gut in both heterozygous and homozygous *dscamb* mutants at 5dpf. After counting the number of ENS neurons in the distal 250μm length of the gut, we found no difference the median number of ENS cells between heterozygous and homozygous mutant embryos (median = 10 ENS neurons in both cases; n = 10 animals per genotype) (Figure 2.9B). These results indicate that Dscamb is not required for the proper migration of ENS neurons into the distal gut in zebrafish.

2.3 DISCUSSION

Using targeted genome engineering and and transgenesis, we have generated the first reported *dscamb* loss-of-function mutants and identified a highly penetrant phenotype in which homozygous mutants die before reaching adulthood. Using BAC transgenesis and targeted enhancer trap insertion, we generated several novel reporters to characterize Dscamb-expressing cell types. Although Dscamb enhancer trap expression was much broader than the BAC reporter, the enhancer trap was expressed in all the same regions as the BAC reporter (Figures 2.2 and 2.5). This suggests that both reporters are specific, but that the BAC reporter is silenced in some Dscamb-expressing cell types, perhaps due to positional effects from its integration into the genome or the absence of regulatory elements in the BAC sequence.

Using the enhancer trap reporter, we found that Dscamb is expressed broadly in neurons throughout the brain, spinal cord, and peripheral nervous system, although it is clearly not expressed in all neurons, and we cannot rule out possible expression in glia (Figure 2.5). This

expression pattern shares many similarities with expression patterns that have been reporter for other DSCAM family members.

Dscamb expression is similar to but not identical to dscama expression

Dscamb enhancer trap expression shares substantial overlap with its paralog *dscama*, which has been previously characterized using wholemount in situ hybridization (Yimlamai et al., 2005). Similar to *dscamb*, *dscama* is broadly expressed throughout the brain and spinal cord, beginning at 1 dpf (Figure 2.5). In contrast, *dscama* expression in the spinal cord was completely absent by 5 dpf, which we did not observe with the Dscamb enhancer trap (Figure 2.5C), suggesting two genes could serve different functions in spinal cord development. However, it is possible that GFP expression from our Gal4 enhancer trap persists past stages when *dscamb* expression has been turned off. In the larval brain, *dscama* is abundantly expressed in the forebrain, midbrain, and hindbrain and is also enriched in the olfactory sensory epithelium, similar to *dscamb* (Figure 2.5). *Dscama* mRNA was also detected in regions of the eye at 3 dpf, including the pigment epithelium, OPL, INL and IPL. However, a more detailed analysis would be required at later stages—when the retina is fully developed—to better understand the degree of retinal overlap between these two genes. Overlapping expression could suggest that these proteins function redundantly in many cell types, which could explain the absence of any apparent structural defects in *dscamb* homozygous mutants. Dscaml1 may also be functionally redundant and compensate for *dscamb* loss-of-function during development, although, to date, there have been no studies investigating the expression or function of this gene.

Dscamb expression resembles the expression of DSCAMs in other vertebrates

The broad, neuronal pattern of Dscamb resembles the expression pattern reported for DSCAM in mice (Yamakawa et al., 1998; Agarwala et al., 2001a; Barlow et al., 2001, 2002). In particular, many of these regions, such as the olfactory bulb, cerebellum, medulla, and spinal cord were also observed in the *dscamb* enhancer trap (Figure 2.5). In mice, DSCAML1 is observed in many of these same brain regions (Agarwala et al., 2001c; Barlow et al., 2002), but often with distinct, inverse patterns of expression, relative to DSCAM. In the embryonic spinal cord, for example, DSCAML1 is enriched in the dorsal sensory regions, while DSCAM predominates in the ventral and lateral regions that give rise to motor and commissural neurons (Barlow et al., 2002). Dscamb was also enriched in the ventral spinal cord (Figure 2.5C), and therefore, more closely resembles the expression pattern of DSCAM. In vivo studies using either knock-down or genomic nulls mutant lines offered conflicting results on DSCAM's role in Netrin-mediated commissural axon guidance (Ly et al., 2008; Liu et al., 2009; Palmesino et al., 2012). Although we did not detect any apparent differences in spinal cord organization in homozygous *dscamb* mutant embryos (Figure 2.5C), closer analysis may identify defects in commissural axon guidance that could resolve the controversy from the mouse literature. Differences in the expression patterns between DSCAM and DSCAML1 have also been reported in the cerebellum, with DSCAM enriched in Purkinje cells and DSCAML1 in granule cells (Barlow et al., 2002). It would be interesting to see if Dscamb expression in the cerebellum is also enriched in Purkinje cells, similar to mouse DSCAM.

DSCAM is expressed in regions of the PNS that were also labeled with the enhancer trap reporter, including the trigeminal ganglion, olfactory epithelium, and enteric neurons (Yamakawa et al., 1998). However, there are several noticeable differences in the peripheral nervous system between the expression patterns of these genes. For instance, dorsal root ganglion neurons, which express DSCAM in mice, did not express Dscamb in fish. Besides the trigeminal ganglion, DSCAM expression has not been reported in other placode-derived cranial ganglia

that were observed in enhancer trap larvae (Figure 2.5). In addition, Dscamb was not expressed in several non-neuronal tissues where DSCAM has been detected, including the heart and liver (Agarwala et al., 2001a). Conversely, mammalian DSCAM expression has not been reported in facial muscles, which express Dscamb. Despite these differences, the overall expression patterns of DSCAM and Dscamb share a striking amount of overlap, suggesting that they could regulate similar aspects of neuronal development.

Dscamb is expressed in all zebrafish sensory systems

Using our enhancer trap reporter, we found that Dscamb is expressed in components of all the major sensory systems during development, including olfactory, gustatory, visual, statoacoustic, somatosensory, and lateral line neurons (Figure 2.5). For several of these systems, such as the olfactory, statoacoustic, and visual systems, Dscamb appeared to be expressed in both primary sensory neurons and their downstream synaptic partners, suggesting that Dscamb homophilic binding could regulate synaptic coupling between these neurons. We investigated this possibility in the olfactory system, but did not observe any obvious defect in ORN axon projections to glomeruli in the olfactory bulb in mutants (Figure 2.7), although it is possible that mutant axons could have more subtle defects in synapse formation that were not detected by our analysis.

Dscamb is expressed in both retinal PRs and ovHCs, which form specialized presynaptic structures, called synaptic ribbons, raising the intriguing possibility that Dscamb could be required for synaptic ribbon synapse development. In *Dscaml1* mutant mouse retinas, rod PRs have rudimentary synaptic ribbons and an overabundance of synaptic vesicles, suggesting that Dscaml1 is required for rod ribbon synapse maturation (Fuerst et al., 2009). We investigate the function of Dscamb in PR ribbon synapse formation in Chapter 3, but future experiments could also assess the development in ovHC ribbon synapse formation.

In Drosophila, Dscam1 is required for dendritic self-avoidance in peripheral touch-sensing neurons (Hughes et al., 2007; Matthews et al., 2007; Soba et al., 2007). In contrast, we did not detect a significant increase in self-crossover events amongst Dscamb-expressing Rohon-Beard peripheral sensory axon branches (Figure 2.3), suggesting that Dscamb is not required for somatosensory self-avoidance. It is possible, however, that Dscamb could mediate this function in other regions of the nervous system.

Dscamb and enteric neuron migration

Dscamb expression in the ENS is consistent with in situ hybridization studies in mice, which showed that *Dscam* mRNA is expressed in enteric neurons of the gut (Yamakawa et al., 1998). Down syndrome (DS) is also the most common chromosomal anomaly associated with Hirschsprung disease (HSCR)—a congenital disorder of severe and intractable constipation caused by an absence of enteric innervation along a variable length of the distal intestine (Amiel and Lyonnet, 2001). Moreover, an association study of SNPs on chromosome 21 in DS patients with HSCR, identified DSCAM as a predisposing locus for HSCR (Jannot et al., 2013). The developmental etiology of HSCR is believed to be a halt in the migration enteric neurons, preventing innervation of the distal region of the colon. We quantified the number of enteric neurons in the distal region of the gut, but found no significant difference in enteric neuron migration between heterozygous and homozygous mutants (Figure 2.9). Since DS is merely a predisposing condition for HSCR, it is likely that other genetic lesions are required in order for disease presentation.

Summary

Although Dscamb is expressed broadly throughout the nervous system, we did not detect any obvious defects in neuronal development across any of the brain regions of that were investigated. Most of our analyses, however, were qualitative and assessed neuronal development at the anatomical scale. Our results do not preclude the possibility of defects at a finer scale, such as synapse formation or subtle changes in neurite branching and organization. *Dscamb* mutants are clearly deficient in their ability to survive, and Dscamb is expressed almost exclusively in the nervous system, making it likely that the underlying cause of mutant mortality is neuropathological. Thus, it is probable that more detailed analysis of neuronal development will uncover the cellular basis of the *dscamb* mutant phenotype.

2.4 ACKNOWLEDGEMENTS

We would like to thank Shin-Ichi Higashijima for the enhancer trap donor plasmid construct (pBluescript-Gbait-Hsp-Gal4ff-BGHpA), Koichi Kawakami for the Tg(UAS:GFP) line, Gage Crump for the Tg(UAS:KikGR) line, and Robert Modlin for the Tg(nbt:DsRed) line. DPJ was supported by a scholarship from the Achievement Rewards for College Scientists (ARCS) Foundation and the UCLA Philip Whitcome Predoctoral Training Program in Molecular Biology. This research was supported by grants to AS from the National Institute of Arthritis and Musculoskeletal and Skin Diseases (R01 AR064582).

2.5 FIGURES

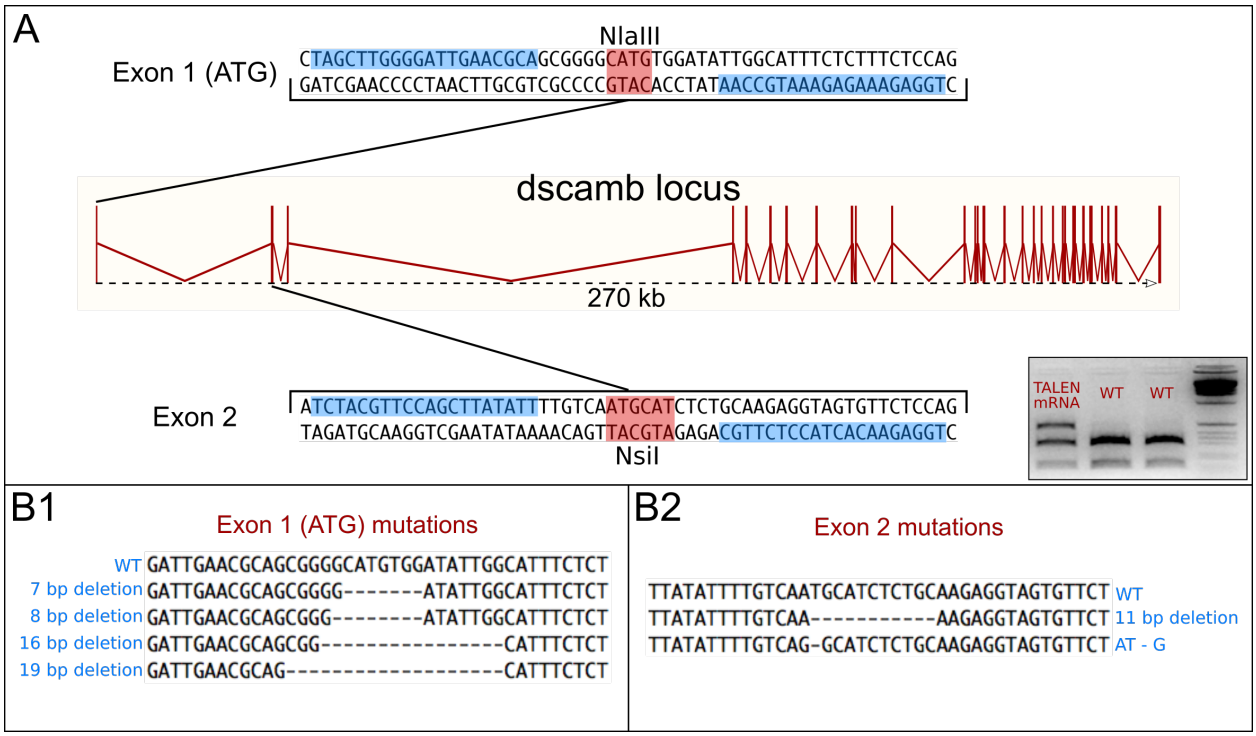

Figure 2.1 – Generation of *dscamb* frame-shift mutations using TALENs
A) The *dscamb* locus, including target sites in exon 1 (top) and exon 2 (bottom) for TALEN mutagenesis. Blue boxes indicate TALEN binding sites. Red boxes indicate restriction enzyme cut sites that were used for RFLP genotyping. The inset shows an example of RFLP genotyping for mutations at exon 2 using genomic DNA from pooled embryos that were either, injected with TALEN-encoding mRNA or uninjected. The upper, uncut band in TALEN-injected embryos indicated TALEN-mediated mutation of the NsiI cut site.
B) Examples of identified TALEN-generated germline mutations at either the exon 1 (B1) or exon 2 (B2) target sites.

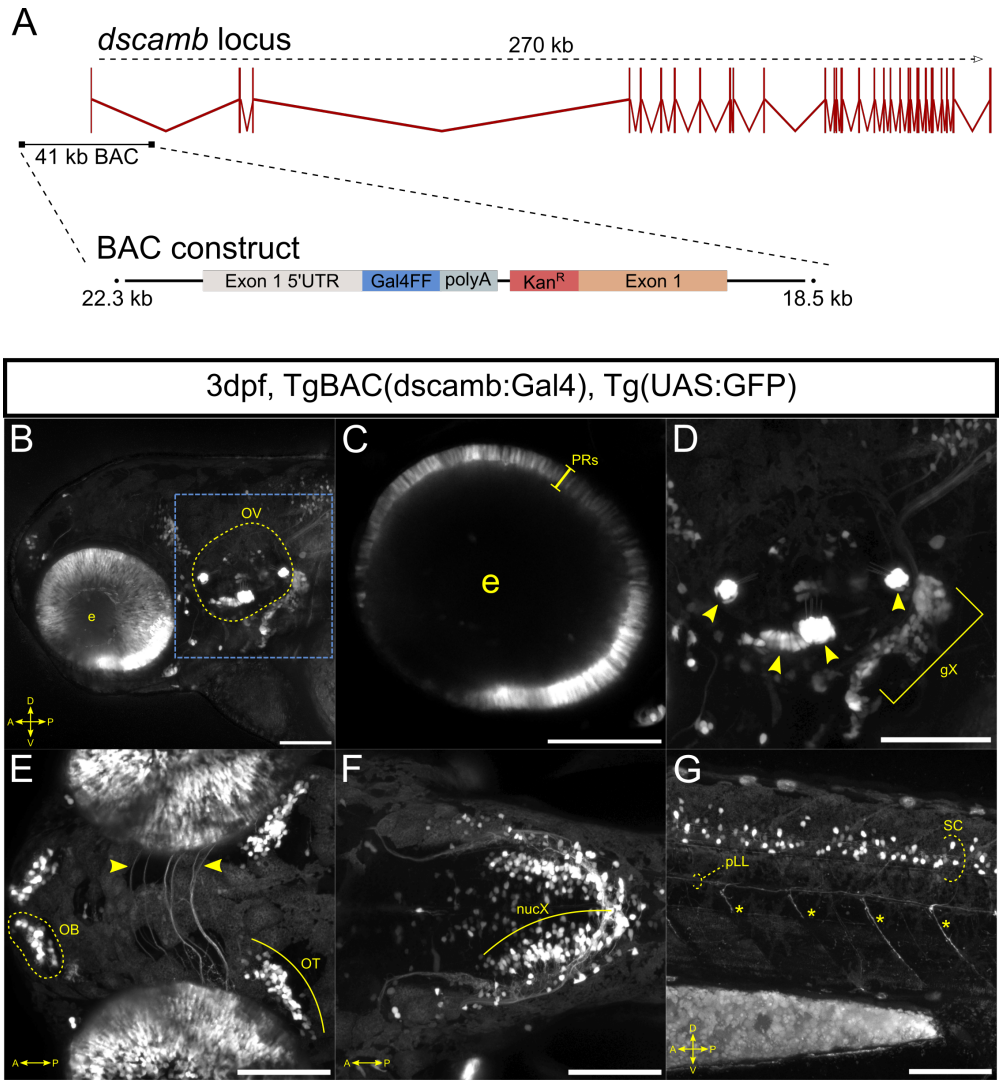

Figure 2.2 – A novel BAC reporter for Dscamb identified gene expression in many regions of the nervous system

A) Top: Location and size of the 41kb *dscamb*-containing BAC (boxed line) relative to the locus. The BAC construct spanned the first exon of *dscamb.* Bottom: A Gal4 reporter cassette was integrated into the BAC the translational start site of exon 1.

B-G) Confocal images showing examples of BAC(dscamb:Gal4) reporter expression after stable integration into the genome.

B) Lateral view of the head, showing Dscamb expression in the peripheral nervous system and sparse expression in the brain. Dashed yellow circle outlines the otic vesicle (OV). e = eye.

C) Higher magnification and single optical section through the eye (e; same as in B), showing that BAC(dscamb:Gal4) is expressed abundantly in photoreceptors (PRs).

D) Higher magnification image of the otic vesicle (blue box in B). Arrowheads indicate expression in the patches of otic vesicle hair cells. Bracket indicates expression in the vagal sensory ganglion (gX).

E) Dorsal view of the anterior head. BAC reporter expression is seen in the olfacoty bulb (OB; yellow dashed circle) and optic tectum (OT; yellow curve). Arrowheads indicate unidentified commissural axons.

F) Dorsal view of the posterior head. Dscamb is expressed in the vagal motor nucleus in the hindbrain (nucX; yellow curve).

G) Lateral view of the trunk. BAC(dscamb:Gal4) expression is seen sparsely throughout the spinal cord (SC). Aterisks mark labeled motor axons innervating the body wall. Expression was also seen in axon of the posterior lateral line (pLL).

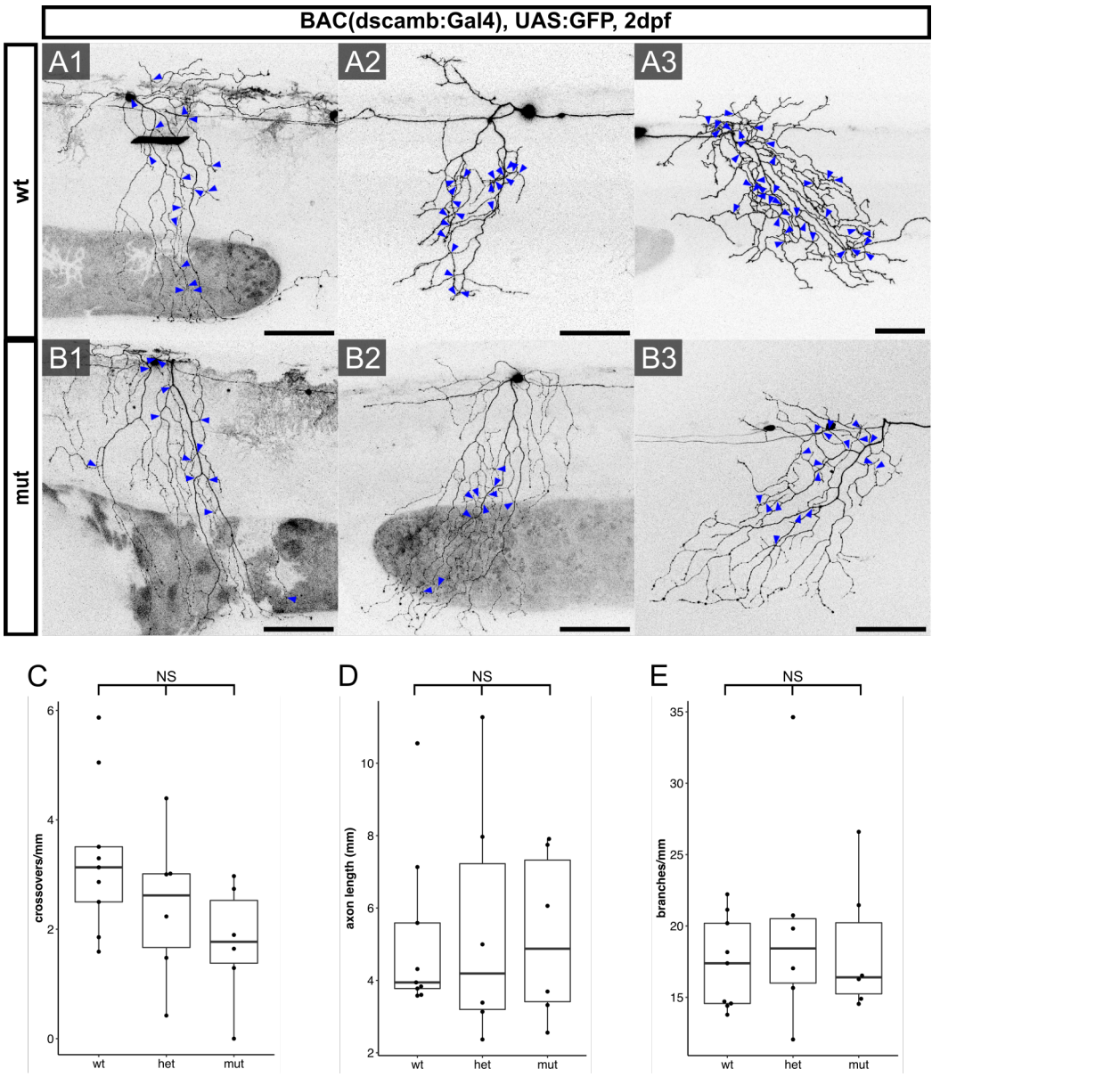

Figure 2.3 – Dscamb is not required for self-avoidance in Rohon-Beard peripheral somatosensory axons

A-B) Confocal images of individual RB neurons labeled with transiently-expressed BAC(dscamb:Gal4) in either wild-type (A) and mutant (B) embryos. Blue arrowheads indicate crossover event between peripheral axon branches.

C-E) Quantification of self-crossovers (C), total axon length (D), and branch number in RB peripheral axons in wildtpe, heterozygous, and homozygous mutant embryos. Middle box line is the median; lower and upper ends of the boxes are 25th and 75th percentiles, respectively. Data points outside of the whiskers are considered outliers. N = 9, 6, 6 RB neurons for wt, het, and mut, respectively. Kruskal-Wallis test p-values: crossovers p = 0.098, axon length p = 0.91, branching p = 0.88.

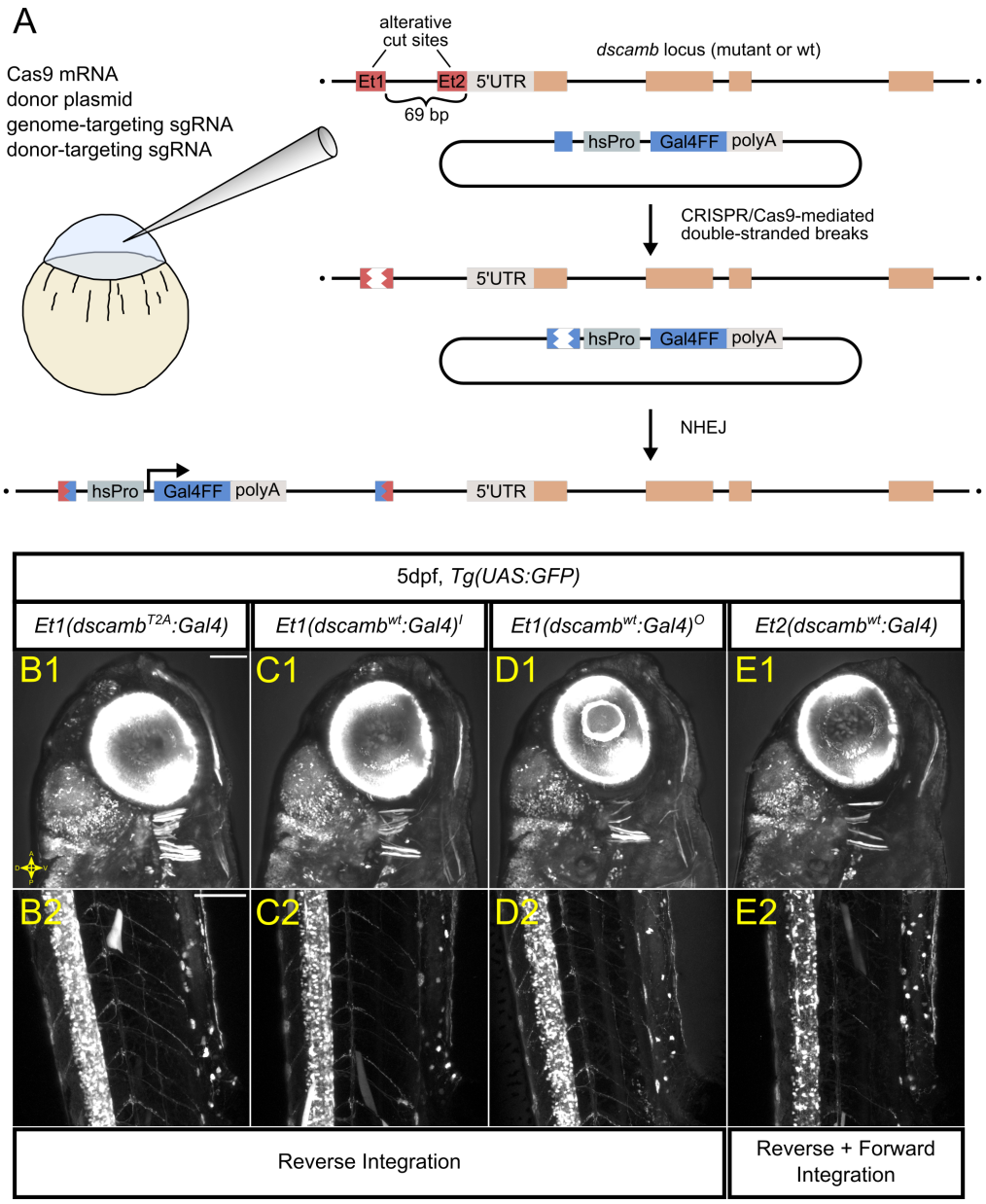

Figure 2.4 – Generation of a Dscamb enhancer trap reporter using CRISPR/Cas9-targeted transgenic insertion

A) Two alternative Cas9 target sites were selected upstream of *dscamb* (Et1 and Et2). CRISPR/Cas9-based strategy for enhancer trap insertion. Cas9-encoding mRNA, a Gal4 donor plasmid, and two gRNAs: one targeting the donor plasmid, and the other targeting either Et1 or Et2. Inside the embryo, Cas9 uses the gRNAs to cut both the genome upstream of *dscamb* and the donor plasmid. Through non-homologous end joining (NHEJ), the donor plasmid will sometimes integrate upstream of *dscamb* and drive expression of Gal4 in Dscamb-expressing cells.

B-E) Example confocal images of 4 independent enhancer trap lines, showing reporter expression in the head (B1, C1, D1, E1) and trunk (B2, C2, D2, E2).

B) A reverse integration at the Et1 target site upstream of the *dscamb*^{t2b} mutant allele. Scale bars = 100um

C and D) Two lines with reverse integrations at the Et1 target site upstream of the wild-type allele.

E) A line with at least two tandem donor plasmid integrations at the Et2 target site upstream of the wildtype allele. The most 5' integration was in the reverse orientation, and the 3' integration was in the forward orientation.

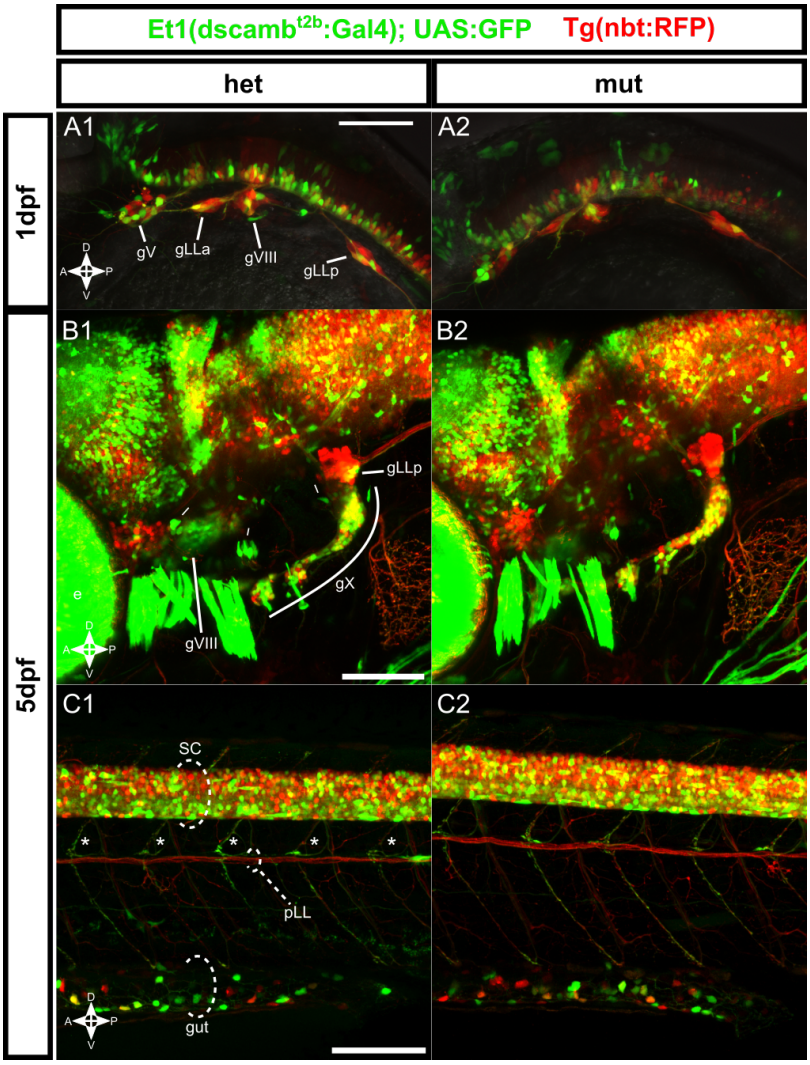

Figure 2.5 – Dscamb enhancer trap reporter is expressed broadly throughout the brain, spinal, cord, and peripheral nervous system, but homozygous mutant embryos show no obvious structural defects

A-C) Et1(dscamb^{t2b}:Gal4) enhancer trap (green) crossed to pan-neuronal Tg(nbt:RFP) for comparison. Left and Right columns show heterozygous and homozygous mutants, respectively.
A1 and A2) Lateral view of the head in 1dpf embryos. gV: trigeminal ganglion, gLLa: anterior lateral line ganglion, gVIII: statoacoustic ganglion, gLLp: posterior lateral line ganglion.
B1 and B2) Lateral view of the head in 5dpf larvae. e: eye, gVIII: statoacoustic ganglion, gX: vagal ganglia, gLLp: posterior lateral line ganglion, white hash marks: otic vesicle hair cell patches.
C1 and C2) Lateral view of the trunk in 5dpf larvae. SC: spinal cord, pLL: posterior lateral line axons, asterisks: motor neuron axons, gut: intestine.
All scale bars: 100um.

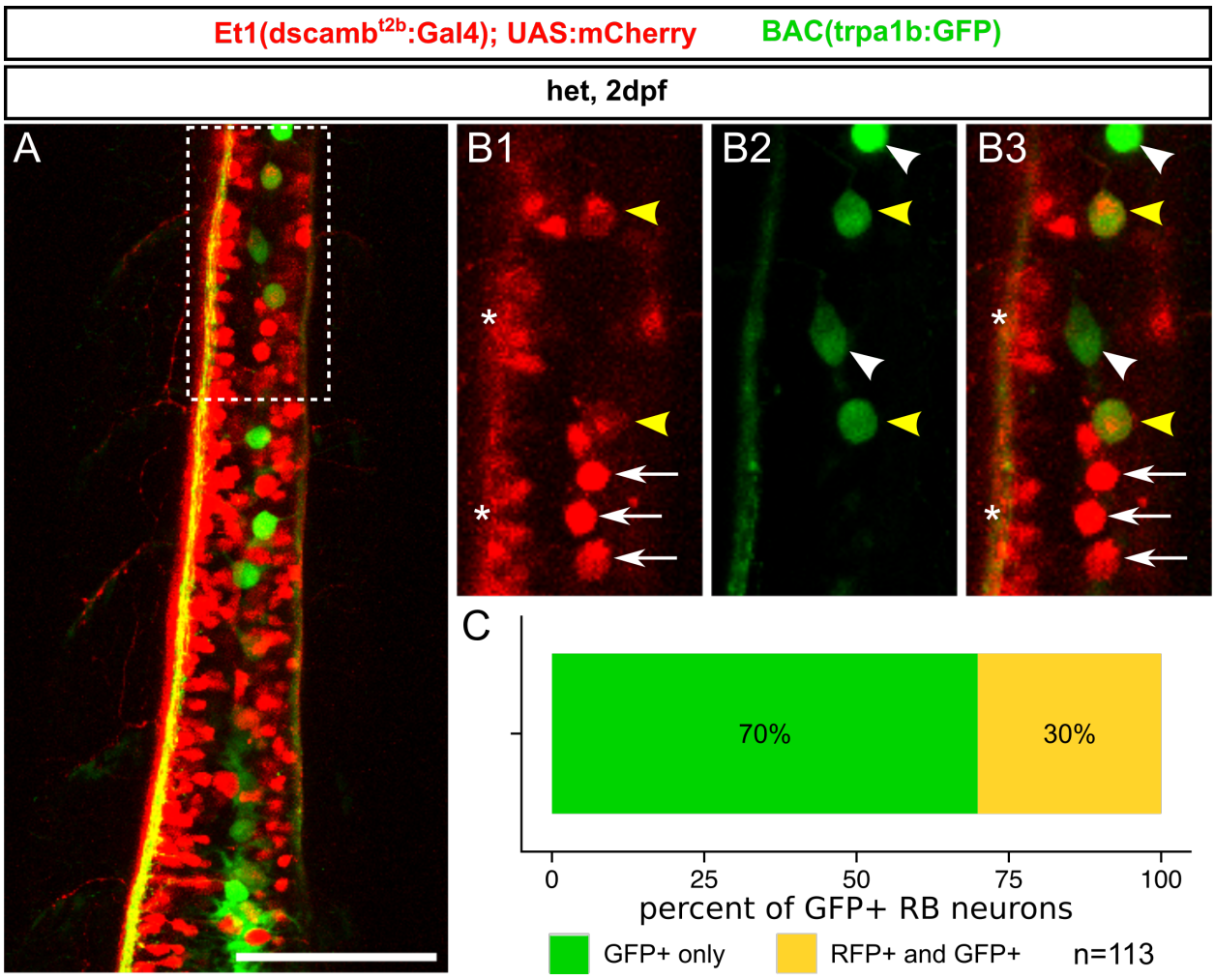

Figure 2.6 – Dscamb is expressed in a subtype of Rohon-Beard neurons that partially overlaps with TrpA1b

A) Dorsal view of the spinal cord in 2dpf embryo showing Et1(dscamb^{t2b}:Gal4) expression in red and BAC(trpa1b:GFP) expression in green. Scale bar: 100um. Anterior is down.

B1-B3) Higher magnification image of boxed region in A. Yellow arrowheads: GFP+/RFP+ RBs, white arrowheads: GFP+ only RBs, white arrows: RFP+ only RBs, white asterisks: other RFP+ spinal cord neurons.

C) Percentage of GFP+ that we either RFP- (green) or co-labeled with RFP (yellow). n = 113 RBs analyzed.

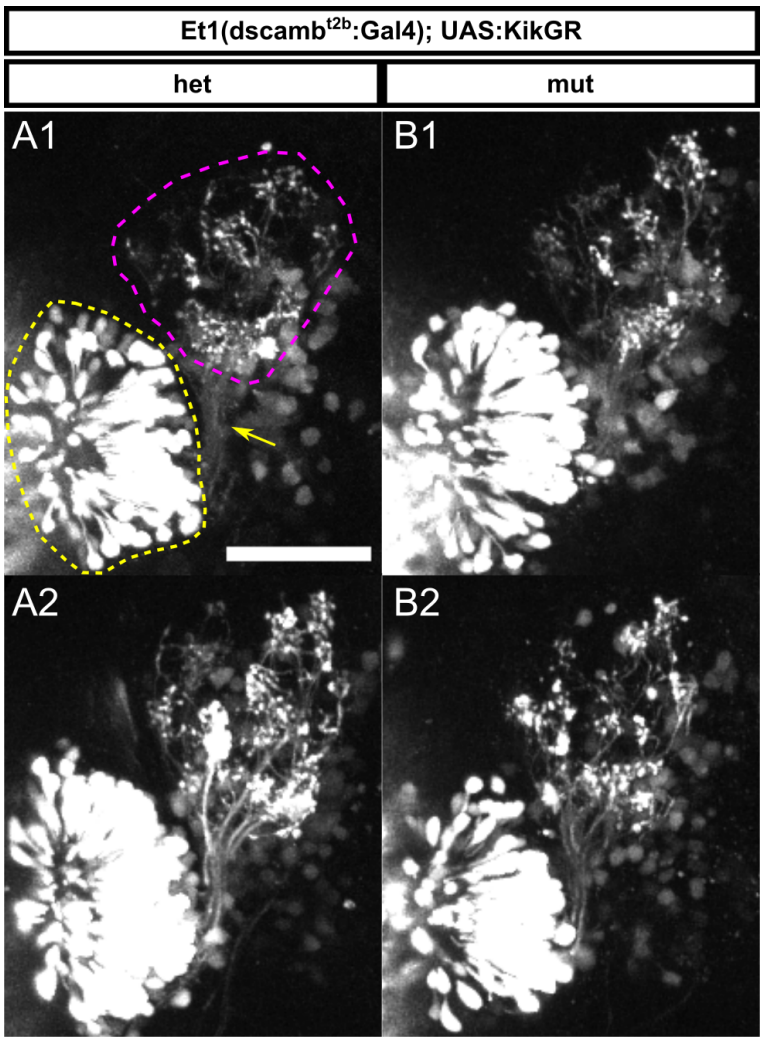

Figure 2.7 Dscamb is not required for olfactory receptor neuron axon innervation of glomeruli in the olfactory bulb
A-B) Et1(dscamb^{t2b}:Gal4) was used to drive expression of photoconvertible KikGR in 3dpf heterozygous (A) and homozygous (B) larvae. KikGR in the ORNs (yellow dashed region) was photoconverted from green to red to better differentiate their axon terminals in the glomeruli (magenta dashed region) from Dscamb-expressing neurons in the olfactory bulb. Yellow arrow: ORN axon coursing to the olfactory bulb. Scale bar: 50um. Dorsal is up and medial is right.

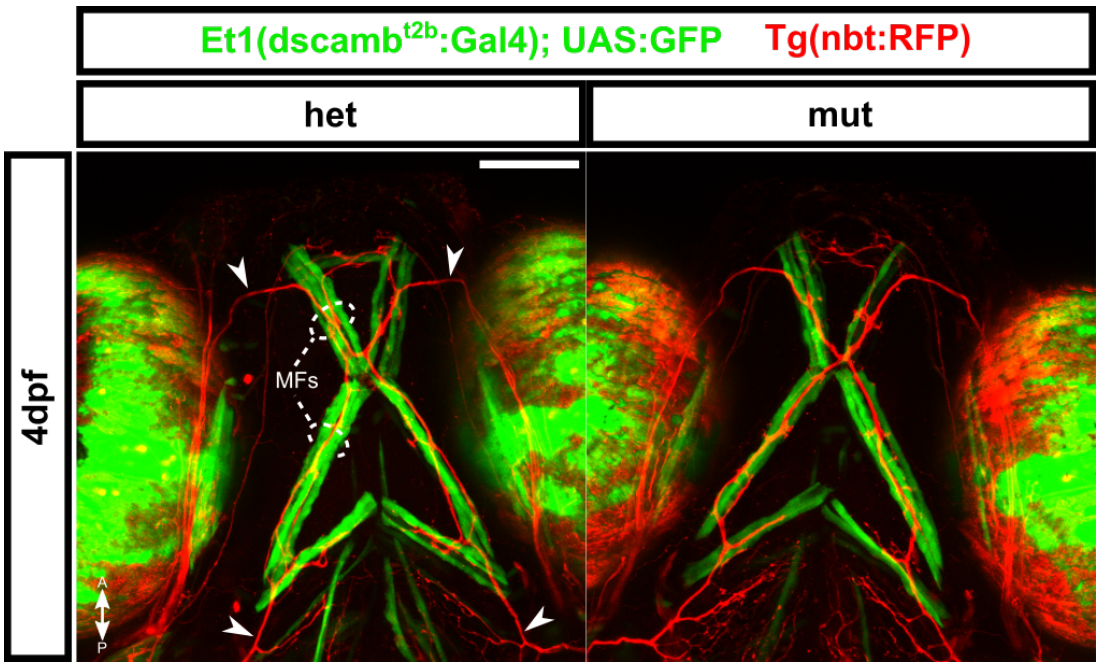

Figure 2.8 Dscamb loss-of-function does not disrupt the overall organization of jaw muscles
Ventral view of the head in 4dpf heterozygous (left) and homozygous (right) *dscamb* mutant embryos. Et1(dscamb^{t2b}:Gal4) expression is labeled in green and pan-neuronal Tg(nbt:RFP) expression is labeled in red. White arrowheads: RFP+ branchiomotor axons, MFs/dashed lines: GFP+ jaw muscle fibers. Scale bar: 100um.

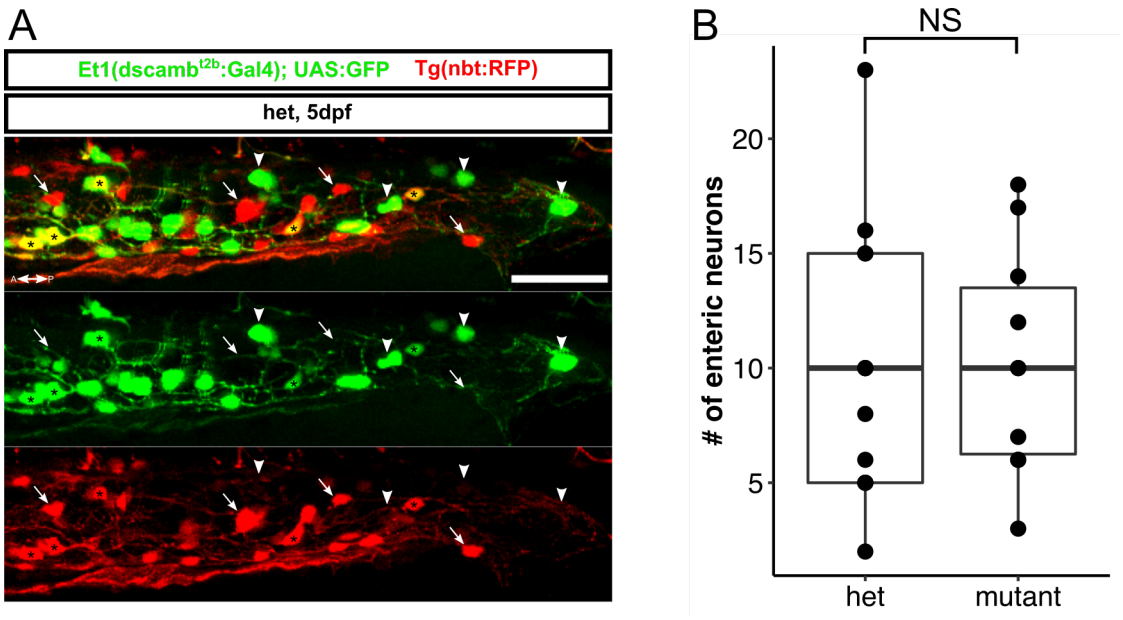

Figure 2.9 Dscamb is expressed in a subtype of enteric neurons, but is not required for their migration into the distal gut.
A) distal portion of the gut in a 5dpf heterozygous *dscamb* mutant, showing Et1(dscamb^{t2b}:Gal4) expression in green and Tg(nbt:RFP) expression in red. Black asterisks: examples of GFP+/RFP+ enteric neurons, white arrowheads: examples of GFP+ only enteric neurons, white arrows: examples of RFP+ only enteric neurons.
Scale bar: 50um
B) Quantification of the number of enteric neurons in the most distal 250um region of the gut. Each data point represents one larvae. Mann-Whitney-Wilcoxon test: p = 0.68. Middle box line is the median; lower and upper ends of the boxes are 25th and 75th percentiles, respectively. Data points outside of the whiskers are considered outliers.

2.6 METHODS

Zebrafish

Zebrafish (Danio rerio) were grown at 28.5°C on a 14 h/10 h light/dark cycle. Embryos were raised at 28.5°C in embryo water (0.3 g/L Instant Ocean Salt, 0.1% methylene blue). For live confocal imaging, embryos were treated with phenylthiourea (PTU) at 24 hpf to block pigmentation. When applicable, embryos and larvae were screened for fluorescent reporter expression using a SteREO Discovery.V12 fluorescent dissecting scope (Carl Zeiss) with a Plan Apo S 1.5x objective. All experimental procedures were approved by the Chancellor's Animal Research Care Committee at UCLA.

For these studies, the following zebrafish lines were used:

AB (wild-type)

Dscamb loss-of-function mutant lines: generated in-house

BAC(dscamb:Gal4): generated in-house

Et(dscamb:Gal4) reporter lines: generated in-house

Tg(UAS:GFP) (Asakawa et al., 2008): provided by Koichi Kawakami (National Institute of Genetics, Mishima)

Tg(UAS:KikGR): provided by Gage Crump (University of Southern California, Los Angeles)

Tg(UAS:nfsb-mCherry) (Davison et al., 2007)

Tg(nbt:DsRed) (Peri and Nüsslein-Volhard, 2008)

BAC(trpa1b:GFP) (Pan et al., 2012)

All experimental procedures were approved by the Chancellor's Animal Research Care Committee at UCLA.

TALEN cloning and and targeted mutagenesis

For each mutant target site in the *dscamb* locus, two 20 bp TALEN binding sites were selected (exon 1: 5'-TAGCTTGGGGATTGAACGCA-3', 5'-TGGAGAAAGAGAAATGCCAA-3'; exon 2: 5'-TCTACGTTCCAGCTTATATT-3', 5'-TGGAGAACACTACCTCTTGC-3'). A restriction enzyme site between each TALEN pair was used for genotyping by restriction fragment length polymorphism (RFLP; exon 1: NlaIII; exon 2: NsiI). TALEN constructs were cloned using a Golden Gate assembly protocol (Cermak et al., 2011) and an accompanying plasmid kit that was purchased from Addgene (Addgene Kit #1000000024). The final TALEN assemblies included half of a homodimerizable Fok1 endonuclease domain for generating DNA double-stranded breaks.

After linearization with StuI, TALEN plasmids were used as templates for in vitro RNA transcription with T7 RNA polymerase (mMessage mMachine kit, Thermo Fisher). Wild-type embryos at the single-cell stage were injected with 1-5 nl of an injection mix containing mRNA encoding a pair of TALENs (100-200 pg/nl for each TALEN mRNA). At 2-5 dpf, pools of 4-6 injected embryos were lysed and genotyped by RFLP. Clutches that demonstrated on-target cutting were raised to adulthood. Adult fish were screened for germline mutations through outcrossing and genotyping offspring embryos. Germline mutations were sequenced from individual embryos to identify frameshift mutations. Founders with demonstrated germline frameshift mutations were used to establish stable mutant lines. For each target site, two independent mutant lines were established , which have each been outcrossed for at least 3 generations (exon 1: *dscamb*^{t1a} [16 bp deletion] *dscamb*^{t2a} [19 bp deletion]; exon 2: *dscamb*^{t2a} [AT-G insertion-deletion] *dscamb*^{t2b} [11 bp deletion]).

Primer Sequence (5'-3')	**Purpose**

CCTCTCAAGTCATTGGCACA	Amplification of *dscamb* TALEN T1 (exon 1) site for genotyping; forward primer
GTGATCACCCGTGACACAAT	Amplification of *dscamb* TALEN T1 (exon 1) site for genotyping; reverse primer
GAGGCCTCTTTAAACAGCAA	Amplification of *dscamb* TALEN T2 (exon 2) site for genotyping; forward primer
GACTGACCGGCCTTAATGTG	Amplification of *dscamb* TALEN T2 (exon 2) site for genotyping; reverse primer
GTGTGCGAAGTGAAAAGAGGAAAATCTA GCTTGGGGATTGAACGCAGCGGgccaccat gaagctactgtcttcta	Amplification of Gal4FF-polyA-Kan with 50 bp *dscamb* homology arms for recombination into the *dscamb* BAC. Forward primer.
GAAGACTAACCATTCAGGATGCTCTGGAG AAAGAGAAATGCCAATATCCAgccctcagaag aactcgtca	Amplification of Gal4FF-polyA-Kan with 50 bp *dscamb* homology arms for recombination into the *dscamb* BAC. Reverse primer.
AAAGCACCGACTCGGTGCCACTTTTTCAA GTTGATAACGGACTAGCCTTATTTTAACTT GCTATTTCTAGCTCTAAAAC	Constant reverse primer for gRNA synthesis
gcgtaatacgactcactataGGAGTGTCTCGGCTC CTTTAgttttagagctagaaatagc	Variable forward primer for gRNA-Et1 synthesis
gcgtaatacgactcactataGGTTATTCTCTAATGC TCTGgttttagagctagaaatagc	Variable forward primer for gRNA-Et2 synthesis
gcgtaatacgactcactataGGCTGCTGCGGTTCC AGAGGgttttagagctagaaatagc	Variable forward primer for gRNA-Mbait synthesis
GCGTAATACGACTCACTATAG	Invariant forward primer for gRNA template amplification
AAAGCACCGACTCGGTGCCAC	Invariant reverse primer for gRNA template amplification
CACGCAGAGTGTTTTTGCTATT	Forward genomic primer for *dscamb* enhancer trap integration PCR
GAACAAAGGTGAGATCCCAGAG	Reverse genomic primer for *dscamb* enhancer trap integration PCR
CTGCGGTCTCTCTTTCGCCC	Outward-facing donor primer. Binds to 5' end of the enhancer trap plasmid
CGGAAGAGCGCCCAATACGC	Outward-facing donor primer. Binds to 3' end of the enhancer trap plasmid

Table 2.1—Primers used in this study

Tissue lysis and genotyping

Tissue lysis for genotyping was carried out according to a previously published protocol (Meeker et al., 2007). In summary, tissue was lysed in PCR tubes containing 50 mM NaOH (lysis buffer) and then heated to 95 degrees Celsius for 20 min in a thermocycler. After cooling to 4 degrees Celsius, the solution was neutralized by adding 1/10th the initial volume of 1M Tris-HCl, pH8.0. The volume of lysis buffer was adjusted according to the amount of tissue to be lysed: individual

embryos/larvae were lysed in 25 ul; larval remains from retinal dissections or cryosectioning were lysed in 20 ul; larval fin biopsies for electron microscopy were lysed in 15 ul; pools of embryos were lysed in 25 ul + 5 ul for each additional embryo over the first; adult fin-clips were lysed in 100 ul. 1 ul of neutralized tissue lysate was used as template for PCR.

For RFLP genotyping *dscamb* mutants, 1 ul of tissue lysate was used as template for a 25 ul PCR in which specific primer were used to amplify either the exon 1 (T1) or exon 2 (T2) TALEN mutation sites. After PCR, a restriction enzyme (NlaIII for T1; NsiI for T2; New England Biolabs) diluted in optimal cutting buffer (CutSmart; New England Biolabs) was added directly to each PCR and digested at 37 degrees Celsius overnight. Entire PCR products were analyzed by gel electrophoresis for restriction fragment length polymorphism. TALEN-mediated mutations ablated the restriction enzyme recognition site, resulting in uncut bands in tissues carrying a *dscamb* mutant allele. Wildtype genotypes were identified by completely digested products, heterozygous mutants by partially digested products, and homozygous mutants by completely uncut products. All genotyping experiments were run with a known wild-type control lysate to verify complete digestion.

BAC cloning and transgenesis

The BAC(*dscamb*:Gal4) construct was created by modifying the Ch73-102M15, a 40.8 kb BAC containing the first exon of *dscamb* along with 22.3 kb upstream and 17.8 kb of the first intron. using in vitro homologous recombination, a Gal4FF-polyA-Kan cassette was inserted in place of the *dscamb* start codon, according to a previously published protocol (Suster et al., 2011). Gal4FF is a zebrafish optimized version of Gal4 (Asakawa and Kawakami, 2009). 1-5 nl of purified BAC(dscamb:Gal4) (50-100 pg/nl) was injected into Tg(UAS:GFP) embryos at the single-cell stage. Embryos were screened at 1 dpf under a fluorescent dissecting microscope

and embryos with the most abundant UAS:GFP expressed were selected to be grown up. Adult fish were screened for germline integration by crossing to Tg(UAS:GFP) and screening for offspring with GFP expression. We identified one founder, which was used to establish a stable line: BAC(dscamb:Gal4).

Enhancer trap cloning and transgenesis

We selected two Cas9 binding sites upstream of the *dscamb* transcriptional initiation site. To generate gRNA's we used a previously published protocol (Talbot and Amacher, 2014), using the "Short oligo method to generate gRNA." In summary, DNA template was PCR synthesized from two primers: 1) a ~60bp variable forward primer containing a 5' T7 RNA polymerase domain, followed by the *dscamb* targeting sequence, and a 3' region of homology with the guide constant reverse primer; 2) a ~80bp guide constant reverse primer containing the gRNA scaffold sequence, including a region of homology with the variable forward primer. Two short invariant primers that bound to the 5' and 3' ends of the 120 bp product were also included for additional amplification. PCR product was used as template for RNA synthesis with T7 RNA polymerase (mMessage mMachine, Thermo Fisher). We synthesized gRNAs that would direct Cas9 to cut both upstream of *dscamb* (gRNA-Et1 and gRNA-Et2) and the enhancer trap donor plasmid (gRNA-Mbait)

A zebrafish codon-optimized Cas9 construct, flanked by nuclear localization signals was used for targeted mutagenesis (Jao et al., 2013). The template plasmid (pCS2-nCas9n) for Cas9 mRNA synthesis was ordered from Addgene.org (Plasmid #47929). The plasmid was linearized by digestion with NotI, before use as a template for RNA synthesis with SP6 RNA polymerase (mMessage mMachine kit, Thermo Fisher).

A plasmid used to generate the enhancer trap donor construct was generously provided by Shin-Ichi Higashijima (pBluescript-SK-Gbait-Hsp-Gal4FF-BGHpA)(Kimura et al., 2014). This plasmid contains a minimal heatshock promoter (Hsp) to drive expression of a zebrafish-optimized Gal4 construct (Gal4FF) when integrated into the genome (Asakawa and Kawakami, 2009). A bovine growth hormone polyadenylation signal (BGHpA) is located downstream of Gal4FF to terminate transcription and stabilize the transcript expression. A gRNA "bait" (Gbait), located 5' to Hsp, is used for Cas9-mediated cleavage/linearization of the donor plasmid in vivo. To create a donor plasmid that was compatible for use in a Tg(UAS:GFP) embryos, the GFP-derived Gbait sequence was replaced with another, highly specific and efficient gRNA target site, Mbait (Kimura et al., 2014). To do this, Hsp-Gal4FF-BGHpA was PCR amplified from the original donor plasmid using a forward primer with the Mbait sequence. Both forward and reverse primers also contained attB recognition sequences, allowing the PCR amplicon to be recombined via Gateway cloning into the middle element entry vector backbone (pDONR 221; Gateway BP Clonase II Enzyme, Thermo Fisher). This plasmid (pME-Mbait-Hsp-Gal4FF-BGHpA) was injected for enhancer trap transgenesis.

Tg(UAS:GFP), *dscamb*^{tr2b} heterozygous embryos were injected at the single-cell stage with 1-5 nl of an injection mix containing Cas9 mRNA (200-300 pg/nl), donor plasmid (10-20 pg/nl), gRNA-Et1/Et2 (20-40 pg/nl), and gRNA-Mbait (20-40 pg/nl). At 1 dpf, injected embryos were screened on a fluorescent dissecting microscope, and those with the most abundant GFP expression were selected to be grown up. To identify founders with germline enhancer trap integration, we crossed adult fish to Tg(UAS:GFP) and screened for fluorescent expression at 1-2 dpf. Gal4+ embryos from identified founders were lysed individually and genotyped to determine if Gal4 expression segregated with the wild-type or mutant *dscamb* allele. Three lines with stable integration upstream of the wild-type allele were established: Et1(dscamb^{wt}:gal4)^{i}, Et1(dscamb^{wt}:gal4)^{o}, and Et2(dscamb^{wt}:gal4). Two of these lines were integrated at the Et1 target

site [Et1(dscamb^{wt}:gal4)^{i} and Et1(dscamb^{wt}:gal4)^{o}], and one line was integrated at the Et2 target site [Et2(dscamb^{wt}:gal4)]. One line with enhancer trap integration upstream of the *dscamb*^{t2b} mutant allele at the Et1 target site was established [Et1(dscamb^{t2b}:gal4)].

Enhancer trap integration PCR

We selected a forward and reverse genomic PCR primers which amplified a region containing both the Et1 and Et2 Cas9 target sites upstream of *dscamb*. For the donor plasmid, we designed two outward-facing primers that bound to either the 5' or 3' end of the linearized plasmid. DNA from lysed enhancer trap-expressing embryos was used as template for PCR with both genomic primers and one of the donor plasmid primers. Enhancer trap integration upstream of *dscamb* will allow one of the genomic primers to generate a PCR product with the donor plasmid primers to produce amplicons of different sizes, depending on the orientation of integration. PCR amplicon sizes was analyzed by gel electrophoresis.

Line name	***dscamb* allele**	**gRNA cut site**	**Integration orientation**
Et1(dscamb^{wt}:gal4)^{i}	wild-type	gRNA-Et1 (69 bp upstream)	Reverse
Et1(dscamb^{wt}:gal4)^{o}	wild-type	gRNA-Et1 (69 bp upstream)	Reverse
Et1(dscamb^{t2b}:gal4)	mutant (t2b)	gRNA-Et1 (69 bp upstream)	Reverse
Et2(dscamb^{wt}:gal4)	wild-type	gRNA-Et2 (4 bp upstream)	Reverse, Forward

Table 2.2—Dscamb enhancer trap integrations

Confocal imaging

Confocal imaging was conducted with a LSM 800 scanning laser confocal microscope (Carl Zeiss). For imaging live embryos, the microscope was equipped with a heated stage set to 28.5 degrees Celsius. We used a 488-nm laser line for imaging GFP, green KikGR, or Alexa-488 and a 561nm laser line for imaging mCherry, red KikGR, or Alexa-568. Unless otherwise stated, all

images were maximum-intensity projections of confocal imaging stacks taken with either a 20x air (0.5 numerical aperture[NA]) or 40x oil (1.3 NA) objectives.

For imaging of live embryos or larvae, fish were anesthetized with 0.02% tricaine and mounted on a coverslip in 1.2% low melt agarose (Promega, V2111) inside a plastic chamber filled with embryo water.

Rohon-Beard self-avoidance analysis

At the single-cell stage, wild-type, heterozygous, and homozygous *dscamb* mutant embryos were injected with a mixture of BAC(*dscamb*:Gal4) (50-100 pg/nl) and a UAS:GFP plasmid (20-30 pg/nl). At 1 dpf, embryos were screened on a fluorescent dissecting scope for GFP-expressing RB neurons. At 2 dpf, embryos were dechorionated and mounted laterally for confocal imaging of RB neurons. After imaging, individual embryos were lysed for genotyping. Individual RB peripheral axons were traced using the ImageJ plugin, Simple Neurite Tracer, which quantifies branch number and length and allows better visualization of branch crossover events. After tracing, total axon length and branch number were tabulated, and crossover events were normalized to total axon length. Tracing and crossover analysis were conducted by an experimenter that was blind to genotype.

Et1(dscamb^{t2b}:Gal4) and TrpA1b Rohon-Beard colocalization

Et1(dscamb^{t2b}:Gal4)/dscamb^{wt}, Tg(UAS:nfsb-mCherry)/+ fish were crossed to BAC(trpa1b:EGFP) fish and embryos were screened at 1 dpf for those expressing both mCherry and GFP. At 2dpf, the dorsal spinal cord was imaged using a confocal microscope. The number of RBs expressing both mCherry and GFP or GFP alone was counted manually.

ORN KikGR photoconversion

Et1(dscamb^{t2b}:Gal4)/*dscamb*^{wt}, Tg(UAS:KikGR) fish were crossed to *dscamb*^{t2b}/*dscamb*^{wt} fish. At 1 dpf, embryos were screened for those expressing KikGR. At 3 dpf, larvae were mounted in agarose on a cover slip so that their nose was positioned against the coverslip. A ROI was drawn around the olfactory sensory epithelium (OSE) on one side of the head, and scanned two times with 405 nm laser for 10 seconds while sweeping the focus through the entire volume of the OSE. Switching between the red and green channels was used to ensure that complete photoconversion of OSE KikGR from green to red fluorescence. After waiting 30 min, the 405 scanning procedure was repeated. After waiting another 30 min to allow red KikGR to diffuse into the ORN axons and glomeruli, we took confocal stacks of the photoconverted, red OSNs and their axons in the olfactory bulb. After imaging, individual larvae were lysed for genotyping.

Enteric neuron cell counting

Et1(dscamb^{t2b}:Gal4), Tg(UAS:GFP) heterozygous and homozygous mutant fish were anesthetized and mounted laterally for confocal imaging of the intestine. To prevent intestinal smooth muscle contractions during imaging, a concentrated tricaine solution (0.1%) was added to the slide chamber just prior to imaging. After confocal imaging of the distal region of the gut, individual embryos were lysed for genotyping. The number of GFP+ enteric neurons in the most distal 250 um region of the gut was counted using the ImageJ plugin, 3D Objects Counter. Genotyping was conducted after cell counting, so the experimenter conducting the analysis was blind to genotype.

2.7 REFERENCES

Agarwala KL, Ganesh S, Amano K, Suzuki T, Yamakawa K (2001a) DSCAM, a Highly Conserved Gene in Mammals, Expressed in Differentiating Mouse Brain. Biochem Biophys Res Commun 281:697–705.

Agarwala KL, Ganesh S, Suzuki T, Akagi T, Kaneko K, Amano K, Tsutsumi Y, Yamaguchi K, Hashikawa T, Yamakawa K (2001b) Dscam is associated with axonal and dendritic features of neuronal cells. J Neurosci Res 66:337–346.

Agarwala KL, Ganesh S, Tsutsumi Y, Suzuki T, Amano K, Yamakawa K (2001c) Cloning and functional characterization of DSCAML1, a novel DSCAM-like cell adhesion molecule that mediates homophilic intercellular adhesion. Biochem Biophys Res Commun 285:760–772.

Amiel J, Lyonnet S (2001) Hirschsprung disease, associated syndromes, and genetics: a review. J Med Genet 38:729–739.

Asakawa K, Kawakami K (2009) The Tol2-mediated Gal4-UAS method for gene and enhancer trapping in zebrafish. Methods 49:275–281.

Asakawa K, Suster ML, Mizusawa K, Nagayoshi S, Kotani T, Urasaki A, Kishimoto Y, Hibi M, Kawakami K (2008) Genetic dissection of neural circuits by Tol2 transposon-mediated Gal4 gene and enhancer trapping in zebrafish. Proc Natl Acad Sci U S A 105:1255–1260.

Avanesov A, Malicki J (2010) Analysis of the retina in the zebrafish model. Methods Cell Biol 100:153–204.

Barlow GM, Micales B, Chen X-N, Lyons GE, Korenberg JR (2002) Mammalian DSCAMs: roles in the development of the spinal cord, cortex, and cerebellum? Biochem Biophys Res Commun 293:881–891.

Barlow GM, Micales B, Lyons GE, Korenberg JR (2001) Down syndrome cell adhesion molecule is conserved in mouse and highly expressed in the adult mouse brain. Cytogenet Cell Genet 94:155–162.

Bussmann J, Schulte-Merker S (2011) Rapid BAC selection for tol2-mediated transgenesis in zebrafish. Development 138:4327–4332.

Cermak T, Doyle EL, Christian M, Wang L, Zhang Y, Schmidt C, Baller JA, Somia NV, Bogdanove AJ, Voytas DF (2011) Efficient design and assembly of custom TALEN and other TAL effector-based constructs for DNA targeting. Nucleic Acids Res 39:e82.

Davison JM, Akitake CM, Goll MG, Rhee JM, Gosse N, Baier H, Halpern ME, Leach SD, Parsons MJ (2007) Transactivation from Gal4-VP16 transgenic insertions for tissue-specific cell labeling and ablation in zebrafish. Dev Biol 304:811–824.

Faucherre A, Nargeot J, Mangoni ME, Jopling C (2013) piezo2b regulates vertebrate light touch response. J Neurosci 33:17089–17094.

Fuerst PG, Bruce F, Tian M, Wei W, Elstrott J, Feller MB, Erskine L, Singer JH, Burgess RW (2009) DSCAM and DSCAML1 function in self-avoidance in multiple cell types in the developing mouse retina. Neuron 64:484–497.

Gau P, Poon J, Ufret-Vincenty C, Snelson CD, Gordon SE, Raible DW, Dhaka A (2013) The zebrafish ortholog of TRPV1 is required for heat-induced locomotion. J Neurosci 33:5249–5260.

Hughes ME, Bortnick R, Tsubouchi A, Bäumer P, Kondo M, Uemura T, Schmucker D (2007) Homophilic Dscam interactions control complex dendrite morphogenesis. Neuron 54:417–427.

Hummel T, Vasconcelos ML, Clemens JC, Fishilevich Y, Vosshall LB, Zipursky SL (2003) Axonal targeting of olfactory receptor neurons in Drosophila is controlled by Dscam. Neuron 37:221–231.

Jannot A-S, Pelet A, Henrion-Caude A, Chaoui A, Masse-Morel M, Arnold S, Sanlaville D, Ceccherini I, Borrego S, Hofstra RMW, Munnich A, Bondurand N, Chakravarti A, Clerget-Darpoux F, Amiel J, Lyonnet S (2013) Chromosome 21 scan in Down syndrome reveals DSCAM as a predisposing locus in Hirschsprung disease. PLoS One 8:e62519.

Jao L-E, Wente SR, Chen W (2013) Efficient multiplex biallelic zebrafish genome editing using a CRISPR nuclease system. Proc Natl Acad Sci U S A 110:13904–13909.

Kimura Y, Hisano Y, Kawahara A, Higashijima S-I (2014) Efficient generation of knock-in transgenic zebrafish carrying reporter/driver genes by CRISPR/Cas9-mediated genome engineering. Sci Rep 4:6545.

Liu G, Li W, Wang L, Kar A, Guan K-L, Rao Y, Wu JY (2009) DSCAM functions as a netrin receptor in commissural axon pathfinding. Proc Natl Acad Sci U S A 106:2951–2956.

Ly A, Nikolaev A, Suresh G, Zheng Y, Tessier-Lavigne M, Stein E (2008) DSCAM is a netrin receptor that collaborates with DCC in mediating turning responses to netrin-1. Cell 133:1241–1254.

Matthews BJ, Kim ME, Flanagan JJ, Hattori D, Clemens JC, Zipursky SL, Grueber WB (2007) Dendrite self-avoidance is controlled by Dscam. Cell 129:593–604.

Meeker ND, Hutchinson SA, Ho L, Trede NS (2007) Method for isolation of PCR-ready genomic DNA from zebrafish tissues. Biotechniques 43:610, 612, 614.

Palanca AMS, Lee S-L, Yee LE, Joe-Wong C, Trinh LA, Hiroyasu E, Husain M, Fraser SE, Pellegrini M, Sagasti A (2013) New transgenic reporters identify somatosensory neuron subtypes in larval zebrafish. Dev Neurobiol 73:152–167.

Palmesino E, Haddick PCG, Tessier-Lavigne M, Kania A (2012) Genetic analysis of DSCAM's role as a Netrin-1 receptor in vertebrates. J Neurosci 32:411–416.

Pan YA, Choy M, Prober DA, Schier AF (2012) Robo2 determines subtype-specific axonal projections of trigeminal sensory neurons. Development 139:591–600.

Peri F, Nüsslein-Volhard C (2008) Live imaging of neuronal degradation by microglia reveals a role for v0-ATPase a1 in phagosomal fusion in vivo. Cell 133:916–927.

Soba P, Zhu S, Emoto K, Younger S, Yang S-J, Yu H-H, Lee T, Jan LY, Jan Y-N (2007) Drosophila sensory neurons require Dscam for dendritic self-avoidance and proper dendritic field organization. Neuron 54:403–416.

Suster ML, Abe G, Schouw A, Kawakami K (2011) Transposon-mediated BAC transgenesis in zebrafish. Nat Protoc 6:1998–2021.

Talbot JC, Amacher SL (2014) A streamlined CRISPR pipeline to reliably generate zebrafish frameshifting alleles. Zebrafish 11:583–585.

Whitfield TT, Riley BB, Chiang M-Y, Phillips B (2002) Development of the zebrafish inner ear. Dev Dyn 223:427–458.

Yamakawa K, Huot YK, Haendelt MA, Hubert R, Chen XN, Lyons GE, Korenberg JR (1998) DSCAM: a novel member of the immunoglobulin superfamily maps in a Down syndrome region and is involved in the development of the nervous system. Hum Mol Genet 7:227–237.

Yimlamai D, Konnikova L, Moss LG, Jay DG (2005) The zebrafish down syndrome cell adhesion molecule is involved in cell movement during embryogenesis. Dev Biol 279:44–57.

Zhu H, Hummel T, Clemens JC, Berdnik D, Zipursky SL, Luo L (2006) Dendritic patterning by Dscam and synaptic partner matching in the Drosophila antennal lobe. Nat Neurosci 9:349–355.

CHAPTER 3

Dscamb expression and function in the zebrafish retina

3.1 INTRODUCTION

Vertebrate DSCAMs have been best studied in the vertebrate retina, where they are involved in three critical aspects of retinal organization: 1) synaptic coupling and lamination, 2) homotypic cell body and branch spacing, and 3) developmentally programmed cell death. For instance, in the chick retina, Dscam and Dscaml1 are expressed in non-overlapping subtypes of BCs, ACs, and RGCs, which project to distinct sublamina in the IPL. Misexpression of either protein causes cells to misproject to inappropriate sublamina, suggesting that DSCAMs are required for synaptic couple between specific pre- and post-synaptic retinal subtypes (Yamagata and Sanes, 2008). Mouse DSCAM and DSCAML1 are also expressed in distinct subtypes of retinal neurons, but most of these cell types target appropriate sublamina in mutant retinas, suggesting that DSCAMs play a more limited role in lamination in the mammalian retina (Fuerst et al., 2008, 2009). Mosaic spacing and homotypic branch avoidance, however, are severely disrupted in *Dscam* and *Dscaml1* mutant mice. Mutant mice also show a dramatic expansion in cell number amongst *Dscam* and *Dscaml1*-expressing cell types due to decreased programmed cell death (Fuerst et al., 2008, 2009). These studies suggest that DSCAMs may have evolutionarily divergent functions in retinal development. We hypothesized that Dscamb could mediate similar aspects of retinal development in zebrafish. Moreover, analysis of DSCAM function in a more evolutionarily ancient vertebrate, such as fish, may shed light on the conservation of DSCAM function in retinal development across vertebrate taxa. Indeed, both our BAC and enhancer trap reporter lines revealed that Dscamb is expressed abundantly in the zebrafish retina. These reporters also provide powerful tools for visualizing the morphology of Dscamb-expressing retinal neurons and identifying defects in *dscamb* mutants.

3.2 RESULTS

Dscamb is expressed abundantly in retinal photoreceptors, amacrine cells, and RGCs, but is not required for retinal lamination

We characterized the expression of Et1(dscambt2b:Gal4) in retinal cryosections from 5dpf larvae, a time point at which the retina is well-stratified and fully functional. Similar to the BAC reporter, the Dscamb enhancer trap was most highly expressed in PRs in the ONL (Figure 3.1). In contrast to the BAC reporter, enhancer trap labeling was much more abundant in the INL and even more prominent in the retinal ganglion layer (RGL). Numerous GFP+ axons were visible in sections through the optic nerve (data not shown), indicating that many of the GFP+ cells in the RGL belonged to RGCs. GFP expression in the INL was most commonly observed in ACs, which were identified by their close proximity to the IPL (Figure 3.1B). GFP+ cells located more centrally in the INL—likely BCs or Muller glia—were also frequently observed extending processes toward both the OPL and IPL (Figure 3.1B). Although less common, we occasionally identified GFP+ HCs, based on their flattened nuclei and immediate proximity to the OPL (data not shown). In summary, although our observations suggest that Dscamb is expressed in all five of the major cell types of the retina (PRs, HCs, RGCs, and possibly BCs or Muller glia), it appears to be most widely expressed in the PRs, RGCs and ACs. Contrary to what has been described in mice, we did not observe an increase in the number of Dscamb-expressing cells or expansion of the IPL in *dscamb* homozygous mutants (Figure 3.1), suggesting that Dscamb is not required for normal programmed cell death in retinal development.

Identification of Dscamb-expressing retinal cell types

We used immunofluorescence to further characterize the expression of Et1(dscambt2b:Gal4) surrounding the inner plexiform layer (Figure 3.2). The zebrafish RGL is composed primarily of RGCs, but also contains a thin layer of displaced amacrine cells (dACs) directly adjacent to the IPL. To determine if enhancer-trap expressing cells in the RGL also contained dACs, we stained 5 dpf retinal cryosections with 5E11, an antibody that labels all amacrine cells (Figure 3.2A,B)(Hyatt et al., 1996; Link et al., 2000). In both the IPL and RGL, many GFP+ cells also stained for 5E11+. However, many (if not most) of the 5E11+ cells on both sides of the IPL were

GFP-. This finding suggests that Dscamb is expressed in subtypes of ACs, which include both ACs in the INL and dACs in the RGL.

To further characterize the Dscamb-expressing AC subtype, we stained retinal cryosections for Parvalbumin (Parv), a marker for an AC subtype located on both sides of the IPL (Figure 3.2C,D) (Nevin et al., 2008). Around half of the Parv+ ACs, were also GFP+, indicating that Dscamb is expressed in a subtype of Parv+ ACs. Conversely, many GFP+ ACs in the inner nuclear layer were Parv-, suggesting that Dscamb is expressed in an additional AC subtype. There were no appreciable differences in either cell number or organization of GFP+ or Parv+ ACs in homozygous *dscamb* mutants.

In the RGL, numerous GFP+ cells were negative for the pan-AC marker, 5E11. Coupled with the fact that we also observed GFP expression in the optic nerve, these observations suggest that Dscamb is expressed in RGCs. To characterize the extent of Dscamb-expressing RGCs, we analyzed the expression of Hermes, a pan-RGC marker (Figure 3.2E,F) (Zearfoss et al., 2004; Hörnberg et al., 2013). Immunofluorescent staining for Hermes demonstrated that most GFP+ cells in the RGL were also Hermes+. However, many Hermes+ cells were GFP-, suggesting that Dscamb is expressed in subtypes of RGCs. *dscamb* mutants displayed no obvious defects in the number or organization of GFP+/Hermes+ RGCs.

Dscamb-expressing retinal neurons concentrate in specific sublamina in the IPL

Parv staining highlights three distinct sublaminae/bands in the IPL. Previous studies categorized these sublaminae as a percentage of the total width of the IPL, with 0% designating the edge closest to the RGL and 100% being closest to the INL (Nevin et al., 2008). Using this convention, they identified the three Parv+ bands as s25, s45, and s85 (i.e. the sublaminae

located at 25%, 45%, and 85% the width of the IPL). These bands also correspond to the stratification of processes from Dscamb-expressing cells (Figure 3.3A). s25, the thickest Parv+ band, located closest to the RGL, was often co-labeled with GFP+, processes. This was immediately followed by a sublaminae with sparse GFP labeling. The Parv+ s45 layer, was flanked by two GFP+ bands. Interestingly, GFP was not expressed in s45, suggest that this sublaminae is composed primarily of process from the GFP- portion of Parv+ ACs. s85, the Parv+ sublamina closest to the INL, was also frequently co-labeled with GFP (Figure 3.3A). Although we could not discern any defects in the localization of these bands in *dscamb* homozygous mutants (Figure 3.3B,C), the absence and aggregation of Dscamb-expressing processes into consistent, identifiable sublaminae suggests that Dscamb expression is specific to certain cells types that synapse in specific regions of the IPL.

In summary, our analysis of retinal Et1(dscambt2b:Gal4) expression suggest that Dscamb is expressed most abundantly in the PRs, ACs, and RGCs. Amongst ACs, Dscamb is expressed in a subtype that partially overlaps with the Parv+ ACs. Dscamb is also expressed in a subtype of RGCs. Dscamb loss-of-function does not appear to affect the number or organization of these neurons neurons, or the spatial arrangement of their endings in the plexiform layers. These results suggest that Dscamb is not required in the retina for normal programmed cell death or synaptic targeting.

Dscamb is not required for the mosaic patterning of retinal PRs

Many retinal cell types are organized into mosaic patterns, with cells evenly-spaced across the retina. This arrangement ensures that the entire visual field is equally competent for processing visual information. In mice, DSCAM and DSCAML1 loss-of-function causes cells of the same subtype to clump together during development, disrupting the orderly mosaic spacing (Masland,

2012). Using our enhancer trap reporter, we identified abundant expression of Dscamb in retinal PRs, which are arranged in a highly regular mosaic pattern. To better visualize the PR mosaic and analyze Dscamb function in its development, we dissected retinas from 7 dpf larvae and stained for markers of rods (zpr3) and red and green cones (zpr1) (Figure 3.4). Retinas were flat-mounted to image the PR mosaic *en face*. Both zpr1 and zpr3 showed complete coexpression with Et1(dscambt2b:Gal4). Moreover, with a few exceptions (likely due to UAS:GFP silencing/variegation) GFP was expressed across the entire PR cell layer, indicating that Dscamb is expressed in all zebrafish PRs. The arrangement of rod and cone photororeceptors were indistinguishable between heterozygous and homozygous *dscamb* mutant retinas, indicating that Dscamb is not required for the development of the PR mosaic.

Dscamb loss-of-function does not disrupt ribbon synapses in cone photoreceptors

The observation that Dscamb is expressed in both PRs and ovHCs, raises the intruiguing possibility that is could be involved in the development of ribbon synapses. In *Dscaml1* mutant mice, rod PRs show defects in synaptic maturation, such as an overabundance of synaptic vesicles and rudimentary synaptic ribbons (Fuerst et al., 2009). Using transmission electron microscopy (TEM), we analyzed the structure of PR synaptic ribbons in 7dpf mutant larvae (Figure 3.5). We focused on cone synaptic peduncles, because they are easy to identify by the presence of multiple synaptic ribbons. We found that *dscamb* mutant cones are able to develop synaptic ribbons, and their structure and organization was indistinguishable from wild-type retinas. In addition, we did not observe any obvious differences in the number of synaptic vesicles (Figure 3.5). This suggests that Dscamb is dispensable for the proper formation of cone synaptic ribbons, although we cannot rule out a possible role in rod ribbon synapse development.

Dscamb is not required for amacrine or retinal ganglion cell branch spacing

In mice, DSCAM and DSCAML1 are expressed in non-overlapping subtypes of ACs and RGCs and are required for maintaining neurite branch spacing. Knockout of either gene causes extensive fasciculation between branches of the same neuron and neighboring neurons of the same subtype(Fuerst et al., 2008, 2009). To investigate the function of Dscamb in RGC and AC branch spacing, we analyzed individual cells in *dscamb* mutant and heterozygous retinas (Figure 3.6). To distinguish individual neurons, we sparsely labeled the retina by injecting Et1(dscamb^{i2b}:Gal4) embryos with a UAS:GFP plasmid at the single cell stage. Over the course of development the UAS:GFP plasmid randomly segregates during cell divisions, driving expression of GFP in Dscamb-expressing cells. We screened for embryos with sparse GFP expression in the retina, then fixed and dissected out retinas at 5 dpf. Retinas were flat-mounted to image individual GFP-expressing ACs and RGCs. ACs were identified by their location within the INL (Figure 3.6A,B). RGCs were identified by their location within the RGL, and their axons, which project along the outer surface of the RGL, towards the optic disk (Figure 3.6C,D). ACs and RGCs were similar in heterozygous and homozygous mutants. We did not observe aberrant fasciculation between neurite branches in homozygous mutants, suggesting that Dscamb is not required for self-avoidance of RGC or AC neurites.

3.3 DISCUSSION

Dscamb expression in the retina resembles other DSCAM family members

In the mouse and chick retinas, DSCAM and DSCAML1 are expressed in distinct, non-overlapping retinal cell types. Extensive study in the mouse retina revealed that DSCAM is expressed in several types of ACs, BCs, and most RGCs (Fuerst et al., 2008, 2009; de Andrade et al., 2014). DSCAML1 is expressed broadly in PRs, and two components of the rod visual circuit (rod BCs and AII ACs), but is excluded from the RGL (Fuerst et al., 2009). Dscamb enhancer trap expression showed similarities with both DSCAM and DSCAML1 (Figure 3.1).

Similar to DSCAML1, Dscamb was abundantly expressed in PRs. On the other hand, Dscamb was also expressed in a large subset of RGCs, which is more reminiscent of DSCAM. In the INL, Dscamb expression was observed in subtypes of ACs, BCs, and rarely in HCs. A more detailed characterization of Dscamb-expressing AC and BC subtypes, using markers that are known to coexpress with DSCAM (e.g. TH, bNOS, etc.) or DSCAML1 (e.g. DAB, PKCα) could identify additional commonalities between the expression patterns of these genes.

Dscamb-expressing processes concentrate in specific sublaminae

Studies in the chick and mouse retina suggest different roles for DSCAM and DSCAML1 in organizing IPL lamination. In chicks, complementary subtypes of neurons on both sides of the IPL express the same IgSF protein and project to the same sublamina. As a result, Dscam and Dscaml1 are enriched in specific sublamina, and disrupting their expression mislocalizes neuronal projections to incorrect layers of the IPL (Yamagata and Sanes, 2008). Mouse DSCAM and DSCAML1 are diffusely localized throughout the IPL, and play a more limited role in directing lamination (Fuerst et al., 2008, 2009). Although Dscamb-expressing processes were also distributed broadly in the zebrafish IPL, we observed specific sublaminae with increased or decreased Dscamb expression, which corresponded to the projections of Parv-expressing ACs (Figure 3.3). Although we did not observe any obvious changes in the structure or location of these bands in *dscamb* mutant embryos, these finding suggest that Dscamb is expressed in specific cell types that project selectively to distinct layers of the IPL. It is possible that, like mouse DSCAMs, Dscamb may regulate lamination in a subset of Dscamb-expressing neurons, and their mislocalization could be difficult to detect in our enhancer trap, which labels all Dscamb-expressing cells. A more detailed understanding of Dscamb expression would allow us to focus our investigations on individual subtypes and identify possible lamination defects. Quantitative measures may also detect subtype changes in the distribution of Dscamb-expressing processes.

Dscamb is not required for homotypic avoidance or mosaic spacing in the retina

DSCAM and DSAML1 are required for mosaic spacing, self-avoidance, and neighbor branch spacing in the mouse retina (Fuerst et al., 2008, 2009). In contrast, we did not detect any obvious fasciculation defects when imaging the arbors of individual ACs and RGCs in *dscamb* mutant zebrafish retinas (Figure 3.6), suggesting that Dscamb is not required for retinal self-avoidance. In the absence of good marker for individual subtypes of Dscamb-expressing retinal neurons, however, we did not directly assess RGC and AC mosaic organization or neighbor branch spacing. Since there were no obvious defects in self-repulsion, it seems unlikely that cell body and branch spacing are disrupted to the extent observed in mutant mice.

We also directly assessed the organization of PR subtypes, including rod and red-green double cones (Figure 3.4). The spacing of these cell types was not affected by *dscamb* loss-of-function. In the mouse retina, DSCAML1 facilitates the maturation of rod ribbon synapses. In *dscamb* mutants, cone ribbon synapses appeared normal by EM (Figure 3.5). Thus, Dscamb is not required for the proper distribution of PRs across the retina, or the development of cone synapses.Future studies could assess the development of rod ribbon synapses in these mutants.

Dscamb is not required for programmed cell death in the retina

Knockout of *Dscam* or *Dscaml1* in the mouse retina disrupts programmed cell death, leading to a dramatic increase in cell number in subtypes of neurons expressing these genes, and a visible increase in the INL and IPL (Fuerst et al., 2008, 2009). We did not observe any changes in the thickness of retinal cell layers in homozygous *dscamb* mutants (Figure 3.1), indicating that Dscamb is also not required for programmed cell death in the zebrafish retina. Changes in

volume or cell number have been reported in other regions of the brain in *Dscam* mutant mice. *Dscam* mutant brains are shorter and wider, but are overall larger in size relative to wild-type (Maynard and Stein, 2012). Closer inspection identified enlargement of the midbrain and medulla (Amano et al., 2009; Maynard and Stein, 2012). Conversely, decreased volume has been reported in regions, such as the posterior cortex and hippocampus in *Dscam* mutant mice (Maynard and Stein, 2012), suggesting that DSCAM may have a more nuanced role in programmed cell death death—or possibly proliferation—in different regions of the brain. Thus, a more careful analysis of brain size in mutant zebrafish larvae may identify brain regions where Dscamb is required for establishing proper cell number.

Summary

Through our analyses, we found that Dscamb is expressed across all the major cell types in the retina, but it is particularly prominent in all PRs and a subset of ACs and RGCs. Dscamb-expressing ACs and RGCs also concentrate their projections in particular sublaminae of the IPL. This expression pattern overlaps with both DSCAM and DSCAML1 in mice, suggesting that Dscamb may regulate different aspects of neuronal development. Along these lines, we did not detect any of the characteristic phenotypes described in mice and chick retinas: defective lamination, branch spacing, or cell number. A more detailed characterization of Dscamb-expressing ACs and RGCs may identify more specific markers, allowing us to home our investigations to individual subtypes and possibly detect more subtype defects in lamination or other aspects of neuronal development.

In vivo studies in mice demonstrate that DSCAM promotes the growth and fasciculation of RGC axons en route to the the dorsal thalamus (Bruce et al., 2017). Upon reaching the thalamus, DSCAM regulates the eye-specific segregation of RGC axon terminals in a dosage-dependent

manner (Blank et al., 2011). It would be interesting to investigate if Dscamb also plays a role in the growth and guidance of RGC axons to their downstream synaptic targets, such as the optic tectum.

3.4 ACKNOWLEDGEMENTS

We would like to thank James Fadool for the 5E11 antibody and Malgorzata Kloc for the Hermes antibody. We also thank Marianne Cilluffo and the UCLA Electron Microscopy Core Facility for conducting the histological processing of larvae for TEM. DPJ was supported by a scholarship from the Achievement Rewards for College Scientists (ARCS) Foundation and the UCLA Philip Whitcome Predoctoral Training Program in Molecular Biology. This research was supported by grants to AS from the National Institute of Arthritis and Musculoskeletal and Skin Diseases (R01 AR064582).

3.5 FIGURES

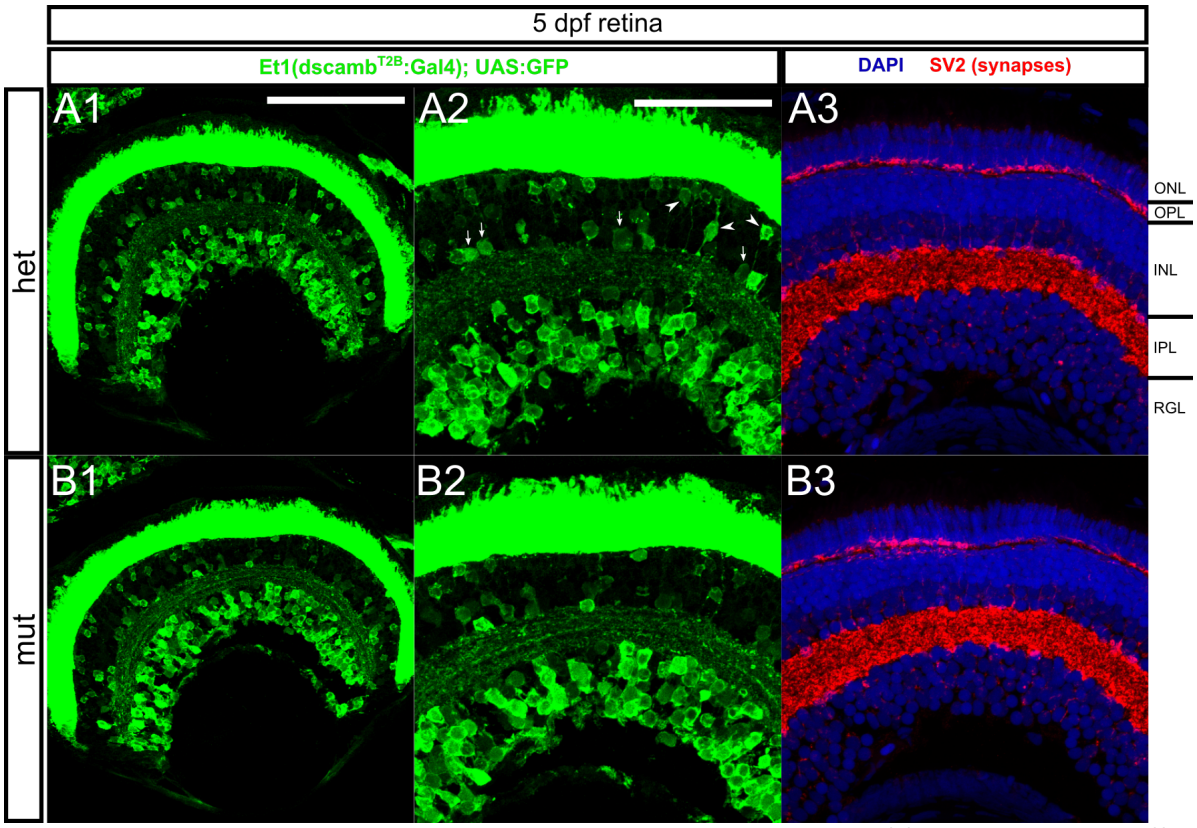

Figure 3.1 Dscamb is expressed in all the major cell layers, but loss-of-function does not affect overall retinal organization

A-B) Et1(dscamb^{t2b}:Gal4) expression (green) in sections from 5dpf heterozygous (A) and homozygous (B) *dscamb* mutant larvae. Dorsal is left and medial is up.

A1 and B1) Confocal image of an entire retinal section. Scale bar: 100um.

A2 and B2) higher magnification images from A1 and B2. White arrowheads: examples of bipolar cell expression, white arrows: examples of amacrine cell expression. Scale bar: 50um.

A3 and B3) Same region as A2 and B2, with nuclei labeled in blue (DAPI) and synaptic vesicles labeled in red (SV2). ONL: outer nuclear layer, OPL: outer plexiform layer, INL: inner nuclear layer, IPL: inner plexiform layer, RGL: retinal ganglion cell layer.

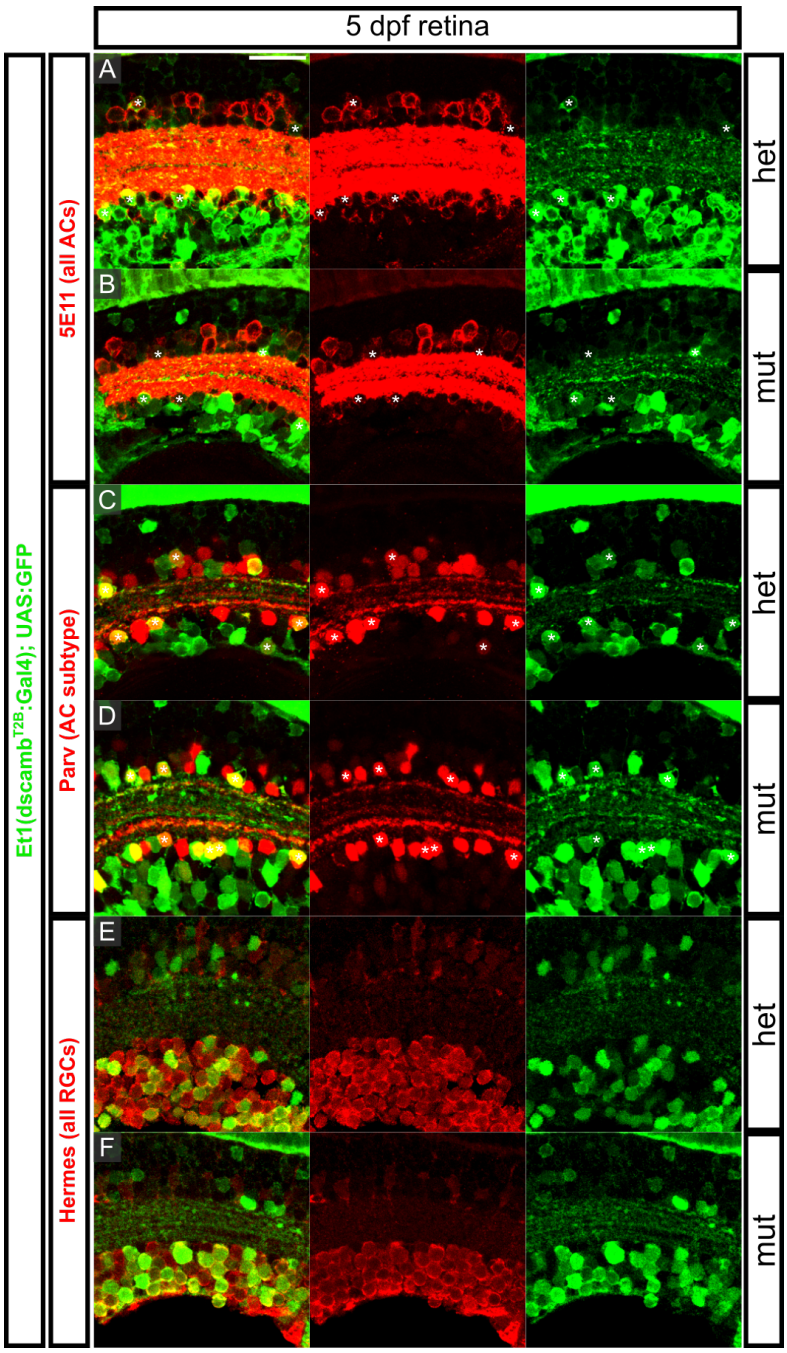

Figure 3.2 Dscamb is expressed in a subtype of amacrine cells and retinal ganglion cells
A-F) Confocal images of the IPL in retinal cryosections from 5dpf heterozygous (A, C, E) and homozygous (B, D, F) *dscamb* mutant larvae. Et1(dscamb^{t2b}:Gal4) expression is labeled in green in all panels. Scale bar in A: 20um.
A and B) Comparison of Et1(dscamb^{t2b}:Gal4) expression to a pan-amacrine cell marker (5E11; red). White asterisks: GFP+/5E11+ amacrine cells.
C and D) Comparison of Et1(dscamb^{t2b}:Gal4) expression to a marker for a subtype of ACs (parvalbumin; red). White asterisks: GFP+/Parv+ amacrine cells.
E and F) Comparison of Et1(dscamb^{t2b}:Gal4) expression to a pan-RGC marker (Herme; red).

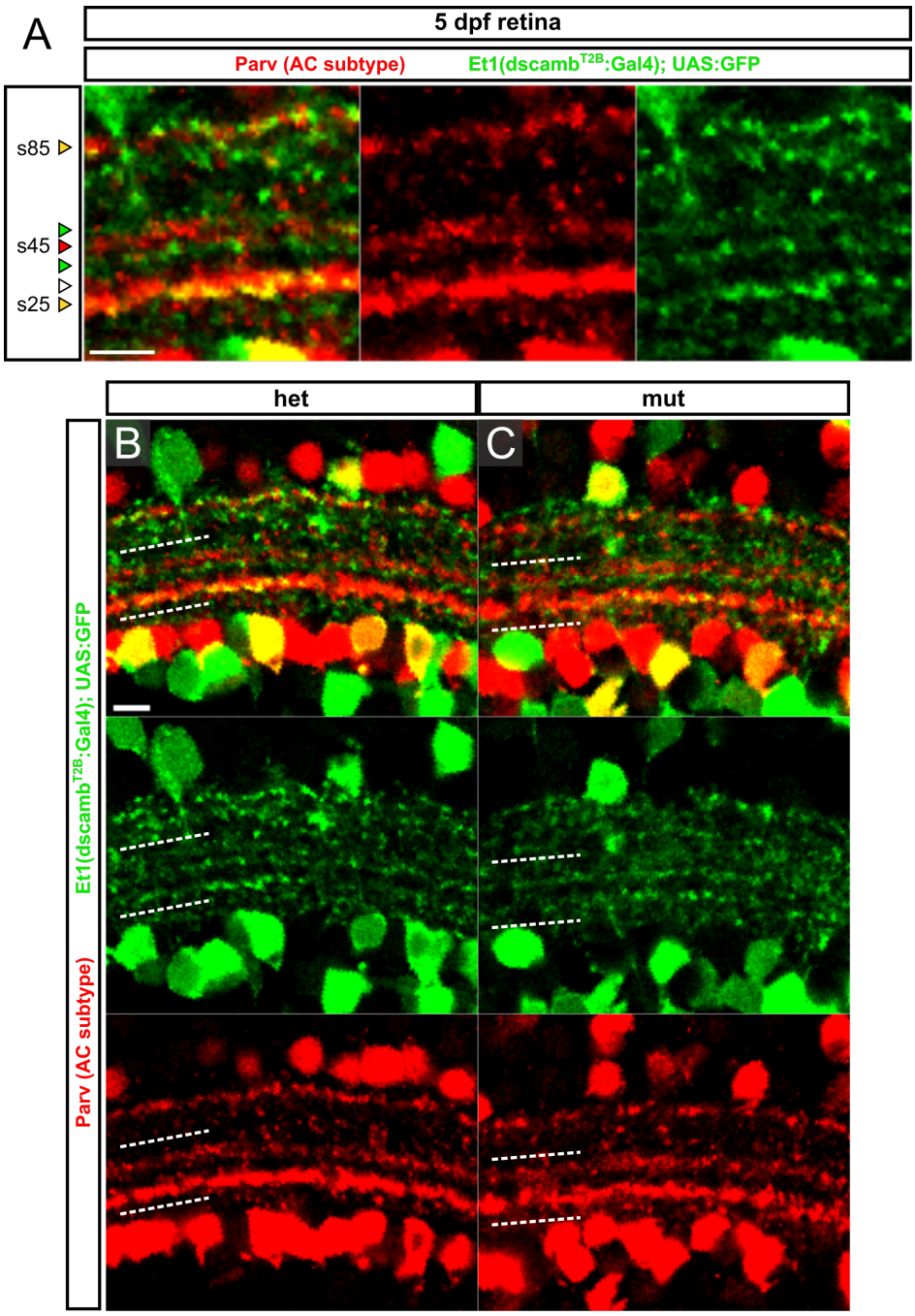

Figure 3.3 Projections from Dscamb-expressing retinal neurons are enriched and depleted in specific sublaminae of the IPL, but these sublaminae are not disrupted in *dscamb* mutants
A-C) Confocal images of the IPL in retinal cryosections from 5dpf heterozygous (A, B) and homozygous (C) *dscamb* mutant larvae. Et1(dscamb^{t2b}:Gal4) is labeled in green and Parv+ amacrine cells in red in all panels.
A) In the left box, s25, s45, and s85 mark previously-identified Parv+ sublaminae in the IPL. The triangles indicate sublaminae that are either GFP+/Parv+ (yellow triangles), GFP+ only (green triangles), Parv+ only (red triangles), or negative for both markers (white triangle). Scale bar: 5um.
B-C) Confocal images of the IPL from 5dpf heterozygous (B) and homozygous (C) *dscamb* mutant larvae. White dashed lines outline the region containing the s25 and s45 Parv+ sublaminae. Scale bar: 5um

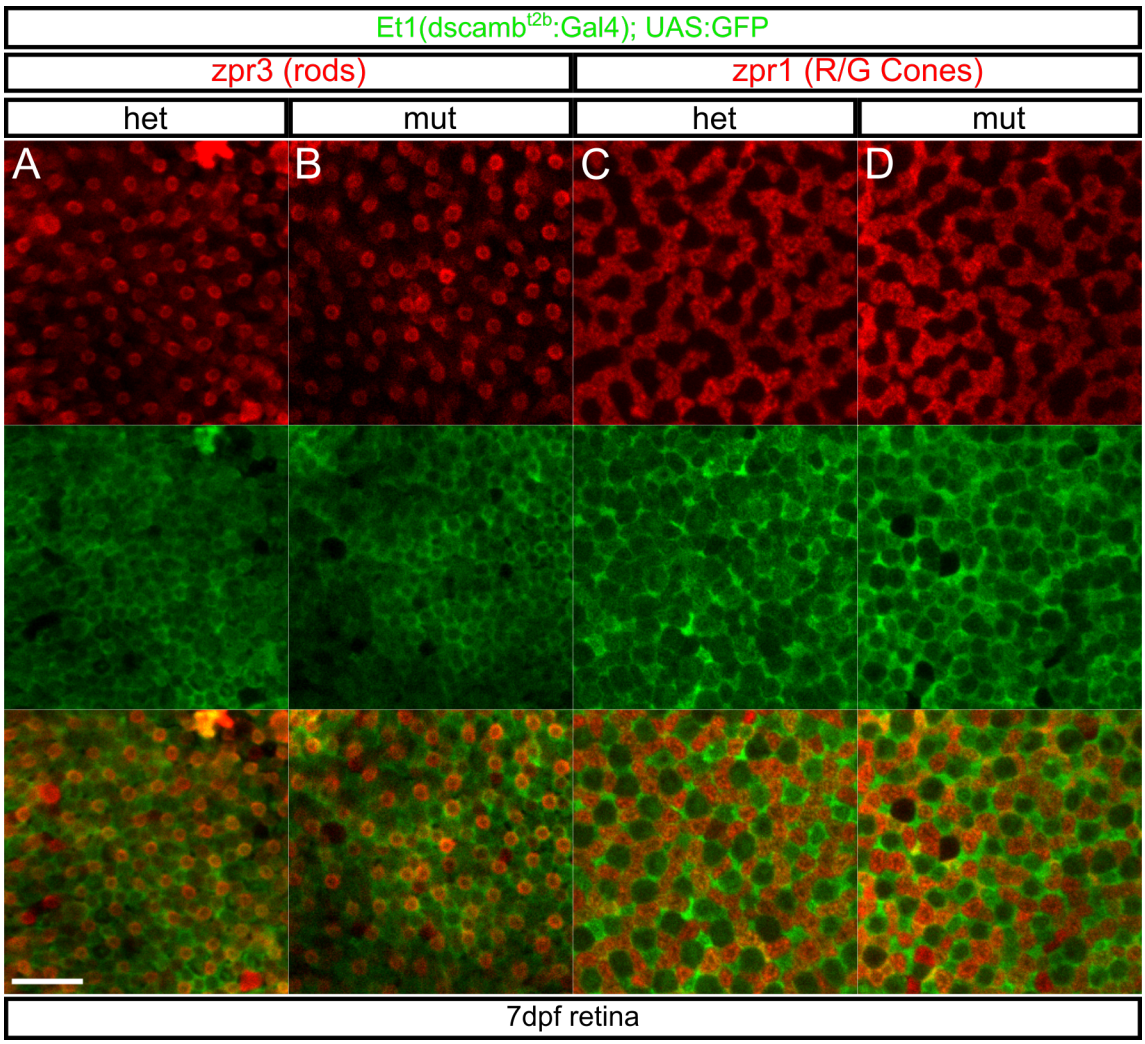

Figure 3.4 Dscamb is expressed in all photoreceptors, but is not required for their proper cell spacing

A and B) Confocal stack through the rod PR synaptic terminals in retinas from 7dpf heterozygous (A) and homozygous (B) *dscamb* mutant larvae. Rod PRs were stained with a specific Ab (zpr3, red) and Et1(dscamb^{t2b}:Gal4) expression is labeled in green. Scale bar in A: 10um.

C and D) Confocal stack through the red and green cone PR nuclei in retinas from 7dpf heterozygous (C) and homozygous (D) *dscamb* mutant larvae. Red and green cone PRs were stained with a specific Ab (zpr1, red) and Et1(dscamb^{t2b}:Gal4) expression is labeled in green.

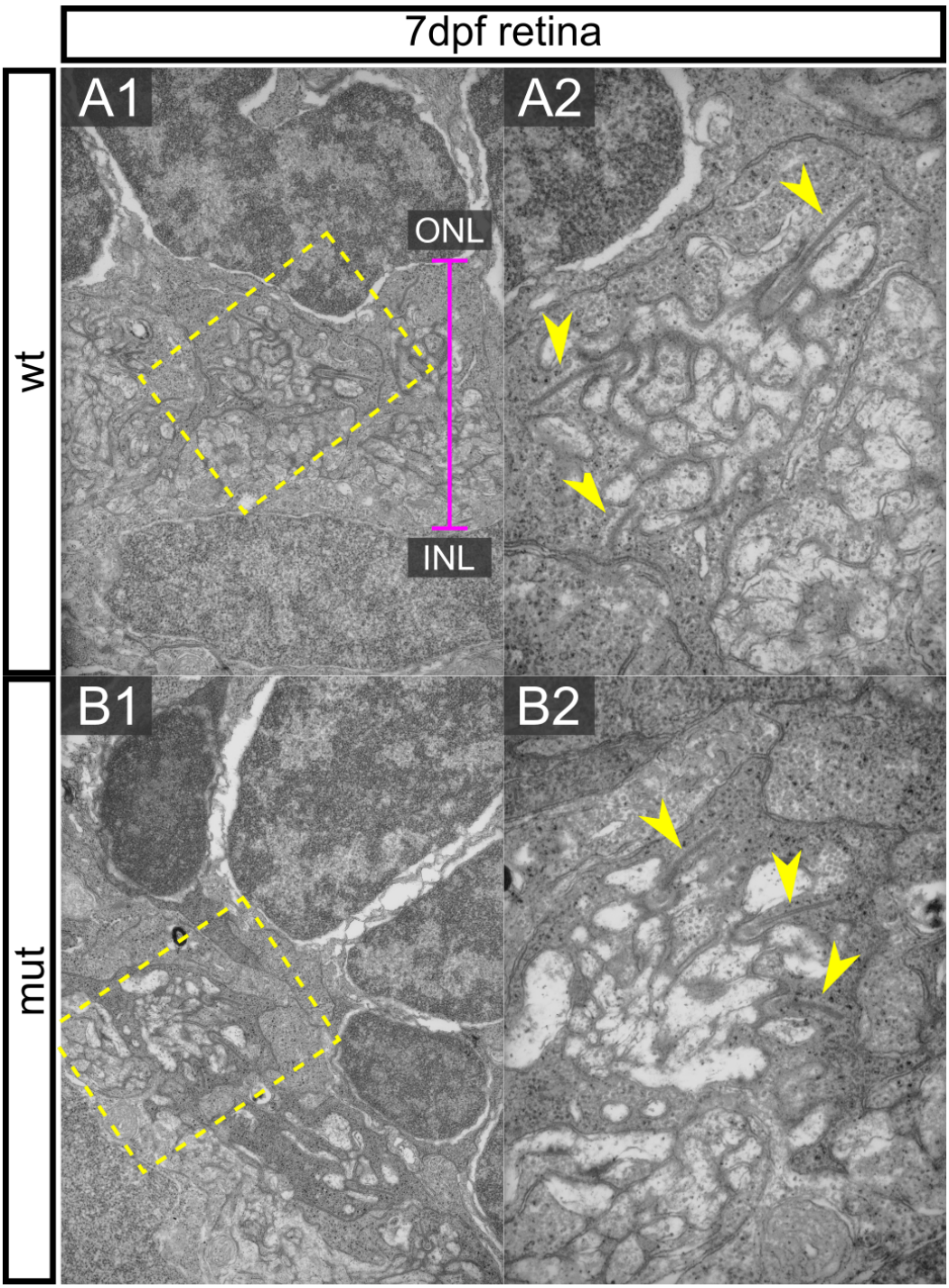

Figure 3.5 Dscamb is not required for cone PR synaptic ribbon development
TEM images of cone photoreceptor synaptic peduncles in 7dpf wildtype (A) and homozygous *dscamb* mutant (B) retinas.
A1 and B1) Images of the OPL (pink bracket). ONL: outer nuclear layer, INL: inner nuclear layer.
A2 and B2) Higher magnification images of the yellow boxed regions in A1 and B1 showing individual cone peduncles in the OPL. Yellow arrowheads indicate synaptic ribbons.

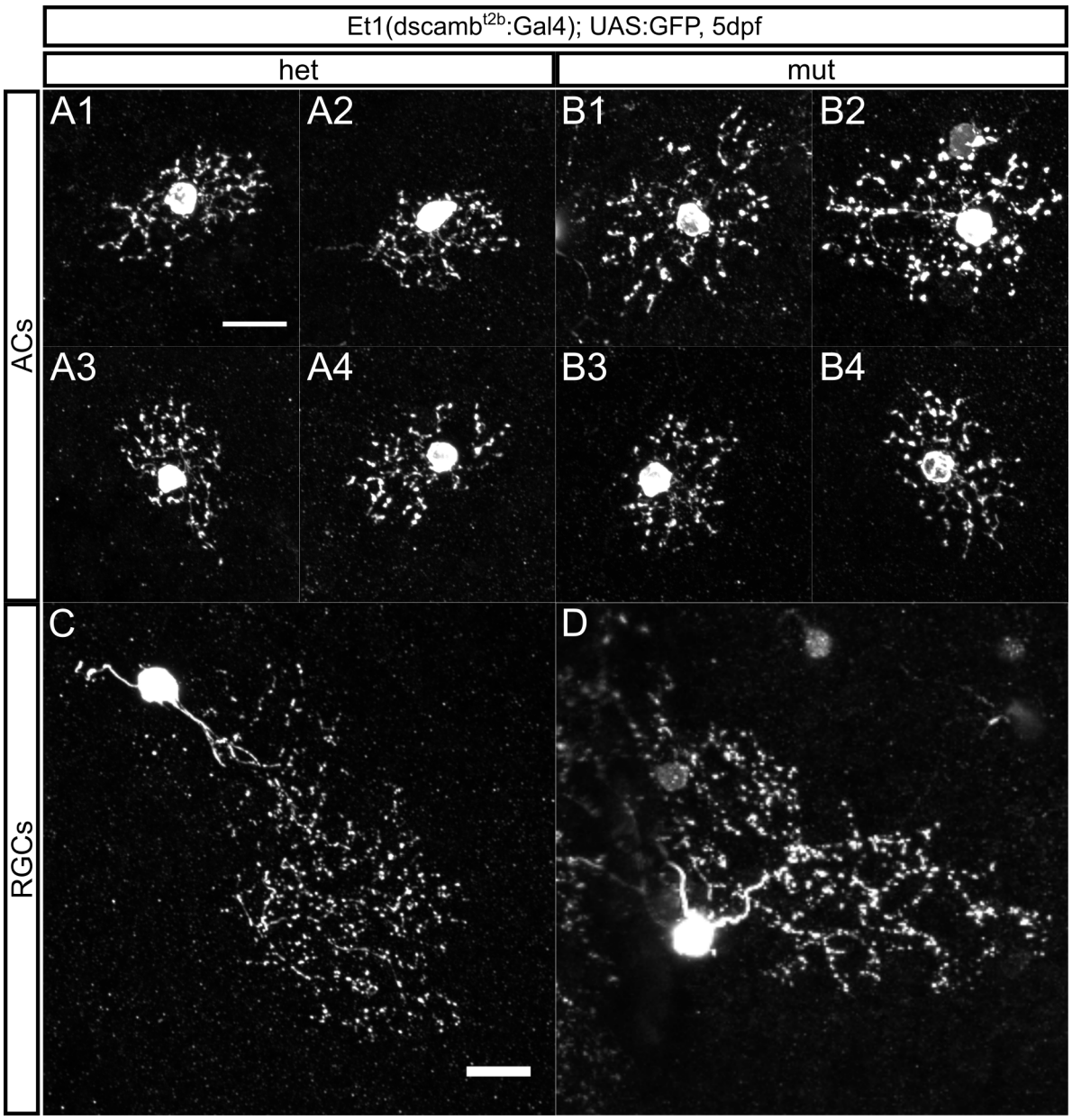

Figure 3.6 *Dscamb* is not required for amacrine and retinal ganglion cell self-avoidance
Sparse Et1(dscamb^{t2b}:Gal4) labeling in individual ACs (A and B) or RGCs (C and D) in 5dpf heterozygous (A and C) and homozygous (B and D) *dscamb* mutant retinas. Scale bars in A1 and C: 10um.

3.6 METHODS

Zebrafish

Zebrafish (Danio rerio) were grown at 28.5°C on a 14 h/10 h light/dark cycle. Embryos were raised at 28.5°C in embryo water (0.3 g/L Instant Ocean Salt, 0.1% methylene blue). For live confocal imaging, embryos were treated with phenylthiourea (PTU) at 24 hpf to block pigmentation. When applicable, embryos and larvae were screened for fluorescent reporter expression using a SteREO Discovery.V12 fluorescent dissecting scope (Carl Zeiss) with a Plan Apo S 1.5x objective. All experimental procedures were approved by the Chancellor's Animal Research Care Committee at UCLA.

Larval fixation and retina cryosectioning

Larvae were prepared for retinal cryosectioning according to a previously published protocol (Uribe and Gross, 2007). In brief, 5 dpf larvae were euthanized on ice in 0.02% tricaine for 10 minutes before being fixed in PBS, 4% paraformaldehyde (PFA) overnight at 4 degrees Celsius. The following morning, embryos were washed three times in PBS for 5 min. Tissue was cryoprotected in PBS, 25% sucrose for 3 hours, followed by PBS, 35% sucrose overnight at 4 degrees. Larvae were then transferred to a small vinyl cryomold (Tissue-Tek) filled with Optimal Cutting Temperature (OCT) compound (Tissue-Tek). After arranging the larvae into an appropriate orientation for cutting, the OCT was flash frozen by floating the cryomold on 100% ethanol, chilled with dry ice. Cryomolds were stored at -80 until cryosectioning.

Cryosectioning was carried out on a Leica CM3050 S cryostat. The specimen and chamber temperatures were set to -16 degrees Celsius and the sectioning thickness was set to 10-12 um. Sections through the retina were captured on positive charge-coated microscope slides (Global Scientific) and stored at -20 degrees until staining. After sectioning, the cryoblocks were

thawed and the remaining tissue from each larva was removed, rinsed in PBS, and lysed for genotyping.

Retinal dissection

5 dpf (for sparse retinal labeling) or 7 dpf (for PR mosaic analysis) were fixed lightly in PBS, 4% PFA for 20 minutes at room temperature, followed by three washes with PBS for 5 min at room temperature. Individual larvae were transferred to a polystyrene petri dish filled with PBS for retinal dissection. Using fine forceps, the body below the head was removed and lysed for genotyping later. After removing the eyes from the head, the retinal pigment epithelium (RPE) was clipped with the fine forceps and the retina was rolled around on the plate. Through gentle rolling, the RPE and lens would adhere to the static charge of the plate and gradually dislodge from the retina. Isolated retinas were then transferred to 0.5 ml centrifuge tubes (Eppendorf), filled with PBS, 0.1% Tween-20, 1% DMSO (PBTD) and stored at 4 degrees until staining.

Sparse retinal labeling

Et1(dscamb^{t2b}:Gal4) heterozygous and homozygous mutant embryos were injected at the single-cell stage with 1-5 nl of a UAS:GFP plasmid (20-40 pg/nl). At 1 dpf, embryos were screened for GFP expression in the retina. At 5 dpf, GFP+ retinas were dissected, and the larval bodies were lysed individually for genotyping. After immunofluorescent labeling for GFP and nuclear staining for DAPI, dissected retinas were flat-mounted for confocal imaging (as described in *Immunofluorescent Staining*). Individual GFP+ ACs and RGCs were distinguished by the positions of their cell bodies in the INL or RGL, respectively.

Immunofluorescent staining

Immunofluorescent staining was carried out using a previously published protocol (Uribe and Gross, 2007), with some modifications. Dissected retinas were stained in 0.5 ml centrifuge tubes. Retinal cryosections were outlined with a hydrophobic PAP pen (Sigma Aldrich), and solutions were pipetted onto the slide (stored in a humidified contained for long incubation times).

Unless otherwise noted, all steps were conducted at room temperature. The tissue was blocked with PBTD, 5% normal goat serum (NGS) (blocking buffer) for 1-2 hours, then incubated with primary antibody diluted in blocking buffer overnight at 4 degrees Celsius. The tissue was rinsed three times with PBTD for 10 minutes. Tissue was incubated in secondary antibody diluted in blocking buffer for 1-2 hours, followed by three washes with PBTD for 10 minutes. To stain nuclei, DAPI was added to the final wash at a concentration of 1 ug/ml. As much PBTD as possible was removed from the slides before coverslipping or mounting.

For retinal cryosections, 40 ul of ProLong Gold Antifade Mountant (Thermofisher) was applied to the sections before coverslipping. Dissected retinas were transferred to a coverslip and clipped 3-4 times with a fine tungsten needle to flatten. Retinas were positioned with the RGL against the coverslip. A small drop of agarose was applied to the retina and allowed to cool for 30 sec, before adding 40-60 ul of ProLong Gold. A dot of vacuum grease was placed in each corner of the coverslip before before applying the microscope slide. Slides were sealed with nail polish and stored at 4 degrees until imaging.

Antibodies

Primary antibodies and dilutions used:

rabbit anti GFP (1:500; Life Technologies A-11122)

mouse anti GFP (1:20; Developmental Studies Hybridoma Bank [DSHB] 12A6)

mouse anti SV2 (1:500; DSHB)

mouse anti 5E11 (1:20; generously provided by James Fadool at Florida State University, Tallahassee, FL) (Hyatt et al., 1996)

mouse anti Parv (1:500; EMD Millipore MAB1572)

rabbit anti Hermes (1:200; generously provided by Malgorzata Kloc at Houston Methodist Research Institute, Houston, TX) (Zearfoss et al., 2004)

mouse anti zpr3 (1:100; Zebrafish International Resource Center [ZIRC])

mouse anti zpr1 (1:100; ZIRC)

Secondary antibodies and dilutions used

Alexa 488 goat anti mouse (1:500; Thermo Fisher)

Alexa 488 goat anti rabbit (1:500; Thermo Fisher)

Alexa 568 goat anti mouse (1:500; Thermo Fisher)

Alexa 568 goat anti rabbit (1:500; Thermo Fisher)

Transmission electron microscopy

Dscamb^{tta} heterozygous adult fish were crossed and the embryos collected. At 3dpf, larvae were anaesthetized and a razor blade was used to dissect a small biopsy of the tail for genotyping, following a previously published protocol (Wilkinson et al., 2013). At 7 dpf, positively identified wild-type, heterozygous, and homozygous mutant larvae were anesthetized and fixed in 4% PFA, 2% glutaraldehyde in PBS, placed on a rotator for 2 hours at room temperature, and incubated at 4 degrees Celsius overnight. Larvae were washed with PBS, postfixed in 1% OsO4 in PB for 1 hour at room temperature, dehydrated in a graded series of ethanol, treated with propylene oxide and infiltrated with Eponate 12 (Ted Pella) (1:1 one hour followed by 1:2

overnight). Larvae were embedded in fresh Eponate, placed under vacuum for several hours and then polymerized at 60oC for 48 hours. Semithin sections (0.2mm) were cut on a RMC MTX ultramicrotome and stained with toluidine blue to identify the area of interest. Approximately 50-60 nm thick sections were cut and picked up on formvar coated copper grids. The sections were stained with saturated uranyl acetate and Reynolds lead citrate and examined on a JEOL 100CX electron microscope at 60kV. Images were collected on type 4489 EM film and the negatives scanned to create digital files.

3.7 REFERENCES

Amano K, Fujii M, Arata S, Tojima T, Ogawa M, Morita N, Shimohata A, Furuichi T, Itohara S, Kamiguchi H, Korenberg JR, Arata A, Yamakawa K (2009) DSCAM deficiency causes loss of pre-inspiratory neuron synchroneity and perinatal death. J Neurosci 29:2984–2996.

Blank M, Fuerst PG, Stevens B, Nouri N, Kirkby L, Warrier D, Barres BA, Feller MB, Huberman AD, Burgess RW, Garner CC (2011) The Down syndrome critical region regulates retinogeniculate refinement. J Neurosci 31:5764–5776.

Bruce FM, Brown S, Smith JN, Fuerst PG, Erskine L (2017) DSCAM promotes axon fasciculation and growth in the developing optic pathway. Proc Natl Acad Sci U S A 114:1702–1707.

de Andrade GB, Long SS, Fleming H, Li W, Fuerst PG (2014) DSCAM localization and function at the mouse cone synapse. J Comp Neurol 522:2609–2633.

Fuerst PG, Bruce F, Tian M, Wei W, Elstrott J, Feller MB, Erskine L, Singer JH, Burgess RW (2009) DSCAM and DSCAML1 function in self-avoidance in multiple cell types in the developing mouse retina. Neuron 64:484–497.

Fuerst PG, Koizumi A, Masland RH, Burgess RW (2008) Neurite arborization and mosaic spacing in the mouse retina require DSCAM. Nature 451:470–474.

Hörnberg H, Wollerton-van Horck F, Maurus D, Zwart M, Svoboda H, Harris WA, Holt CE (2013) RNA-binding protein Hermes/RBPMS inversely affects synapse density and axon arbor formation in retinal ganglion cells in vivo. J Neurosci 33:10384–10395.

Hyatt GA, Schmitt EA, Fadool JM, Dowling JE (1996) Retinoic acid alters photoreceptor development in vivo. Proc Natl Acad Sci U S A 93:13298–13303.

Link BA, Fadool JM, Malicki J, Dowling JE (2000) The zebrafish young mutation acts non-cell-autonomously to uncouple differentiation from specification for all retinal cells. Development 127:2177–2188.

Masland RH (2012) The neuronal organization of the retina. Neuron 76:266–280.

Maynard KR, Stein E (2012) DSCAM contributes to dendrite arborization and spine formation in the developing cerebral cortex. J Neurosci 32:16637–16650.

Nevin LM, Taylor MR, Baier H (2008) Hardwiring of fine synaptic layers in the zebrafish visual pathway. Neural Dev 3:36.

Uribe RA, Gross JM (2007) Immunohistochemistry on Cryosections from Embryonic and Adult Zebrafish Eyes. Cold Spring Harb Protoc 2007:db.prot4779.

Wilkinson RN, Elworthy S, Ingham PW, van Eeden FJM (2013) A method for high-throughput PCR-based genotyping of larval zebrafish tail biopsies. Biotechniques 55:314–316.

Yamagata M, Sanes JR (2008) Dscam and Sidekick proteins direct lamina-specific synaptic connections in vertebrate retina. Nature 451:465–469.

Zearfoss NR, Chan AP, Wu CF, Kloc M, Etkin LD (2004) Hermes is a localized factor regulating cleavage of vegetal blastomeres in Xenopus laevis. Dev Biol 267:60–71.

CHAPTER 4

Dscamb mutant sensory function and behavior

4.1 INTRODUCTION

Our investigations of Dscamb expression identified no obvious structural defects in homozygous *dscamb* mutants. However, Dscamb may be involved in subtle aspects of neuronal development, such as synapse formation or branch spacing, which could be difficult to detect in our analyses. Subtle defects in neural circuit formation could, however, manifest in detectable deficits in sensory or motor function. Indeed, behavioral defects have been reported in DSCAM mutant flies and mice. For instance, analysis of visual perception in *dscam2* mutant flies showed that while mutant flies can see, they move in the opposite direction of wild-type controls in response to moving stimuli (Bosch et al., 2015). Dscam overexpression in Drosophila scutellar mechanosensory neurons, which disrupts their synaptic targeting of the ventral nerve cord, reduced their ability to detect touch stimuli (Cvetkovska et al., 2013). *Dscam* mutant mice have defective motor coordination and impaired sensory reflexes (Xu et al., 2011; Lemieux et al., 2016; Thiry et al., 2016), which correlated with synaptic changes onto motor neurons in the spinal cord (Thiry et al., 2016). *Dscam* mutant mice also show signs of vestibular defects. For example, postnatal day two mice struggle to maintain balance and frequently rest on their backs. Adult mutant mice fail to stay afloat or swim in a straight line (Fuerst et al., 2010). Both of these defects indicate defects in the ability to sense and maintain equilibrium, suggesting that DSCAM could be required for proper development of the vestibular system, although these behaviors have not been quantitatively analyzed or investigated at the molecular and cellular scale.

Our enhancer trap revealed Dscamb expression in all of the major sensory systems: olfactory, gustatory, visual, auditory, lateral line, and somatosensory (Figure 2.5). Although we did not detect any obvious defects in the organization of these sensory systems, we hypothesized that more subtle defects may be detectable at the behavioral level and allow us to home in on particular sensory pathways for more detailed cellular analyses. To test this hypothesis and

characterize the role of Dscamb in sensorimotor development, we subjected *dscamb* mutant larvae to a series of sensory behavioral assays.

4.2 RESULTS

Dscamb is not required for somatosensory, visual, and auditory function

Somatosensory responses

Dscamb is expressed in trigeminal and Rohon-Beard somatosensory neurons at early developmental stages, when these sensory neurons are first innervating the skin. Although in *dscamb* mutants, the overall architecture of RB peripheral sensory axons appeared normal (Figure 2.3), it is possible that subtle defects in the association between RB neurons, the skin, or downstream synaptic partners caused defects in somatosensation. To analyze somatosensory function, we lightly touched 3 dpf zebrafish larvae on the tail three times and recorded the number of touch trials that elicited an escape behavior, comparing touch responses between wild-type, heterozygous, and homozygous *dscamb* mutants (Figure 4.1A). In all three genotypes, all three touch trials elicited an escape response in the majority of larvae. There was no statistically significant difference in the distribution of responses of wild-type larvae, heterozygous and homozygous mutant larvae (wt-het: $p = 0.127$, wt-mut: $p = 0.332$), indicating that Dscamb is not required for the detection of touch stimuli in zebrafish larvae.

Visual responses

To assess visual responses, we first analyzed larval pigmentation changes in response to light. On a dark background, zebrafish melanocytes spread out their melanosomes across their stellate cell projections, creating a dark appearance; when exposed to a light background, melanosomes aggregate, giving larvae a paler appearance. This visually-mediated background adaptation (VBA) is controlled by a neuroendocrine circuit dependent upon RGCs signaling to

the hypothalamus (Neuhauss et al., 1999). We compared the VBA response between wild-type, heterozygous, and homozygous *dscamb* mutants (Figure 3.1C). At 7 dpf, larvae that had adapted to a dark environment for several hours were placed under a bright light for at least 30 minutes. We segregated fish with a light pigmentation pattern (appropriate VBA response) from those that maintained dark pigmentation (failed VBA). Similar proportions of wild-type, heterozygous, and homozygous mutants adjusted their pigmentation appropriately in response to a bright environment (light-adapted percentage: wild-type = 63%, heterozygous = 73%, homozygous = 74%; Fisher's exact test: $p = 0.725$), demonstrating that *dscamb* mutants have at least a partially functional RGL in the retina.

Zebrafish, and many other organisms, have a tendency to swim in the direction of a moving stimulus. This behavior, called the optomotor response (OMR), can be observed in larval zebrafish as early as 6 dpf (Fleisch and Neuhauss, 2006). We assessed the OMR in *dscamb* heterozygous and homozygous mutants at 7 dpf by placing fish in a circular arena lined with arrays of computer-controlled LEDs (Figure 4.1B). The LED arrays allowed us to project rotating bar stimuli with precise control over its width and rotational speed. In each experiment, 4 larvae were tested simultaneously, with each larva occupying its own petri dish (35mm diameter). We presented larvae with a stimulus that fluctuated in direction and angular speed along a 0.05 Hz sine wave and recorded the response of each larva on video camera. Each fish was exposed to six consecutive stimulus trials, where the direction of rotation changed between trials. For each trial, larval swimming responses were scored on a 1-3 scale: 1 = swimming in the opposite direction of the stimulus, 2 = direction of swimming uncertain, 3 = swimming in the same direction as the stimulus. For each fish we averaged the response scores across all 6 trials and found the median average score for both heterozygous and mutant homozygotes was the same (median score = 2.17; n = 31 heterozygotes; n = 40 homozygotes). The distribution of OMR

responses was similar between the two genotypes (Fisher's exact test: p = 0.379), demonstrating that *dscamb* mutants have a functional retina.

Auditory responses

DSCAM mutant mice show some evidence of vestibulocochlear defects, although these phenotypes have not been thoroughly investigated (Fuerst et al., 2010). Our Dscamb BAC and enhancer trap lines corroborated expression in all of the otic hair cell patches (Figures 2.2 and 2.5). The enhancer trap was also observed in statoacoustic axons innervating the ovHCs, suggesting that Dscamb could be required for statoacoustic sensory transduction. We used a prepulse inhibition assay to characterize auditory function in larval *dscamb* mutants (Figure 4.1D,E). PPI is a well-studied phenomenon in which the presentation of an initial, weak stimulus inhibits the behavioral response to a second stronger stimulus. This effect has been observed across different species and sensory systems, and, in zebrafish, is a more sensitive measure of auditory function than standard acoustic startle response assays (Bhandiwad et al., 2013). 6-8 dpf larvae were exposed to a strong startle-inducing acoustic stimulus either by itself or preceded by a weaker non-startling stimulus, and their escape responses (c-bends) were recorded using a high-speed camera. The inhibitory effect of the prepulse on the startle response was then calculated by comparing these two trial types. We found no significant differences in PPI between wild-type, heterozygous, and homozygous mutant embryos. The latency of the c-bend responses was also similar between genotypes, indicating that Dscamb is not required for auditory function or gross motor function.

Dscamb mutants die during the first month of life and have defective feeding behavior

Mortality

In the absence of marked sensory defects in *dscamb* mutant larvae, a more detailed characterization of *dscamb* mutant mortality could point to underlying mechanisms. To determine the timeline of *dscamb* mutant mortality, we crossed *dscamb* heterozygotes, genotyped their offspring at regular timepoints between 7 and 60 dpf, and compared the proportion of wild-type, heterozygous, and homozygous mutant siblings to the theoretical Mendelian inheritance (0.25 : 0.5 : 0.25, respectively) (Figure 4.2A). We observed a gradual, albeit fluctuating, downward trend in the survival of homozygous mutants, which reached statistical significance at 16 dpf (Fisher's exact test: $p = 0.0455$). Although the proportion of genotypes was not statistically different at 19 dpf ($p = 0.2473$), by 34 and 60 dpf ($p = 0.0013$, $p = .0017$, respectively) there were significantly fewer mutants. Homozygous mutants did not survive to 60 dpf. The gradual loss of *dscamb* mutants indicates a defect in survival that may vary between individual fish, enabling some homozygous mutants to survive longer than others.

Feeding analysis

We hypothesized that a deficit in feeding could cause the gradual lethality of *dscamb* mutants. Zebrafish larvae begin to acquire their nutrients from exogenous food sources at ~7 dpf, when the yolk sac is completely absorbed. In the absence of food, larvae perish from starvation, starting around 10 dpf, and completely succumb by 15 dpf (Versonnen et al., 2004; Wilson, 2012). Since we first observed a statistically significant decline in *dscamb* mutants at 16 dpf, we hypothesized that *dscamb* mutants may have a deficit in either finding or capturing food. To assess food intake, we exposed 7 dpf zebrafish embryos to larval food coated with fluorescent microspheres (Figure 4.2B-D). After allowing fish to feed on the fluorescent food for 90 minutes, we assessed food intake into the foregut (anterior intestine). Larvae were categorized as having full, empty, or partially-filled foreguts (Figure 4.2B). Wildtype and heterozygous mutants had a similar ability to ingest food (Fisher's exact test, Bonferroni-corrected: wt x het: $p = 0.807$), but homozygous mutants showed a marked increase in the proportion of larvae with empty or

partially-filled foreguts, and a corresponding decrease in the number of full larvae, compared to wild-type and heterozygotes (Fisher's exact test, Bonferroni-corrected: wt x mut: $p < 0.001$, het x mut: $p < 0.001$) (Figure 4.2D). Between wild-type and homozygous mutants, the proportion of larvae with empty foreguts increased fourfold, from 12.5% to 46.5%, while the number of full larvae decreased five fold (76.8% wild-type to 15.1% mutants). It is possible that the paucity of full homozygous mutants is caused by an increased rate of food evacuation from the intestine. To rule out this possibility, we selected larvae with full stomachs and time-lapse imaged the transit of food through the gut between 2 and 6 hours post-feeding (data not shown). Because few mutants started off with full foreguts, and because we were blind to genotype when performing the experiment, we were only able to image two homozygous mutants in this analysis. Nonetheless, we found no evidence that food moved through the gut more rapidly in homozygous mutants. In summary, *dscamb* homozygous mutants have an impaired ability to capture food, suggesting that Dscamb plays an important role in the development or maintenance of neuronal systems or muscles that mediate feeding behavior.

Gulping behavior

In Chapter 2, we found that Dscamb is expressed in muscles that regulate the opening and jaw movement (Figures 2.5 and 2.8). We hypothesized that Dscamb may be required for the proper activation and coordination of these muscle fibers as defects in these processes would provide a plausible explanation for the mutant feeding phenotype. To determine if there were functional defects in jaw movement, we immobilized awake, behaving 7 dpf larvae in 3% methylcellulose and time-lapse imaged their spontaneous jaw movements (or "gulps") (Figure 4.2E). Over a 20 second imaging period, we observed no difference in the median number of gulps between heterozygous and homozygous *dscamb* mutant siblings (median: het = 21, mut = 19 gulps/20sec; Mann-Whitney-Wilcoxon p-value = 0.9872). A more detailed analysis of jaw behavior would be required to rule out subtle defects, such as the speed or amplitude of mouth

openings, but our results demonstrate that *dscamb* mutants are capable of at least some degree of jaw function.

4.3 DISCUSSION

Dscamb is not required for somatosensory, visual, auditory, or motor function

Dscamb is expressed in primary sensory neurons in the somatosensory (trigeminal and RB neurons), visual (PRs), and statoacoustic (ovHCs) sensory systems. We also identified expression in cell types of downstream circuitry in the statoacoustic (statoacoustic ganglion) and visual systems (HCs, BCs, ACs, and RGCs). Despite this intriguing expression pattern, we did not identify any defects in the function of these three sensory pathways (Figure 4.1). We previously noted abundant Dscamb expression in motor axons innervating the muscle fibers along the trunk, suggesting that it could be required for motor neuron development or function. However, *dscamb* mutants respond with normal latencies to auditory stimuli, indicating normal motor function (Figure 4.1D).

For assessing visual function, it is possible that our optomotor analysis was not sensitive enough to detect possible defects in visual function. Our optomotor assay was categorical, but quantitative measures of OMR have also been used by other labs, in addition to other visually-elicited behaviors, such as the optokinetic response for assessing visual function (Bilotta and Saszik, 2001; Muto et al., 2005). In future experiments, we could use these more sensitive assays to better interrogate the function of Dscamb in visual function.

Dscamb mutants respond normally to a physical touch stimulus. However, as we reported in Chapter 2, Dscamb is expressed in a subtype of RB somatosensory neurons (Figure 2.6), which could mediate the detection of a different sensory modality such as chemical or thermal stimuli.

Dscamb-expressing neurons partially overlap with the chemosensory TrpA1b-expressing subtype (Prober et al., 2008; Palanca et al., 2013). Other sensory ion channels, including TrpV1 (Gau et al., 2013) and piezo2b (Faucherre et al., 2013), are expressed in RB subtypes and detect specific types of stimuli. Further characterization of Dscamb expression relative to other sensory channels, coupled with thermal and chemosensory behavior assays could uncover a particular somatosensory modality for Dscamb-expressing neurons and suggest a possible role in their development.

Dscamb mutant mortality is likely due to defective feeding

Dscamb mutant larvae are impaired in their ability to take in food (Figure 4.2C,D), providing a plausible behavioral mechanism for homozygous mutant mortality around 2-3 weeks post-fertilization (Figure 4.2A). This finding raises the question: What is the neurodevelopmental basis for defective food intake in *dscamb* mutant larvae? A recent study provides convincing evidence that hindbrain branchiomotor neurons are indispensable for feeding behavior in zebrafish (Allen et al., 2017). In particular, it was found that genetic, chemical, or laser ablation of branchiomotor caused a dramatic decrease in larval food intake that was strikingly similar to what we observed in *dscamb* mutants. This raises the intriguing possibility that Dscamb could be required for the development of branchiomotor circuits. In zebrafish, food intake requires the coordinated interaction of jaw and opercular/gill muscles (Allen et al., 2017). In Chapter 2, we identified Dscamb expression in many of these muscle fiber groups, which are located on the lateral and ventral side of the head, although we did not detect any obvious structural defects in homozygous mutants (Figures 2.5 and 2.8).

Jaw muscles receive innervation from facial and trigeminal branchiomotor neurons, while gill muscles are controlled primarily by vagal branchiomotor neurons (Schilling and Kimmel, 1997).

Abundant Dscamb expression in the brain made it difficult to assess whether Dscamb is expressed in the branchiomotor nuclei. However, using the more sparsely expressed BAC reporter, we identified Dscamb expression in the vagal branchiomotor nucleus (Figure 2.2F). In future experiments, we could combine our enhancer trap with known reporters for branchiomotor neurons to determine if Dscamb is also expressed in the trigeminal and facial motor nuclei. Using the nbt:dsRed reporter to distinguish branchiomotor axons, we found that both ventral and lateral muscle fibers received motor innervation in *dscamb* mutants. However, more detailed morphological analysis could identify defects in the organization of the motor axon terminals. In certain cell types, such as cortical neurons (Maynard and Stein, 2012) and rod PRs (Fuerst et al., 2009), *Dscam* loss-of-function causes defect in synapse formation and maturation even in the absence of changes in neuronal morphology. A critical experiment would be to analyze the organization of branchiomotor neuromuscular junctions using pre- and postsynaptic markers.

Our analysis of gulping behavior demonstrated that *Dscamb* mutants can open and close their mouths, suggesting that there are some functional neuromuscular junctions (Figure 4.2E). However, spontaneous gulping behavior is unlikely to be a reliable measure for the motor patterns that are required for feeding. Fish capture food through a process called “suction feeding,” where upon approaching potential prey they open their their mouth and expand their oral cavity to create an inward flow that forces the prey into the mouth. This complex motor behavior requires the coordinated movement of the jaw, operculum (gill cover), and gills (China and Holzman, 2014). A more detailed analysis of feeding behavior, perhaps in response to a potential prey item, may defects in particular motor programs or stages of the process that underlie the mutant phenotype.

Feeding behavior is likely modulated by input from multiple sensory systems in the brain, such as the visual, olfactory, and gustatory systems. For instance, laser ablation of the retinotectal neuropil impairs prey capture in larval zebrafish (Gahtan et al., 2005), and surgical lesion of the olfactory tract reduced odorant-induced feeding behaviors in carp (Hamdani et al., 2001). Dscamb was expressed in the olfactory (ORNs and the olfactory bulb) and gustatory (facial, glossopharyngeal, and vagal ganglia) sensory systems, both of which are important for zebrafish feeding behavior (Hamdani et al., 2001; Okada, 2015). We were unable to find an olfactory behavioral assay that worked reliably in our hands, and gustatory assays usually involve assessing food intake (Okada, 2015), the interpretation of which would be confounded by possible defects in branchiomotor function. Therefore, we were unable to analyze the olfactory and gustatory sensory systems, making it possible that deficits in these sensory modalities could contribute to the feeding phenotype.

It is possible that defective neuronal systems mediating satiety or appetite could also contribute to the reduced feeding in *dscamb* mutants. For instance, it has been reported that larval zebrafish feeding state influences their response to whether a visual stimulus is perceived as either food or a potential predator (Filosa et al., 2016). When exposed to moving visual stimuli of different sizes, zebrafish will approach small objects, but avoid larger objects, suggesting that they perceive these stimuli as either prey or predatory, respectively. Interestingly, fish that have been recently fed are more likely to avoid smaller objects than fish that have been starved. This shift in preference is regulated by neuroendocrine signaling from the hypothalamus-pituitary-interrenal axis and serotonergic system. It would be interesting to determine if these systems are disrupted in *dscamb* mutants.

Summary

Thus, feeding is a complex behavior that is modulated by input from multiple sensory and neuroendocrine systems and requires the coordinated output of multiple muscles groups. Due to the broad neuronal expression pattern of *dscamb*, identifying which of these disparate systems is affected in mutant larvae could prove challenging. One approach would be to use a more complex behavioral analysis, such as a prey capture assay, to identify the specific point in the feeding process—either the detection, approach, or capture—that mutants are failing to ingest food. Alternatively, we could use transgenic promoters to drive expression of Dscamb in specific cell types, such as branchiomotor, sensory, or hypothalamic neurons, and assess whether this rescues the phenotype.

4.4 ACKNOWLEDGEMENTS

We would like to thank Mark Frye for setting up an LED array for us to use in his lab, and for providing guidance in testing zebrafish OMR responses. We also thank Joshua Barrios in Adam Douglass' lab for conducting the auditory behavioral assays. DPJ was supported by a scholarship from the Achievement Rewards for College Scientists (ARCS) Foundation and the UCLA Philip Whitcome Predoctoral Training Program in Molecular Biology. This research was supported by grants to AS from the National Institute of Arthritis and Musculoskeletal and Skin Diseases (R01 AR064582).

4.5 FIGURES

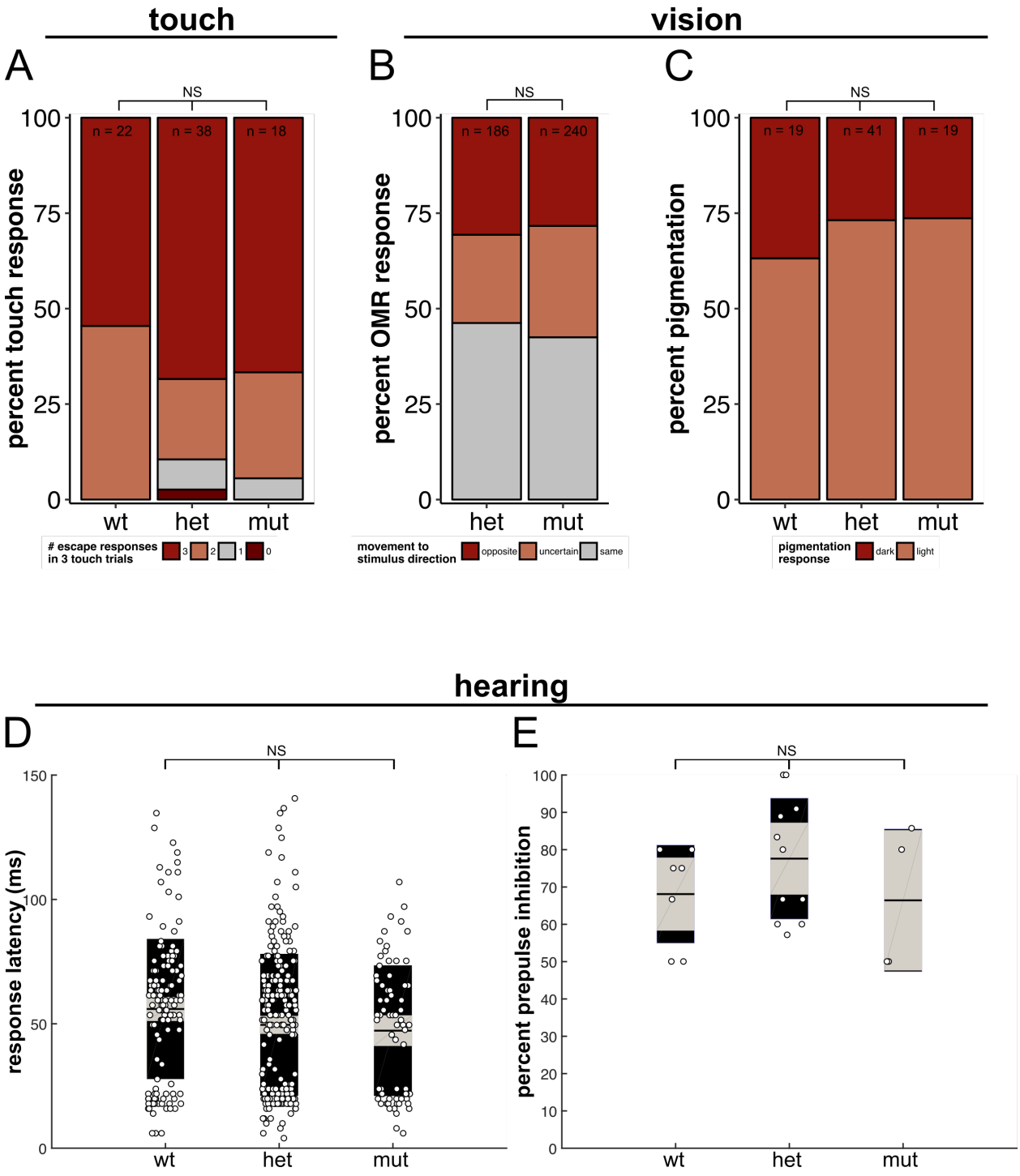

Figure 4.1 *Dscamb* is not required for somatosensory, visual, or olfactory function
A) Percentage of 2 dpf wildtype, heterozygous, and homozygous *dscamb* mutant larvae that responded with 0, 1, 2, or 3 escape behaviors in during three 3 trials of lightly touching their tails with a probe. Fisher's exact test of independence: p = 0.40
B) Optomotor response (OMR). Percentage of trials in which 7dpf heterozygous and homozygous mutant *dscamb* larvae that responded to a rotating visual stimulus by either moving in the same, opposite, or an

uncertain direction, relative to direction of the stimulus rotation. Each fish was exposed to 6 trials with the stimulus changing directions between each trial. 31 het larvae were tested for a total of 186 trials. 40 mut larvae were tested for a total 240 trials. Fisher's exact test of independence: p = 0.39.
C) Visually-mediated background adaptation. Percentage of 7dpf larvae of each genotype that adapted their pigmentation either correctly (light) or incorrectly (dark) in response to a bright background. Fisher's exact test: p = 0.72.
D) Auditory startle response latency. Latency time between the application of a startle-inducing acoustic stimulus and escape behavior in 6-8dpf larvae of each genotype. Middle black bar: mean. Grey boxes: 95% confidence intervals. Outer black boxes: one standard deviation. Each data point is one trial, and each fish was tested in 30 trials. n fish = 7 wt, 11 het, 4 mut; therefore, n trials = 210 wt, 330 het, 120 mut. ANOVA: p = 0.46.
E) Pre-pulse inhibition (PPI). 6-8dpf larvae of each genotype were exposed to 15 startle-only trials and 15 PPI trials (sub-startle stimulus, following by a stronger startle-stimulus). The percent PPI for each fish was calculated as [(% of startle trials showing short-latency C-bends) – (% of PPI trials showing short-latency C-bends)] / (% of startle trials showing short-latency C-bends) * 100. Each data point is one fish (the same fish tested in D): n = 7 wt, 11 het, 4 mut. ANOVA: p = 0.98.

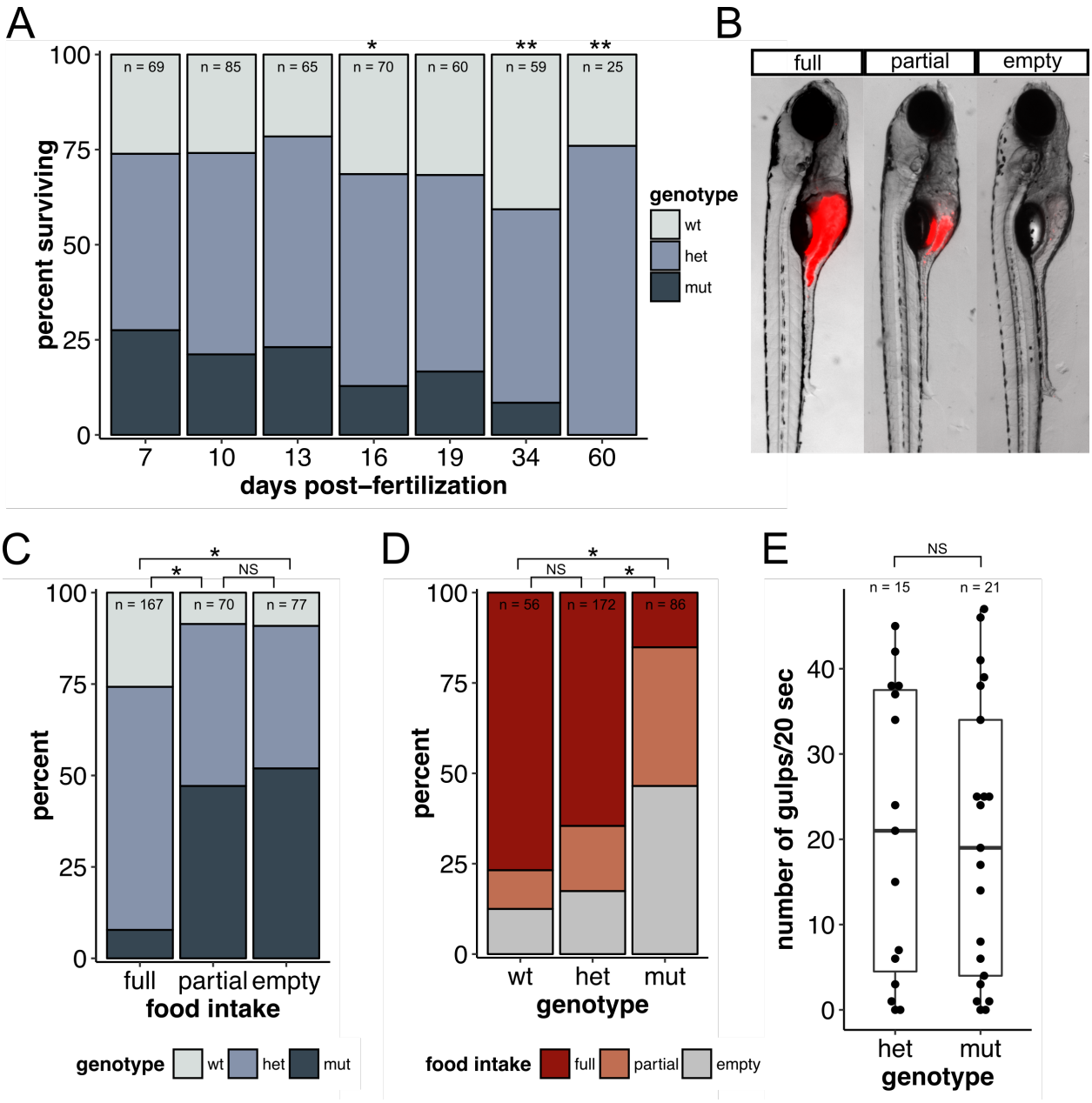

Figure 4.2 Dscamb mutants have defective feeding behavior and die at 2-3 weeks of age
A) *Dcamb* mutant mortality. After crossing heterozygous *dscamb* mutant fish, we sacrificed and genotyped offspring at different time points post-fertilization and quantified the percentage of offspring of each genotype. Multinomial exact test for goodness-of-git (predicted proportions wt:het:mut = 0.25:0.75:0.25) p-value for each time point: 7dpf = 0.80, 10dpf =0.74, 13dpf =0.73, 16dpf =0.046, 19dpf =0.25, 34dpf =0.0013, 60dpf =0.0017.
B) Example images of different states of food intake after exposing 7dpf larvae to fluorescently-labeled food.
C) Percentage of 7dpf fish in each food-intake state that were wild-type, heterozygous, or homozygous mutants after being exposed to fluorescently-labeled food. Fisher exact test of independence across all groups: p = 0.00050. Post-hoc Fisher's exact test with Bonferroni correction: full x partial p = 1.2e-10, full x empty p = 4.1e-13, partial x empty p = 1.0.

D) Same data as in C, broken down by the percentage of 7dpf fish in each genotype with full, partial, or empty foreguts. Fisher exact test of independence across all groups: p = 0.00050. Post-hoc Fisher's exact test with Bonferroni correction: wt x het p = 0.81, wt x mut p = 2.2e-12, het x mut p = 1.8e-13.
E) Quantification of the number of gulps during a 20sec movie for 7dpf heterozygous and homozygous mutants. Each data point represents one fish. Mann-Whitney-Wilcoxon test: p = 0.99. Middle box line is the median; lower and upper ends of the boxes are 25^{th} and 75^{th} percentiles, respectively. Data points outside of the whiskers are considered outliers.

4.6 METHODS

Zebrafish

Zebrafish (Danio rerio) were grown at 28.5°C on a 14 h/10 h light/dark cycle. Embryos were raised at 28.5°C in embryo water (0.3 g/L Instant Ocean Salt, 0.1% methylene blue). For live confocal imaging, embryos were treated with phenylthiourea (PTU) at 24 hpf to block pigmentation. When applicable, embryos and larvae were screened for fluorescent reporter expression using a SteREO Discovery.V12 fluorescent dissecting scope (Carl Zeiss) with a Plan Apo S 1.5x objective.

Touch assay

At 2 dpf, individual wild-type, heterozygous, and homozygous *dscamb*^{tz2b} mutant larvae were isolated in a petri dish and subjected to three touch trials. For each touch trial, a small metal needle was used to light graze the tail, and whether the larva responded with a movement or escape behavior in each of the three touch trials was record. Each touch trial was separated by at least 10 seconds. After testing behavior, individual fish were lysed for genotyping. The experimenter was blind to genotype while testing.

Visually mediated background adaptation assay

At 7 dpf, wild-type, heterozygous, and homozygous *dscamb*^{tz2b} mutant siblings were placed in the dark for several hours to adapt to adapt their pigmentation to a dark environment. Larvae were then placed under bright illumination from gooseneck lamps. After allowing at least 30 minutes for pigment adaptation. Pigmentation was assessed on a dissecting microscope and larvae were separated into either light (correct background adaptation) or dark (incorrect background adaptation) pigmentation groups and lysed for genotyping. The experimenter was blind to genotype while testing.

Optomotor response assay

At 7 dpf, Et1(dscamb:Gal4), Tg(UAS:GFP) heterozygous and homozygous mutant fish were transferred to a 35 mm petri dish inside circular arena lined with arrays of computer-controlled LEDs. Using MatLab software, the illumination of the LED arrays was coordinated into bar stimuli that rotated across the circumference of the chamber. The angular velocity and direction of the rotating stimuli was adjusted along a 0.05 Hz sine wave. Thus, during a 60 sec testing period, the rotating stimulus changed directions six times. Four larvae, each in their own petri dish were tested simultaneously during each experiment, and their movement was recorded on a camera positioned above the testing chamber. After testing, individual larvae were lysed for genotyping.Each change of the stimulus direction was counted as one trial. For each trial we ranked the swimming behavior of each fish on a 1-3 scale: 3 = movement in the same direction as the stimulus; 2 = movement in an uncertain direction, relative to the stimulus; 1 = movement in the opposite direction of the stimulus. Scoring was conducted by an observer that was blind to genotype. These categorical measures were used to calculate an average OMR score for each fish, or to calculate the percentage of trials for each genotype that had a score of either 1, 2, or 3.

Auditory response assay

Larval fish 6-8 dpf were placed in custom made agarose chambers flooded with E3 solution and imaged with a Pike IEEE 1394b camera (Allied Vision Technologies) at 544 frames per second. Startle stimuli consisted of 10ms, 1 KHz acoustic/vibrational pulses delivered by a speaker mounted directly to the imaging platform 6cm away from the dish. Image acquisition and stimulus delivery were driven using custom software written in LabView (National Instruments). At the end of the experiment, individual larvae were lysed for genotyping.

For prepulse inhibition (PPI) testing, each dish was subjected to fifteen startle-only trials and fifteen PPI trials. PPI trials consisted of a non-startling prepulse followed by a startling stimulus with a 400ms inter-stimulus interval. Startle stimulus amplitude was defined as the lowest amplitude that evoked c-bend startle behaviors in at least 90% of embryos over six stimulus repetitions. Prepulse stimulus amplitude was defined as the highest amplitude that evoked c-bend startle behaviors in less than 10% of embryos over six stimulus repetitions. Percent inhibition was calculated for each fish as [(% of startle trials showing short-latency C-bends) – (% of PPI trials showing short-latency C-bends)] / (% of startle trials showing short-latency C-bends) * 100.

Mortality analysis

A mixture of wild-type, heterozygous, and homozygous *dscamb*^{j2b} mutant siblings were distributed into tanks at a density of 20-40 fish/tank and raised under standard rearing conditions. At select time-points (7, 10, 13, 16, 19, 34, and 60 dpf), whole tanks were euthanized in 0.02% tricaine on-ice for 10 min, and individual fish were either lysed whole or fin clipped (34 and 60 dpf only) for genotyping.

Food intake assay

Analysis of food intake was adapted from a previously published protocol (Field et al., 2009). In summary, fluorescent food was made by combining 100 mg of 50-100 um powdered larval fish food with 150 ul of red fluorescent microspheres (FluoSpheres carboxylate, 2.0 um diameter, 580/605 nm, Life Technologies F8826) and 50 ul of water in a glass depression well. The

mixture was dried overnight, in the dark, then ground into a fine powder using a small pestle and stored at 4 degrees until use.

At 5 and 6 dpf wild-type, heterozygous, and homozygous *dscamb*^{i2b} mutant siblings were fed 2-4 mg of non-nonfluorescent 50-100 um larval fish food each morning, when the lights turned on. At 7 dpf, 2-4 mg of fluorescent food was added to the tank in the morning. After feeding for 1.5 hours the fluorescent food was washed out and fish were anaesthetized in 0.02% tricaine for screening. Food intake in the anterior intestinal bulb was assessed using a SteREO Discovery.V12 fluorescent dissecting microscope by an observer that was blind to genotype. Larvae with intestinal bulbs that were completely filled with fluorescent food were selected as "full", and "empty" fish had no fluorescence in the gut, except a few occasional fluorescent specs. "Partial" fish were those with any amount of fluorescence between full and empty. After separating fish by feeding state, individual larvae were euthanized and lysed for genotyping.

Gulp assay

At 7 dpf, Et1(dscamb:Gal4), Tg(UAS:GFP) heterozygous and homozygous mutant siblings were immobilized in 3% methylcellulose, with the ventral side facing up to better visualize jaw movements. 20 sec videos of spontaneous jaw movements (or "gulps") were recorded on an AxioCam MRm CCD camera mounted on SteREO Discovery.V12 dissecting microscope with a frame interval of 0.076 frames/sec. After recording, individual larvae were lysed for genotyping. Videos were analyzed by counting the total number of gulps during each video. The observer was blind to genotype while counting.

Statistical analyses

All statistical analyses were performed using the R software package.

4.7 REFERENCES

Allen JR, Bhattacharyya KD, Asante E, Almadi B, Schafer K, Davis J, Cox J, Voigt M, Viator JA, Chandrasekhar A (2017) Role of branchiomotor neurons in controlling food intake of zebrafish larvae. J Neurogenet:1–10.

Bhandiwad AA, Zeddies DG, Raible DW, Rubel EW, Sisneros JA (2013) Auditory sensitivity of larval zebrafish (Danio rerio) measured using a behavioral prepulse inhibition assay. J Exp Biol 216:3504–3513.

Bilotta J, Saszik S (2001) The zebrafish as a model visual system. Int J Dev Neurosci 19:621–629.

Bosch DS, van Swinderen B, Millard SS (2015) Dscam2 affects visual perception in Drosophila melanogaster. Front Behav Neurosci 9:149.

China V, Holzman R (2014) Hydrodynamic starvation in first-feeding larval fishes. Proc Natl Acad Sci U S A 111:8083–8088.

Cvetkovska V, Hibbert AD, Emran F, Chen BE (2013) Overexpression of Down syndrome cell adhesion molecule impairs precise synaptic targeting. Nat Neurosci 16:677–682.

Faucherre A, Nargeot J, Mangoni ME, Jopling C (2013) piezo2b regulates vertebrate light touch response. J Neurosci 33:17089–17094.

Field HA, Kelley KA, Martell L, Goldstein AM, Serluca FC (2009) Analysis of gastrointestinal physiology using a novel intestinal transit assay in zebrafish. Neurogastroenterol Motil 21:304–312.

Filosa A, Barker AJ, Dal Maschio M, Baier H (2016) Feeding State Modulates Behavioral Choice and Processing of Prey Stimuli in the Zebrafish Tectum. Neuron 90:596–608.

Fleisch VC, Neuhauss SCF (2006) Visual behavior in zebrafish. Zebrafish 3:191–201.

Fuerst PG, Bruce F, Tian M, Wei W, Elstrott J, Feller MB, Erskine L, Singer JH, Burgess RW (2009) DSCAM and DSCAML1 function in self-avoidance in multiple cell types in the developing mouse retina. Neuron 64:484–497.

Fuerst PG, Harris BS, Johnson KR, Burgess RW (2010) A novel null allele of mouse DSCAM survives to adulthood on an inbred C3H background with reduced phenotypic variability. Genesis 48:578–584.

Gahtan E, Tanger P, Baier H (2005) Visual prey capture in larval zebrafish is controlled by identified reticulospinal neurons downstream of the tectum. J Neurosci 25:9294–9303.

Gau P, Poon J, Ufret-Vincenty C, Snelson CD, Gordon SE, Raible DW, Dhaka A (2013) The zebrafish ortholog of TRPV1 is required for heat-induced locomotion. J Neurosci 33:5249–5260.

Hamdani EH, Kasumyan A, Døving KB (2001) Is feeding behaviour in crucian carp mediated by the lateral olfactory tract? Chem Senses 26:1133–1138.

Lemieux M, Laflamme OD, Thiry L, Boulanger-Piette A, Frenette J, Bretzner F (2016) Motor hypertonia and lack of locomotor coordination in mutant mice lacking DSCAM. J Neurophysiol 115:1355–1371.

Maynard KR, Stein E (2012) DSCAM contributes to dendrite arborization and spine formation in the developing cerebral cortex. J Neurosci 32:16637–16650.

Muto A, Orger MB, Wehman AM, Smear MC, Kay JN, Page-McCaw PS, Gahtan E, Xiao T, Nevin LM, Gosse NJ, Staub W, Finger-Baier K, Baier H (2005) Forward Genetic Analysis of Visual Behavior in Zebrafish. PLoS Genet 1:e66.

Neuhauss SC, Biehlmaier O, Seeliger MW, Das T, Kohler K, Harris WA, Baier H (1999) Genetic disorders of vision revealed by a behavioral screen of 400 essential loci in zebrafish. J Neurosci 19:8603–8615.

Okada S (2015) The taste system of small fish species. Biosci Biotechnol Biochem 79:1039–1043.

Palanca AMS, Lee S-L, Yee LE, Joe-Wong C, Trinh LA, Hiroyasu E, Husain M, Fraser SE, Pellegrini M, Sagasti A (2013) New transgenic reporters identify somatosensory neuron subtypes in larval zebrafish. Dev Neurobiol 73:152–167.

Prober DA, Zimmerman S, Myers BR, McDermott BM Jr, Kim S-H, Caron S, Rihel J, Solnica-Krezel L, Julius D, Hudspeth AJ, Schier AF (2008) Zebrafish TRPA1 channels are required for chemosensation but not for thermosensation or mechanosensory hair cell function. J Neurosci 28:10102–10110.

Schilling TF, Kimmel CB (1997) Musculoskeletal patterning in the pharyngeal segments of the zebrafish embryo. Development 124:2945–2960.

Thiry L, Lemieux M, D Laflamme O, Bretzner F (2016) Role of DSCAM in the development of the spinal locomotor and sensorimotor circuits. J Neurophysiol 115:1338–1354.

Versonnen BJ, Roose P, Monteyne EM, Janssen CR (2004) Estrogenic and toxic effects of methoxychlor on zebrafish (Danio rerio). Environ Toxicol Chem 23:2194–2201.

Wilson C (2012) Aspects of larval rearing. ILAR J 53:169–178.

Xu Y, Ye H, Shen Y, Xu Q, Zhu L, Liu J, Wu JY (2011) Dscam mutation leads to hydrocephalus and decreased motor function. Protein Cell 2:647–655.

CHAPTER 5

Concluding Remarks

5.1 SYNTHESIS OF THE RESULTS AND POTENTIAL PITFALLS

Dscams have been relatively understudied in zebrafish, although this model offers many advantages for investigating their function. The present study is an example of how genome engineering techniques can be applied to zebrafish to efficiently generate genomic null mutations and endogenous reporter lines. These techniques are relatively easy to perform and, when combined with dynamic in vivo imaging, make the larval zebrafish a powerful model for investigating gene function in neuronal development. Using these techniques, we conducted the first detailed analysis of the expression and function of a DSCAM family member in the zebrafish nervous system and uncovered a novel, critical role for this gene in regulating feeding behavior.

We found that Dscamb is expressed abundantly throughout the nervous system in a pattern that resembles the patterns that have been described for other DSCAM genes in other vertebrate models (Yamakawa et al., 1998; Barlow et al., 2002; Yimlamai et al., 2005; Morales Diaz, 2014). Despite broad neuronal expression, we were unable to identify any cellular or structural defects in *dscamb* mutants. There are several possible explanations for this outcome. First, *dscamb* could be required for subtle aspects of neuronal development. Precedence for this is found in studies of *Dscam* mutant mice, in which, despite broad expression during development, the overall architecture of the brain is largely preserved (Amano et al., 2009; Maynard and Stein, 2012). In most cases, defects were only identified in a few select regions of the brain, such as the cortex , brainstem, and spinal cord following detailed cellular or electrophysiological analysis (Amano et al., 2009; Maynard and Stein, 2012; Thiry et al., 2016). An accumulation of subtle developmental insults could lead to a dramatic deficit in a complex behavior such as feeding, which requires the coordinated activity of sensory, motor, and neuroendocrine systems.

A second, more prosaic, possibility is that our analyses were misled by inaccurate expression from our enhancer trap reporter. The fact that we observed similar patterns of expression with independent enhancer trap integrations at two separate target sites argues against this possibility. Moreover, although our BAC reporter was expressed more sparsely, it overlapped completely with our enhancer traps, further indicating that these reporters were likely accurate. Nonetheless, our two enhancer trap integration sites were only 65 bp apart, so it is possible that both integrations disrupt the same regulatory sequence, resulting in similar patterns of misexpression. Alternative insertional strategies, such as targeted gene trap or splice trap insertion have also been reported in zebrafish (Gonzales and Yeh, 2014) and could be used to validate enhancer trap expression.

Third, gene expression could be incompletely knocked out in our *dscamb* mutant lines. Highly penetrant homozygous mutant lethality occurred across mutant lines containing independent mutations at two different target sites. This provides strong evidence that our phenotype was specific and that we deleteriously altered gene function. However, there could be alternative splice forms of Dscamb, which exclude the first two exons, although no such alternative isoforms are currently predicted for this gene. Genomic insults may also activate alternative start codons or splice sites, allowing cells to excise the deleterious mutations (Kochetov, 2008; Nilsen and Graveley, 2010; Ohno et al., 2017). Using TALENs or CRISPR/Cas9, it is possible to generate large genetic deletions (as opposed to point mutations) (Varshney et al., 2015). We could use this approach to ensure complete loss-of-function by generate mutations in that remove functionally critical domains of *dscamb*, in addition to generating frameshift mutations.

Lastly, Dscamb could be functionally redundant with one or both of its paralogs, Dscama and Dscaml1. Although the expression and function of Dscaml1 has never been investigated,

Dscama shows a similar expression pattern to Dscamb, suggesting that it could be expressed in the same cells and perform similar functions (Yimlamai et al., 2005). Additional functional analyses of these genes could shed light on this possibility. It has also been reported in zebrafish that deleterious mutations can stimulate the upregulation of closely related genes and compensate for loss-of-function (Rossi et al., 2015). We could test for this possibility by generating expression profiles of mutant larvae, and assessing whether similar genes, such as *dscama*, *dscaml1*, or other IgSF cell adhesion molecules are upregulated with *dscamb* loss-of-function. However, even if compensation is occurring, is it clear that it is incomplete, as *dscamb* mutant larvae are defective in their ability to find and capture food.

In summary, these studies uncover a novel role for a DSCAM family member in regulating feeding behavior and survival. Although we were unable to elucidate a cellular mechanism for this behavior, we are the first to identify that Dscamb is expressed in the muscle fibers and innervating neurons of the jaw and operculum, critical structures for food capture. Moreover, that Dscamb is also expressed in all sensory systems may indicate its potential role in the sensory systems coordinating complex behaviors such as detecting or capturing food. The results reported in this body of work blossomed from the development of novel genetic tools that now poise our lab and others in the field to further map specific functions of Dscamb in the wiring of neuronal circuits. In total, the studies encompassed by this dissertation demonstrate the power of engineering genetic tools in the zebrafish model, and may open new investigations in uncovering the roles of IGSF family members in neuronal development.

5.2 REFERENCES

Amano K, Fujii M, Arata S, Tojima T, Ogawa M, Morita N, Shimohata A, Furuichi T, Itohara S, Kamiguchi H, Korenberg JR, Arata A, Yamakawa K (2009) DSCAM deficiency causes loss of pre-inspiratory neuron synchroneity and perinatal death. J Neurosci 29:2984–2996.

Barlow GM, Micales B, Chen X-N, Lyons GE, Korenberg JR (2002) Mammalian DSCAMs: roles in the development of the spinal cord, cortex, and cerebellum? Biochem Biophys Res Commun 293:881–891.

Gonzales APW, Yeh J-RJ (2014) Cas9-based genome editing in zebrafish. Methods Enzymol 546:377–413.

Kochetov AV (2008) Alternative translation start sites and hidden coding potential of eukaryotic mRNAs. Bioessays 30:683–691.

Maynard KR, Stein E (2012) DSCAM contributes to dendrite arborization and spine formation in the developing cerebral cortex. J Neurosci 32:16637–16650.

Morales Diaz HD (2014) Down syndrome cell adhesion molecule is important for early development in Xenopus tropicalis. Genesis 52:849–857.

Nilsen TW, Graveley BR (2010) Expansion of the eukaryotic proteome by alternative splicing. Nature 463:457–463.

Ohno K, Takeda J-I, Masuda A (2017) Rules and tools to predict the splicing effects of exonic and intronic mutations. Wiley Interdiscip Rev RNA Available at: http://dx.doi.org/10.1002/wrna.1451.

Rossi A, Kontarakis Z, Gerri C, Nolte H, Hölper S, Krüger M, Stainier DYR (2015) Genetic compensation induced by deleterious mutations but not gene knockdowns. Nature 524:230–233.

Thiry L, Lemieux M, D Laflamme O, Bretzner F (2016) Role of DSCAM in the development of the spinal locomotor and sensorimotor circuits. J Neurophysiol 115:1338–1354.

Varshney GK, Pei W, LaFave MC, Idol J, Xu L, Gallardo V, Carrington B, Bishop K, Jones M, Li M, Harper U, Huang SC, Prakash A, Chen W, Sood R, Ledin J, Burgess SM (2015) High-throughput gene targeting and phenotyping in zebrafish using CRISPR/Cas9. Genome Res 25:1030–1042.

Yamakawa K, Huot YK, Haendelt MA, Hubert R, Chen XN, Lyons GE, Korenberg JR (1998) DSCAM: a novel member of the immunoglobulin superfamily maps in a Down syndrome region and is involved in the development of the nervous system. Hum Mol Genet 7:227–237.

Yimlamai D, Konnikova L, Moss LG, Jay DG (2005) The zebrafish down syndrome cell adhesion molecule is involved in cell movement during embryogenesis. Dev Biol 279:44–57.